Centro de Investigación Científica y de Educación Superior de Ensenada, Baja California

Programa de Posgrado en Ciencias en Electrónica y Telecomunicaciones

Design and implementation of IR-UWBoF systems with spectral line suppression capabilities

Tesis

para cubrir parcialmente los requisitos necesarios para obtener el grado de Doctor en Ciencias

Presenta:

Aldo Eleazar Pérez Ramos

Ensenada, Baja California, México
2016

Tesis defendida por

Aldo Eleazar Pérez Ramos

y aprobada por el siguiente Comité

_____   _____
Dr. Salvador Villarreal Reyes   **Dr. Arturo Arvizu Mondragón**
Codirector   Codirector

Dra. Catherine Lepers
Miembro del comité

Dr. Miguel Ángel Alonso Arévalo
Miembro del comité

Dr. David Hilario Covarrubias Rosales
Miembro del comité

Dr. Roberto Conte Galván
Miembro del comité

_____
Dr. Miguel Ángel Alonso Arévalo
Coordinador del Posgrado en Electrónica y Telecomunicaciones

_____
Dra. Rufina Hernández Martínez
Directora de Estudios de Posgrado

Resumen de la tesis que presenta **Aldo Eleazar Pérez Ramos** como requisito parcial para la obtención del grado de Doctor en Ciencias en Electrónica y Telecomunicaciones con orientación en Telecomunicaciones.

Diseño e implementación de sistemas de ancho de banda ultra-amplio sobre fibra (IR-UWBoF) capaces de eliminar líneas espectrales

Resumen aprobado por:

_____   _____
Dr. Salvador Villarreal Reyes   **Dr. Arturo Arvizu Mondragón**
Codirector de tesis   Codirector de tesis

La eliminación de líneas espectrales es un tema de gran importancia en el diseño de sistemas de ancho de banda ultra-amplio (UWB), en particular de aquellos que utilizan pulsos de ultra-corta duración (Impulse-Radio, IR) para transmitir información. Es un hecho comprobado que la presencia de líneas espectrales en la densidad espectral de potencia (DEP) de señales IR-UWB puede afectar el desempeño del sistema, esto debido a que, generalmente, se reduce la potencia de transmisión de dichos sistemas para cumplir con las regulaciones UWB vigentes. La reducción de esta potencia de igual forma puede afectar la distancia de las comunicaciones entre dispositivos IR-UWB. Aunque trabajos previos han mostrado interesantes ventajas al implementar IR-UWB sobre fibra óptica (IR-UWBoF), principalmente para extender el área de cobertura de comunicaciones UWB por varios kilómetros, el tema de eliminación de líneas espectrales en la DEP no ha sido desarrollado por completo. Para abordar el tema antes mencionado, en esta tesis se proponen dos sistemas IR-UWBoF que utilizan códigos convolucionales (CC) supresores de líneas espectrales: "*spectral line supressive*" (SLS) y "*spectral line free*" (SLF). Además, estos sistemas han sido diseñados para establecer comunicaciones de alta y baja tasa de datos entre una oficina central y puntos de acceso remoto emplazados a varios kilómetros de distancia. La arquitectura radio sobre fibra (RoF) utilizada en ambos sistemas propuestos se basa en la técnica de modulación de intensidad con detección directa (IM/DD). Dicha arquitectura facilita la implementación de sistemas de bajo costo y baja complejidad. Resultados experimentales muestran que los sistemas propuestos ofrecen DEPs con características espectrales convenientes si se comparan con implementaciones de sistemas IR-UWBoF convencionales. Además, se ha demostrado experimentalmente que el sistema SLF IR-UWBoF-IM/DD puede entregar una DEP sin líneas espectrales considerando un canal óptico-inalámbrico formado de 30 km de fibra óptica monomodo y 20 cm de transmisión inalámbrica.

Palabras clave: Sistemas IR-UWB, radio sobre fibra, densidad espectral de potencia, eliminación de líneas espectrales, códigos convolucionales.

Abstract of the thesis presented by **Aldo Eleazar Pérez Ramos** as a partial requirement to obtain the Doctor of Science degree in Electronics and Telecommunications with orientation in Telecommunications.

Design and implementation of IR-UWBoF systems with spectral line suppression capabilities

Abstract approved by:

_____   _____
Dr. Salvador Villarreal Reyes   **Dr. Arturo Arvizu Mondragón**
Thesis Codirector   Thesis Codirector

The topic of spectral line suppression is of major importance when designing impulse-radio ultra-wideband (IR-UWB) systems. The presence of spectral lines in the power spectral density (PSD) may limit the maximum transmission power in order to comply with UWB regulations, thus, affecting the system performance. In fact, the transmitted power diminishes could lead to a range reduction of the UWB system. Although previous works have shown the advantages of IR-UWB over fiber (UWBoF) implementations (mainly to extend the coverage area of UWB communications by several kilometers), the topic of spectral line suppression in such systems has not been entirely addressed. This thesis proposes two IR-UWBoF systems using spectral line suppressive and spectral line free (SLF) convolutional codes to address the spectral line suppression problem. Furthermore, these systems have been designed to implement high data rate and low data rate communications from a central office to remote access points located several kilometers away. The radio over fiber (RoF) architecture implemented in both systems is based on the intensity modulation with direct detection technique which allows the implementation of low cost and low complexity systems. Experimental results show that the proposed systems offer improved PSD characteristics compared to conventional IR-UWBoF implementations. Furthermore, it was experimentally demonstrated that the proposed SLF IR-UWB system is able to deliver a spectral line free PSD considering an optical-fiber channel formed by 30 km of single-mode fibers and 20 cm of wireless transmission.

Keywords: Impulse-radio ultra-wideband, radio over fiber, power spectral density, spectral line suppression, convolutional codes.

Dedicatory

<div align="right">

A Dios

A mi padre y madre

Eleazar Pérez Santiago e Inés Nancy Ramos Miguel

</div>

Acknowledgements

It is important to me give my special thanks to all those people I met in CICESE and in Ensenada during my postgraduate studies.

Your friendship and support will never be forgotten

Table of contents

List of figures

List of tables

Chapter 1. Introduction

Recent advances in microelectronics, signal processing, computation, communication protocols and highly capable wireless networking technologies developed in last decade, have led to arise new ways to convey information between people and devices, which also can be connected to the Internet. Today, it is common having services such as: high definition (HD) and ultra-high definition (UHD) video streaming, massively multiplayer online games (MMO), high-speed transfers of massive files, environmental and health care telemonitoring systems, among others. These new usage models in the telecommunications area demand robust and reliable wireless technologies. In this sense, wireless systems have increased their capacities in order to meet with this demand, such as is shown in Figure 1. From here, it is possible to see that capacity of wireless personal area networks (WPAN) appears to be rising at a much faster rate than wireless technologies included within wireless metropolitan networks (WMAN). This fact is due to smaller coverage areas enables the implementation of high bandwidth communications (hundreds of Mb/s) and multi-Gb/s wireless communication by using wireless technologies operating below 10 GHz and 60 GHz, respectively, (Abraha S. T., 2012).
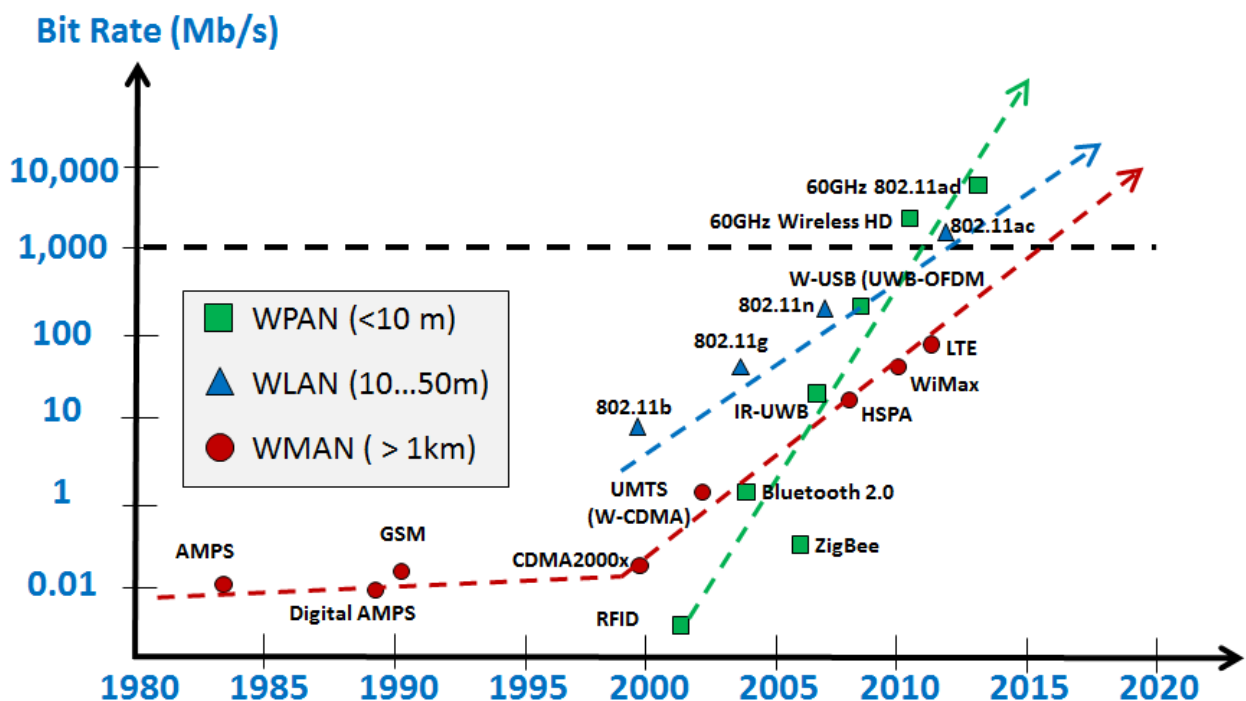
Figure 1: Wireless technology trends.

Typically, wireless services previously mentioned use the most widely deployed wireless technologies such as Wi-Fi (IEEE802.11b/g/n), Bluetooth and ZigBee, which transmit radio signals over the Industrial, Scientific and Medical (ISM) frequency bands (i.e. 900 MHz and 2.4 GHz). During the last decade, the dramatic increasing of WPAN deployments have originated overcrowding in these ISM bands. This fact produces interference between wireless systems operating in the same frequency bands, which considerably degrades WPAN communication performance. In this context, PHY-MAC layer improvements such as those shown in (Zhu, Waltho, Yang, and Guo, 2007, Huang, Lee, and Park, 2009, Roy and Jamadagni, 2010, Kumar, Shin, Choi, and Niculescu, 2012) were recently proposed to counter these issues.

An interesting technology proposed over the last decade was ultra-wideband (UWB) radio. UWB technology has gained a lot of attention by academics and industry because of its low power consumption, high capacity, spectrum coexistence, tolerance against multipath fading, and comparatively high data rates (HDR), (Win and Scholtz, 1998, Aiello and Rogerson, 2003, Roy, Foerster, Somayazulu, and Leeper, 2004). Due to the characteristics previously mentioned, this technology has been considered to be suitable for HDR-WPANs, low data rate (LDR) WPANs, sensor networks, imaging systems, precision navigation systems, vehicular radar systems, medical monitoring, among others. In all these applications, the transceivers range usually covers an area of a few meters. Thus, when information has to be exchanged between several of these UWB networks separated by hundreds or thousands of meters, it is necessary to use a long range technology to interconnect them. Recently, Radio over Fiber (RoF) systems have been used to transport UWB signals over long distances, extending the coverage area of these UWB-WPANs. This relatively new technique disclosed as UWB over fiber (UWBoF) by Yao, Zeng, and Wang (2007), allows to overcome the coverage limitation of WPANs and providing availability of undisrupted UWB service across different networks, (Pan and Yao, 2010-A, Pan and Yao, 2011-A). In addition, this technique will be able to overcome the last mile bottleneck problem expected due to the rapid increase in the capacity of WPAN services.

Nevertheless, despite of the potential offered by the introduction of UWB technology combined with RoF systems, the compliance of UWB emissions with spectral masks defined by various regulatory body such as the Federal Communications Commission (FCC) in the United States and the European Conference of Postal and Telecommunications Administrations/Electronic Communications Committee (CEPT/ECC) (FCC, 2002, CEPT/ECC, 2006-A) is an important topic that must be considered. The spectral masks aim is to enable harmonious coexistence between UWB signals and narrow band wireless systems (WiFi, Bluetooth, Zigbee). In this context, the design of compliant UWB systems and as well as compliant UWBoF systems are topics of major interest for implementing the next generation WPANs.

1.1 Ultra-Wideband over Fiber (UWBoF) systems

The UWB "plus" Radio over Fiber (UWB + RoF) or simply UWB over Fiber is a relatively new cost-effective technique used to extend the range, to interconnect isolated UWB networks, and to integrate UWB services into fixed wired or wireless communications networks, (Yao , 2009, Pan and Yao, 2010-A).

The distribution of UWB signals over fiber has been considered for two main applications. One of these applications are the distributed antenna systems (DAS), which can be implemented in buildings to extend the reach of UWB signals, (Xianbin Yu et al., 2013). The fiber lengths used in these DAS are relatively short (tens of meters). In the second application, the UWB signals are distributed from a central office (CO) to end-users using optical fiber transmission followed by wireless UWB transmission (Pan and Yao, 2011-A). The distances can be several kilometers (20-km and 30-km can be the distance from the local exchange to wireless user in households).

Typically, the design and implementation of UWBoF systems reported in the literature consider two widely adopted UWB technologies: Impulse Radio (IR) and Multi Band (MB) OFDM. The UWB MB-OFDM consists in transmitting orthogonal frequency division multiplexing (OFDM) symbols successively over frequency channels allocated by communication standards such as the ECMA-368 (WiMedia PHY), (ECMA-368, 2008). On the other hand, IR-UWB technology is based on the transmission of very short-time

pulses (in the order of hundreds of picoseconds), optimized to meet spectral masks defined regulatory bodies such as the U.S. FCC and the CEPT/ECC, (Di Benedetto and Giancola, 2004, Di Benedetto, Kaiser, Molisch, Oppermann, Politano and Porcino, 2006). Although both technologies enable the implementation of robust short-range wireless networks of high capacity, with tolerance against multipath fading, spectrum coexistence and comparatively high data rate, IR technology can also offer variable low complexity, low cost, low power consumption and very good time domain resolution, (Zhang, Orlik, Sahinoglu, Molisch, and Kinney, 2009-A). These last characteristics allow the implementation of low data rate (LDR) wireless sensor networks deployments. On the other hand, RoF architectures used by the UWBoF systems reported in the literature consider simple to complex optical transmission techniques. As a pair of examples of the most used techniques to transmit UWB signals over single-mode and multi-mode optical fibers we have the intensity modulation with direct detection (IM-DD) technique and phase modulation-to-intensity modulation (PM-to-IM) conversion with direct detection technique, (Yao et al., 2007, Pan and Yao, 2010-C, Abraha, Okonkwo, Gamage, Tangdiongga, and Koonen, 2012). Furthermore, there exist other complex optical transmission techniques such as "all optical up-conversion" based on advanced configurations of Mach Zehnder Modulators (MZM), and "heterodyne detection" methods based on dual-wavelengths system, injection locking, dual-mode lasers, and mode-locked lasers, (Guillory, 2012). These techniques have been mainly proposed to generate electrical millimeter-waves for UWB MB-OFDM networks working at 60 GHz. It is important to mention that IM/DD systems could be easily integrated with next generation optical communication systems (e.g. Wavelength Division Multiplexing Passive Optical Networks, WDM-PONs), (Pan and Yao, 2010-C), taking advantage of preexistent infrastructure widely deployed since more than 20 years, (Cox, Ackerman, Betts, and Prince, 2006). Furthermore, the combination of this optical system (IM/DD) with impulse radio UWB systems results in low-complexity/low-power consumption IR-UWBoF deployments. This latter point resulting important to this research work.

In brief, the IR-UWBoF-IM/DD systems convey information by generating trains of short-time pulses (on the order of hundreds of picoseconds) modulated by schemes such as pulse position modulation (PPM), pulse amplitude modulation (PAM), binary phase shift

keying (BPSK), biorthogonal PPM (BOPPM) and pulse shape modulation (PSM), which are then transmitted through optical fiber links by means of the intensity modulation (IM) technique. This latter technique is carried out modulating the optical power of a laser diode by means of two methods. In one of these methods, referred to as "direct modulation", the IR-UWB signal can be converted into an optical signal by means of the modulation of the laser diode's injection current. This modulation can be achieved since there exist a direct relationship between the laser diode output optical power and its injection current. In the second method, referred to as "external modulation", a laser diode operating in continuous wave (CW) mode is connected to an external electro-optic Mach Zehnder modulator (MZM). This MZM is used to modulate the CW optical signal according to voltage changes determined by the electrical IR-UWB signal. At the end of the optical link, the electrical IR-UWB signal is recovered by using a direct detection schema using a PIN photodiode. This device detect the magnitude-squared of the real envelope of the optical field received.

Another important characteristic of typical IR-UWBoF systems is that IR-UWB signals usually employ pseudo-random (PR) time hopping (TH) and/or PR direct sequence (DS) multiplication for multiple access and/or PSD shaping purposes, (Win and Scholtz, 1998, Win and Scholtz, 2000, Aiello and Rogerson, 2003, Di Benedetto and Giancola, 2004, Roy et al., 2004, Di Benedetto et al., 2006, Arslan, Chen, and Di Benedetto, 2006, Ghavami, Michael, and Kohno, 2007). Basically, a TH-IR UWBoF system transmits pulses with a very low duty cycle. The relative position of each pulse within a specified time frame is then determined by a PR-TH sequence. In a pure DS-IR UWBoF system the relative position of each pulse within a time frame remains unchanged but the pulse amplitude is multiplied by a PR-DS usually taking values of the set $\{-1, +1\}$. Thus the duty cycle of a DS-IR UWB signal can be higher than the duty cycle of a TH-IR-UWB signal. Finally a TH/DS IR-UWB signal combines both techniques and its duty cycle can be as low as that of a TH-IR-UWB signal.

1.2 Problem statement

As previously mentioned, one of the main constraints when designing IR-UWB deployments and IR-UWBoF systems is compliance with the spectral masks issued by regulatory bodies such as the U.S. FCC and CEPT/ECC. The aim of these masks is to

enable the harmonious coexistence between UWB systems and the already established wireless systems such as Global Position Systems (GPS), WiFi, Bluetooth, ZigBee, 2G to 4G cellular networks, among others. Thus, one of the main research areas when IR-UWB systems are considered, it is the maximization of the transmit power while maintaining compliance with the spectral mask limits imposed by current UWB regulations.
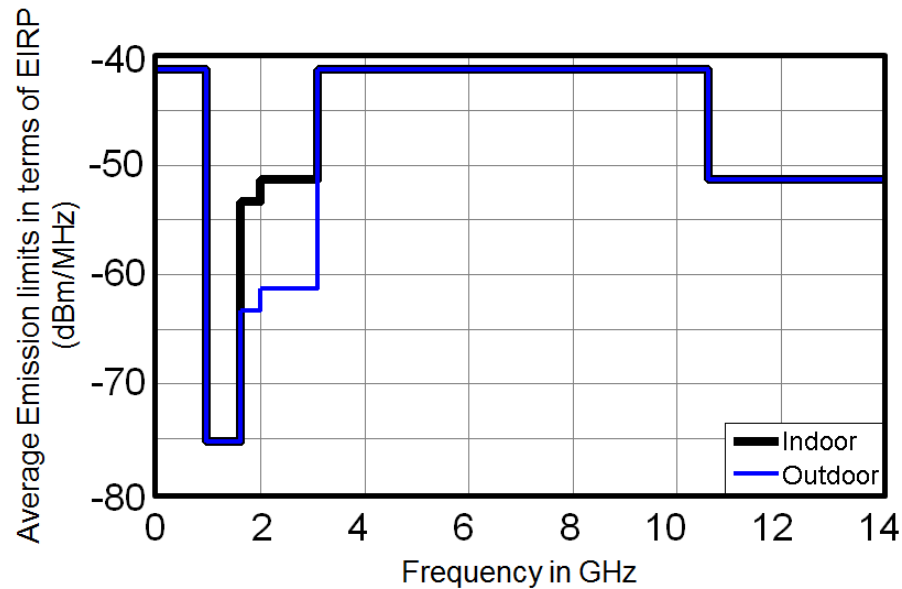
Figure 2. FCC's spectral masks for UWB systems, (Federal Communication Commission, 2002).

As an example, the spectral masks issued by the U.S. FCC for indoor and outdoor UWB systems, (FCC, 2002), are shown in Figure 2. These spectral masks are specified in terms of Power Spectral Density (PSD) in dBm as measured with a 1 MHz resolution bandwidth (RBW), root mean square (RMS) average detector and an average time of 1 ms or less, (FCC, 2002).

Recently several previous studies dealing with IR-UWBoF systems usually report measured and/or analytical PSDs for the analyzed IR-UWBoF signals, (Qing Wang, Fei Zeng, Blais, and Yao, 2006, Wang and Yao, 2006, Zeng and Yao, 2006-A, Zeng and Yao, 2006-B, Dong, Zhang, Xu, and Huang, 2007, Jianji Dong, et al., 2007, Qing Wang and Yao, 2007, Wang, Zeng, and Yao, 2007, Yao, Zeng, and Wang, 2007, Zeng, Wang, and Yao, 2007, Abtahi, Magne, Mirshafiei, Rusch, and LaRochelle, 2008-B, Chang, Tian, Ye, Gao, and Su, 2008, Dong, Zhang, Zhang and Huang, 2008, Jazayerifar, Cabon, and

Jawad, 2008, Huang, et al., 2008, Jianqiang Li, et al., 2008, Pan Ou, Ye Zhang, and Chun-Xi Zhang, 2008, Abtahi, Dastmalchi, LaRochelle, and Rusch, 2009, Bolea, Mora, Ortega, and Capmany, 2009, Hanawa, et al., 2009, Li, Kuo, and Wong, 2009, Pan and Yao, 2009, Xianbin Yu et al., 2009, Yao, 2009, Bolea, Mora, Ortega, and Capmany, 2010, Dong, Zhang, Yu, Huang, and Zhang, 2010, Gibbon, et al., 2010, Jian-Yu Zheng, Ming-Jiang Zhang, An-Bang Wang, and Yun-Cai Wang, 2010, Lopez, et al., 2010, Pan and Yao, 2010-A, Pan and Yao, 2010-B, Pan and Yao, 2010-C, Rodes, et al., 2010-A, Rodes, Pham, Jensen, Gibbon, and Monroy, 2010-B, Valente and Cartaxo, 2010, You Min Chang, Junsu Lee, and Ju Han Lee, 2010, Abtahi and Rusch, 2011, Abraha et al., 2011, Chang, Lee, Lee, Yan, and Lee, 2011, Ming-Jiang Zhang et al., 2011, Pan and Yao, 2011-A, Pan and Yao, 2011-B, Pham, Yu, Dittmann, and Monroy, 2011, Sakib, Huang, Gross, and Liboiron-Ladoucer, 2011, Xu, et al., 2011, Abraha et al., 2012, Abraha S. T., 2012, Gang Chen and Shilong Pan, 2012, Guillory, 2012, Li, Chen, Chen, and Xie, 2012, Wang, Zhu, and Gomes, 2012, Xianbin Yu et al., 2013, Zhang et al., 2013, Chengliang et al., 2014-A, Chengliang et al., 2014-B, Feng, Xiao, Yi, and Hu, 2014-A, Feng et al., 2014-B, Le, Briggmann, and Kuppers, 2014, Moreno, Rius, Mora, Muriel and Capmany, 2014, Quang Trung Le, Briggmann, and Kuppers, 2014, Moreno, Mora, and Capmany, 2015). However, most of the PSDs reported in these works show spectral lines. The spectral lines can be result of periodicity in the data, modulation schemes used in the signal and/or optical configurations implemented.
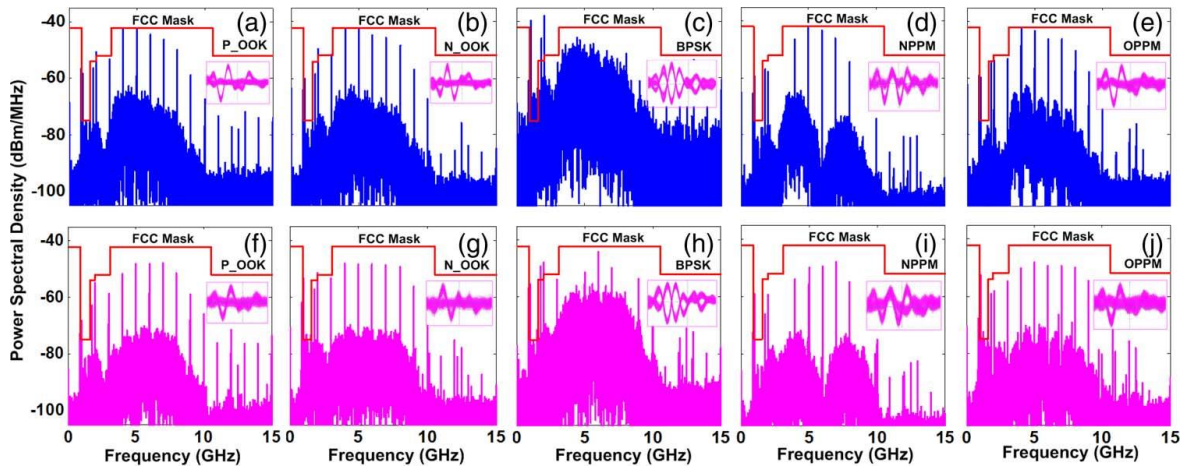
Figure 3. Electrical spectra and eye diagrams of the UWB signals generated by the IR-UWBoF system reported in (Li, Chen, Chen, and Xie, 2012). (a)-(e) with wireless transmission; (f)-(j) with combined 20-km SMF and wireless transmission.

Figure 3 shows the experimental PSDs reported by Li, et al. (2012), and as it can be seen in this figure, most of them exhibit spectral lines, which are violating the spectral mask power limits. The problem with the spectral lines presence is that the maximum achievable transmit power has to be reduced in order to comply with the spectral masks. Comparatively, an IR-UWB system with a spectral line free (SLF) PSD will be able to transmit with more power over the wireless link than an IR-UWB system whose PSD shows spectral lines. Furthermore, theoretically, when using BPSK (which is equivalent to BPM, Bi-phase modulation mentioned in some works) and the input data stream consists of random binary data with uniform distribution, the PSD should not show any spectral lines (Villarreal-Reyes, 2007). Nevertheless, as shown by the experimental PSDs reported by Pan and Yao (2010-A and 2011-A), Xianbin Yu et al., (2009), Feng et al., (2014-B), and Abraha et al., (2011), the photonic implementation of some IR-UWBoF systems can generate spectral lines even when using BPSK schemes with pseudorandom sequences of very long period (i.e., resembling a perfectly random binary data stream with uniform distribution). In addition, strong spectral lines in the PSD of BPSK signals naturally appear when the binary data stream is not perfectly random (that is, the data stream is an i.i.d sequence of binary random variables with uniform distribution), (Pan and Yao, 2010-A, Villarreal-Reyes, 2007), which is the most commonly observed case. Thus, to fully exploit the maximum transmit power allowed by the spectral masks, it is desirable to design IR-UWBoF schemes whose PSD is SLF, this even when the data stream consists of non-uniform distributed bits (i.e., nonrandom binary data streams).

Previously, spectral line suppressive (SLS) and spectral line free (SLF) convolutional codes (CC) have been proposed to achieve both elimination of spectral lines and BER improvement, (Villarreal-Reyes, 2007). Analytical and simulation-based performance evaluations have shown that it is possible to eliminate spectral lines on the PSD of IR-UWB systems, even when the encoder input does not consist of a perfectly random binary data stream.

Based on the previous discussion it can be said that the analysis, estimation and shaping of the PSD of IR-UWB signals is a topic of major interest for the design of compliant IR-UWB systems and IR-UWBoF systems as well. This research deals with the proposal of

IR-UWBoF systems that simultaneously provide improved BER performance and convenient PSD characteristics. Therefore the use of SLS/SLF CC is important for this thesis work.

1.3 Aim of thesis

The research presented in this thesis work deals with the design and implementation of Impulse Radio Ultra-Wideband over Fiber (IR-UWBoF) systems compliant with the FCC UWB regulations. The proposed systems can be able to offer both convenient PSD characteristics and bit error rate (BER) improvement over traditional IR-UWBoF systems reported in the literature.

The particular objectives of this thesis work can be listed as follows:

- Investigate the state of the art of IR-UWBoF systems.
- Perform a theoretical study of IR-UWBoF systems that use the Intensity Modulation with Direct Detection (IM/DD) technique.
- Propose IR-UWBoF-IM/DD systems that use spectral line suppressive (SLS) or spectral line free (SLF) convolutional codes for eliminating spectral lines in the power spectral density of M-PPM and BPSK/Q-BOPPM IR-UWB signals.
- Design and Implement of a High Data Rate (HDR) IR-UWBoF-IM/DD simulation testbed for evaluating PSD characteristics of IR-UWB signals.
- Implement IR-UWBoF-IM/DD systems with spectral line suppression capabilities designed for low data rate (LDR) and HDR applications.
- Perform experimental evaluations of spectral line suppression capabilities of proposed systems.

1.4 Literature survey of spectral shaping techniques for UWBoF systems

As established in Section 1.3, this work deals with the implementation of IR-UWBoF systems with spectral line suppression capabilities. Thus a summary of previous research

related to spectral shaping techniques for IR-UWBoF systems is presented in the following paragraphs.

The current approaches used for spectral shaping in wireless IR-UWB systems can be classified into the categories of pulse shape based spectral shaping, time hopping (TH) code based spectral shaping, direct sequence (DS) code based spectral shaping, orthogonal/antipodal modulation based spectral shaping and convolutional codes based spectral shaping. All these approaches look to shape the transmitted signal's PSD such that compliance with emission limits is achieved and/or interference from/to narrowband users of the spectrum is minimized.

The practical implementation of these spectral shaping methods for IR-UWBoF systems have been carried out using well known microwave techniques and/or novel optical configurations. In the literature, several works related with IR-UWBoF systems focus on photonics generation of UWB waveforms using hybrid (electrical and optical devices) and all-optical radio over fiber (RoF) architectures have been reported, (Yao, Zeng, and Wang, 2007, Zeng and Yao, 2006-A, Zeng and Yao, 2006-B, Chengliang et al., 2014-A, Chengliang et al., 2014-B, Zeng, Wang, and Yao, 2007, Zeng, Wang, and Yao, 2007, Qing Wang et al., 2006, Wang and Yao, 2006, Qing Wang and Yao, 2007, Wang et al., 2007, Bolea et al., 2010, Jianqiang Li, et al., 2008, Dong, et al. 2007, Jianji Dong, et al., 2007, Gang Chen and Shilong Pan, 2012, Dong et al., 2008, Huang, et al., 2008; You Min Chang, et al., 2010, Li et al., 2009, Chang et al., 2011). In some of these works, complex RoF configurations employed to generate optical UWB waveforms compliant with the FCC spectral masks are shown, (Xianbin Yu et al., 2009), Bolea et al., 2009, Feng et al., 2014-A, Feng et al., 2014-B, Moreno et al., 2014, Moreno et al., 2015, Abtahi et al., 2008-A, Abtahi et al., 2009, Abtahi and Rusch, 2011, Abraha et al., 2011, Quang Trung Le et al., 2014, Dong et al., 2010, Xu, et al., 2011, Li et al., 2011). There exist other works that show non-compliant IR-UWBoF systems that have been forced to fit under the frequency limits of spectral masks by using commercial microwave filters, (Xianbin Yu et al., 2013, Gibbon, et al., 2010), custom-designed UWB antennas and/or by using a combination of band pass UWB antennas with dispersion compensating fibers, (Hanawa, et al., 2009). Although pulse shape based spectral shaping techniques applied to IR-UWBoF systems

have demonstrated their effectiveness, these are not able to suppress spectral lines in the PSD.

The TH codes applied to wireless IR-UWB systems were widely studied during the last decade, (Win and Scholtz, 1998, Win and Scholtz, 2000, Aiello and Rogerson, 2003, Di Benedetto and Giancola, 2004, Roy et al., 2004, Di Benedetto et al., 2006, Arslan et al., 2006, Ghavami et al., 2007, Villarreal-Reyes, 2007). The use of these codes have been mainly used for multiple access purposes and to suppress spectral lines in the PSD of the transmitted signal. In addition, some works have proposed the use of TH codes to produce spectral notches in specific frequency bands of the PSD in order to reduce the mutual interference between UWB and narrow band systems, (Piazzo and Romme, 2003, Wu, Wang, and Chao, 2003, Bellorado, Ghassenzadeh, Kavcic, Tarokh, and Tarokh, 2004, Majhi, Madhukumar, Nasser, and Hélard, 2010). Nevertheless, despite the advantages offered by the introduction of TH codes, the TH-IR UWB systems do not provide a SLF PSD. This latter fact holds even when independent identically distributed (i.i.d.) binary data streams with uniform distribution (perfectly random) are modulated with TH-PPM schemes, (Villarreal-Reyes, 2007). It is important to mention that the use of perfectly random TH is an idealization that in practice is addressed by generating a pseudo-random (PR) TH sequence with extremely long period. The use PR-TH sequences with extremely long period increases the transmitter and receiver complexity without a significant BER performance improvements (when comparing systems with the same transmit power), (Villarreal-Reyes, 2007). Thus, IR-UWBoF systems that implement TH code based spectral shaping methods also will show spectral lines in the PSD, such as is reported by Pan and Yao, (2011-A).

Alternatively, it has been analytically demonstrated by Villarreal-Reyes (2007) that the use of a perfectly random DS code taking values on the set $\{-1, 1\}$ can provide a SLF PSD for IR-UWB systems. Nevertheless, the acquisition and synchronization of extremely long DS codes becomes a challenge in terms of large acquisition times and complexity of the acquisition system, (Ramachndran and Roy, 2005, Aedudodla, Vijayakumaran, and Wong, 2006, Ibrahim and Buehrer, 2006). These kind of DS code sequences have been also implemented optically in IR-UWBoF systems. However, Pan Ou, Ye Zhang, and

Chun-Xi Zhang (2008) have used these sequences to address the multiple-user communications issues in current IR-UWBoF technology, without analyzing the spectral line suppression capabilities of these DS code sequences.

The use of orthogonal/antipodal modulation schemes applied on wireless IR-UWB systems and IR-UWBoF systems have been widely reported in the literature. It is well-known that the PSD of IR-UWB signals modulated by orthogonal formats such as on-off keying (OOK) and pulse position modulation (PPM) exhibit strong spectral lines, even when perfectly random data streams with uniform distribution are transmitted. Therefore these schemes have been mainly used to validate novel IR-UWBoF configurations and for implementing low-cost and low-complexity LDR UWB-WPANs. On the other hand, perfectly random data streams modulated with antipodal formats (i.e. BPSK and quaternary biorthogonal PPM) should not produce spectra lines in the PSD, (Villarreal-Reyes, 2007, Majhi et al., 2010). However, if the statistics of the data streams change slightly and/or the negative and positive pulses form are not fully complementary, then strong spectral lines will appear in the PSD, (Villarreal-Reyes, 2007, Pan and Yao, 2010-A). In this context, it could be expected that the use of BPSK with PR-DS sequences would be a favorable solution to suppress spectral lines in the PSD of unbalanced (that is, the total number of 1's and 0's of the data transmitted is not the same) binary data streams. However, it has been analytically demonstrated that if the period of the PR-DS code is relatively short the height of the spectral lines may be reduced but the actual number of spectral lines in the PSD may be simultaneously increased, (Villarreal-Reyes, 2007).

During the last decade, convolutional codes with convenient PSD characteristics were proposed by Villarreal-Reyes (2007) for IR-UWB systems in order to achieve both spectral line suppression and BER improvement. Analytical and simulation-based performance evaluations have shown that the spectral lines free (SLF) convolutional codes generate a SLF PSD in BPSK and quaternary biorthogonal PPM (Q-BOPPM) IR-UWB systems, even when unbalanced binary data streams are inputted to the SLF convolutional encoder (CE), (Villarreal-Reyes, Edwards, Villasenor-Gonzalez, Conte-Galvan, and Aquino-Santos, 2011). However, the spectral line suppression capabilities of SLF-CCs have not been previously evaluated experimentally. *Thus, the implementation and experimental*

evaluation of this spectral shaping technique to IR-UWBoF systems result of particular interest for this research.

Recently a novel optical spectral line suppression technique based on the chaotic dynamics of a laser diode with optical feedback was experimentally demonstrated by Jian-Yu Zheng, et al., (2010) and Zhang et al., (2013). The main advantage provided by this spectral shaping technique over those previously mentioned was the generation of a SLF-PSD of IR-UWB signals modulated with a simple OOK scheme. In addition, this SLF PSD holds over 20-km fiber followed by a 0.6-m wireless link without any processing of dispersion compensation. Despite the benefits offered by this optical spectral shaping technique, the PSD generated not fulfill with the FCC spectral masks. Thus, in order to meet with the power limits that protect the Global Positioning Systems (GPS), it would be necessary to reduce considerably the transmit power. However such a method would have the drawback that less energy would be transmitted per data symbol and thus the BER may worsen.

1.5 Thesis outline

Chapter 2 introduces concepts, terminology and definitions that will be used throughout this entire thesis. In this chapter, three main areas can be identified. The first area shows concepts related to Radio over Fiber systems. The Intensity Modulation with Direct Detection (IM/DD) optical transmission technique, main architectures and applications areas of these systems are discussed. The second area describes the UWB approach adopted in this research. Several important topics such as the signal model for non-coded and convolutionally-coded IR-UWB systems, current UWB regulations, as well as spectral shaping mechanisms are also reviewed. Finally, the third area provides an overview of the state of the art of IR-UWBoF systems. The photonics UWB pulse generation, transmission and spectral characteristics of these systems are analyzed.

In Chapter 3, the analytical model of IR-UWBoF-IM/DD systems with spectral line suppression capabilities proposed in this research work are provided. Furthermore, the design and implementation of IR-UWBoF-IM/DD testbeds in *VPITransmissionMaker^{TM}*

simulation software are described. Preliminary results of the spectral line suppression capabilities of proposed systems are obtained.

In Chapter 4 we look at the practical implementation of IR-UWBoF IM/DD systems designed for Low Data Rate (LDR) and High Data Rate (HDR) applications. In these systems the spectral line suppression capabilities of a rate 1/4 spectral line suppressive convolutional encoder (SLS-CE) and a rate 1/2 SLF-CE are experimentally evaluated. The impact of the chromatic dispersion and wireless transmission over the PSDs generated by both IR-UWBoF IM/DD systems, SLS and SLF, are also reported.

Finally, in Chapter 5, the contributions, general conclusions and areas of future research derived from these thesis work are provided.

A schematic diagram with the structure of this thesis is shown in Figure 4.
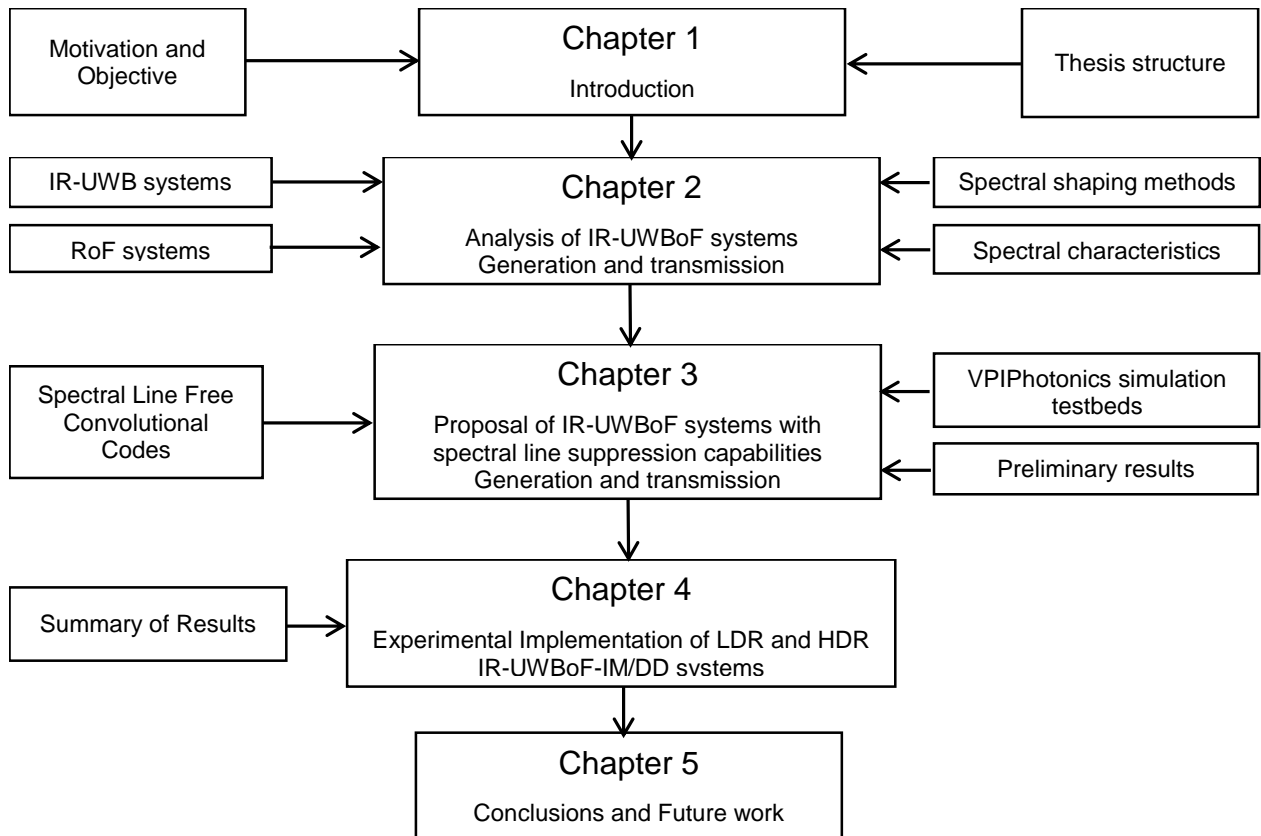
Figure 4. Thesis structure**.**

1.6 Main outcomes and contributions of this thesis

Derivative of this research work, the main outcomes were published in the following journals and conferences:

- Perez-Ramos, A. E., Villarreal-Reyes, S., Lepers, C., Arvizu, A., Muller, M. and Abib, G. I. (2015), Low complexity M-PPM impulse-radio ultra wideband over fiber system for wireless sensor networks applications. IEEJ Trans Elec Electron Eng, 10: S162–S164. doi:10.1002/tee.22178.

- Arvizu-Mondragón, A., Villarreal-Reyes, S., Perez-Ramos, A.E., Santos-Aguilar, J., Muller, M., Abib, G. I., Lepers, C. (2015). Optical channel impact over the PSD of UWB over FSO links, in Free-Space Laser Communication and Atmospheric Propagation XXVII, Proceedings of SPIE *9354*.

- Pérez-Ramos, A. E., Arvizu, A., Villarreal-Reyes, S., Lepers, C., Santos-Aguilar, J., y Covarrubias Rosales D. H. (2014). Desarrollo de una cama de pruebas experimental para sistemas IR-UWBoF-IM/DD basándose en el uso de la plataforma de simulación VPIphotonics. *Revista mexicana de física*, *60*(2014), 435-442.

- Perez-Ramos, A. E., Villarreal-Reyes, S., Arvizu-Mondragon, A., Lepers, C. and Santos-Aguilar, J. (2014), Spectral line suppression capabilities of spectral line free convolutional codes in UWB over fiber systems. Microwave Optical Technology Letters, *56*, 1712–1715. doi: 10.1002/mop.28424

- Espinosa, L.A.L.; De Dios Lopez Sanchez, J.; Hipolito, J.I.N.; Vazquez Briseno, M.; Perez-Ramos, A.E.; Villarreal-Reyes, S., (2013), Viterbi Decoders Generation for FPGA Platforms, in *Mechatronics, Electronics and Automotive Engineering (ICMEAE), 2013 International Conference on*, 211-215.
doi:10.1109/ICMEAE.2013.32

Chapter 2. Theoretical background

2.1 Introduction

The purpose of this chapter is to introduce the concepts, terminology and definitions that will be used in future chapters. As previously mentioned, an important topic of this research is the implementation of low-complex IR-UWB over fiber systems with spectral line suppression capabilities. Therefore three main areas can be identified in this chapter. The first area is covered in Section 2.2 and describes the Radio over Fiber technology, optical transmission techniques, architectures and recent application areas. The second area is written in Sections 2.3 to 2.5 and concerns about several important concepts related to the UWB approach adopted for this work. Finally, the third area is shown in subsection 2.6 and 2.7. The state of the art of IR-UWBoF systems and their spectral characteristics are investigated and analyzed.

2.2 Radio over Fiber systems

Radio over fiber (RoF) is a mature technology used for distributing radio frequency (RF) signals through optical fiber links, (Cooper, 1990, Fye, 1990, Wake, Webster, Wimpenny, Beacham, and Crawford, 2004). It was originally proposed to distribute analog Cable TV (CATV) signals, (Chiddix, Laor, Pangrac, Williamson, and Wolfe, 1990), and radio cellular services using one of its main applications, the distributed antenna system (DAS), (Cooper, 1990, Fye, 1990, Wake et al., 2004). In DAS, RoF links are used to interconnect a central office/node/unit (CO/CN/CU), which contains radio base stations, towards a number of remote antenna units (RAUs) distributed in areas such as city centers, shopping malls, stadiums, airports, railway stations, buildings, households, among others. This kind of systems provides excellent coverage and dedicated capacity for enabling short range communications in each of the above places mentioned, (Wake et al., 2004). Furthermore, RoF technology can be used to transmit RF/analog signals whose frequencies (e.g. 60 GHz) are difficult to transport through traditional coaxial cables, and this technology can also be used to provide wireless connectivity where dead-zone radio coverage are present, (Mitchell, 2009). Figure 5 shows the DAS concept for distributing cellular communications radio services to office buildings, cell towers and railway stations.

Here, it can be observed that the base transceiver stations (BTS) are located inside a building, sometimes known as a base station hotel, where the wireless services are transmitted to RAUs by using point-to-point or point-to-multipoint RoF links, (Wake et al., 2004, Mitchell, 2009). It is important to mention that, the DAS general structure is similar for all cases, however there exist several proposed optical configurations to offer specific functionalities. Figure 6 shows a generic point-to-multipoint RoF architecture. As noted, important radio system functionalities such as data modulation, signal processing, frequency conversion (up and down) and optical transmission/reception techniques are performed in the CO. In downlink communications, the optical carrier modulated by the RF signal, or by an intermediate frequency (IF) signal generated in the CO, is transmitted across the optical network towards the RAU. At this point the RF/analog signal is recovered from the optical carrier and it is electrically amplified (if necessary) to tune up for a wireless transmission, (Mitchell, 2009).
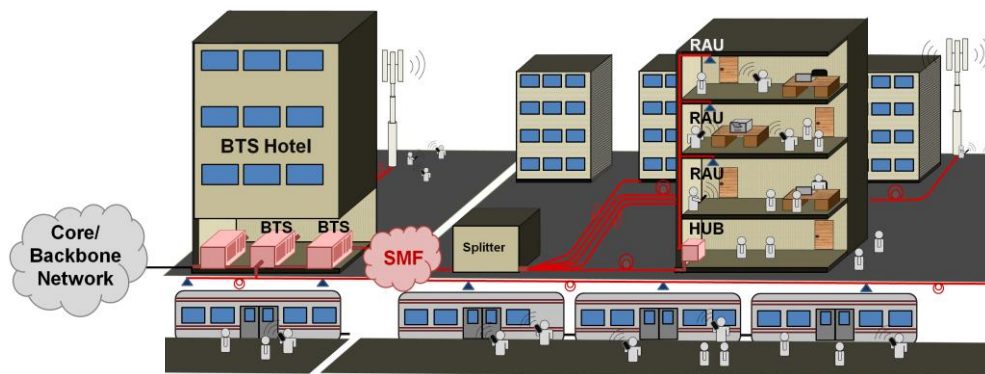
BTS: Base Transceiver Station; RAU: Remote Antenna Unit;

Figure 5. Typical application of radio-over-fiber technology.
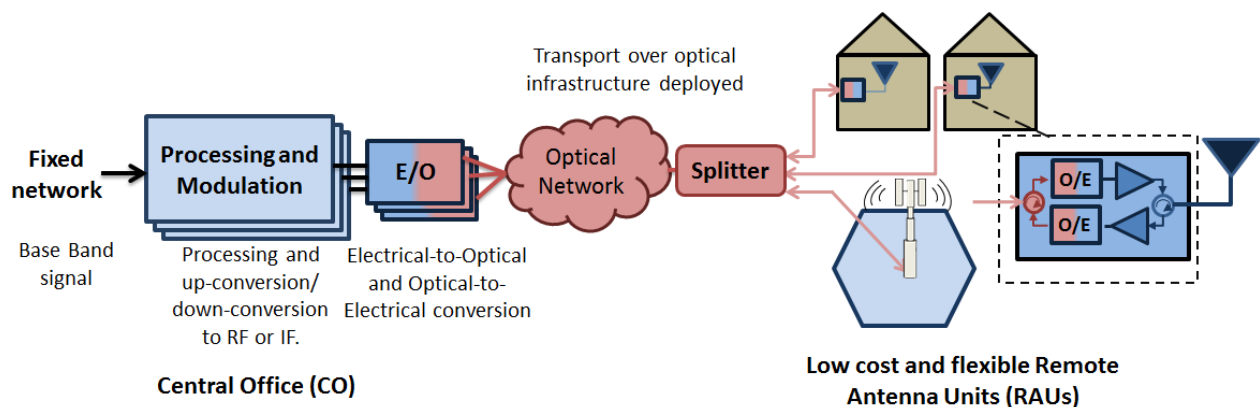
Figure 6. Generic schematic of a radio-over-fiber system.

For uplink communications, similar functionalities of modulation onto an optical carrier, transport, and recovery are performed. However, as the main aim of RoF technology is reducing the cost, size, and power requirements of the RAU, a large research effort has been expended in the development of low-cost devices for this part of the network, (Mitchell, 2009). Even in some cases, this return path is performed by a simple and mature wireless communication technique (such as a wireless local area network-WLAN) due to the low-data-rate nature of upstream transmission, (Yao, 2009).

As noted in Figure 6, the main advantage of RoF systems is the ability to concentrate the heavy, complex and costly equipment in the CO, thereby the deployment of compact and simple remote antenna units can be achieved. Furthermore, advantages of optical fibers such as light weight, immunity to electro-magnetic interference (EMI) and huge bandwidth allow the distribution of signals of typical wireless systems, regardless of their frequency bands, over several hundreds of meters. In addition, a low power consumption system may be achieved through dynamic allocation of resources (power and data on demand) in time and space, (Trevor, et al., 2013).

2.2.1 Optical transmission techniques

In the literature, simple and complex optical transmission techniques of RoF systems have been reported. For example, intensity modulation with direct detection (IM-DD) and phase modulation with coherent detection (PM-CD) are the two techniques most often used to transport RF (Analog) signals over single-mode fiber (SMF) and multi-mode fiber (MMF), (Lethien, Loyez, and Vilcot, 2005, Cox, et al., 2006, Lin et al., 2007, Zhu, et al., 2013). Furthermore, there exist other complex optical transmission techniques such as "all optical up-conversion" based on advanced configurations of electro-optic Mach Zehnder Modulators (EO-MZM), and "heterodyne detection" methods based on dual-wavelengths system, injection locking, dual-mode lasers, and mode-locked lasers, (Guillory, 2012). Some of these complex techniques have been proposed to generate analog millimeter-waves used in wireless personal area networks (WPANs) working at 60 GHz, (Beltran, Jensen, Llorente, and Monroy, 2011-A, Omomukuyo, Thakur, and Mitchell, 2013). It is important to mention that the IM/DD optical systems have been widely deployed for

providing digital optical communications services, (Cox et al., 2006). *Therefore, it is desirable to exploit the preexistent optical fiber infrastructure in order to deploy simple, low cost and low power consumption RoF-IM/DD systems.*

2.2.1.1 Intensity Modulation with Direct Detection (IM/DD)

The IM/DD optical systems use mainly two methods to modulate the output optical power of a laser diode. In one of these methods, referred as "direct modulation", the RF (Analog) signal that would be transmitted over the optical fiber is converted to optical domain by modulating the injection current of the laser diode. This electrical-to-optical conversion process can be accomplished due to the linear relationship between the output optical power and the injection current of the laser. In spite of direct modulation is a very simple and low cost intensity modulation method, it produces a phenomena known as "frequency chirp", which usually broadens the spectral bandwidth of the modulated optical signal and introduces additional performance degradation when the optical signal propagates through a dispersive media, (Hui and O'Sullivan, 2009). Typically, direct modulation is available in frequencies below 10 GHz (although some devices mentioned by Kaszubowska, Anandarajah, and Barry, 2002, work above 10 GHz). It is important to mention that if low modulation depth is used then a reasonable performance in terms of distortion can be achieved, (Mitchell, 2009).
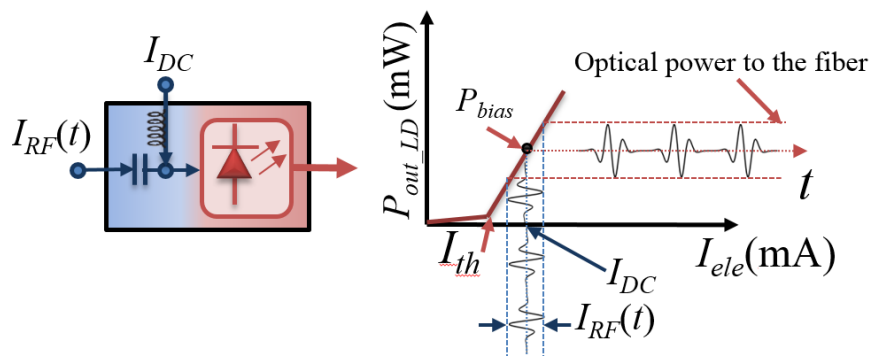
Figure 7. Direct intensity modulation of a Distributed Feedback (DFB) laser diode. (a) Internal configuration of a directly modulated laser and (b) transfer function of a DFB laser.

Figure 7 illustrates the operating principle of direct intensity modulation (DIM) of a Distributed Feedback (DFB) laser. To ensure that the laser diode operates above lasing

threshold, a DC bias current I_{DC} is usually required. A bias-Tee combines the electrical signal, $I_{RF}(t)$, with I_{DC} to modulate the injection current of the laser diode. The modulation efficiency is then determined by the slope of the laser diode P-I curve (transfer function). Therefore, if the P-I curve has a linear form, the output optical power is linearly proportional to the modulating current, which can be mathematically expressed by

$$R_C = \Delta P_{out\_opt} / \Delta I_{ele} \tag{1}$$

$$P_{out\_LD}(t) \approx R_C \, (I_{DC} - I_{th}) + R_C \, I_{RF} \tag{2}$$

where I_{th} is the lasing threshold current and $R_C = \Delta P_{out\_opt} / \Delta I_{ele}$ is the slope of the laser diode P-I curve.

As it is well-known an amplitude modulation is a double side band modulation, (Guillory, 2012), therefore the optical spectrum exhibit two adjacent sidebands placed at both sides of the carrier frequency as depicted in Figure 8. It is important to mention that chromatic dispersion and the frequency chirp can limit considerably the reach of optical links.
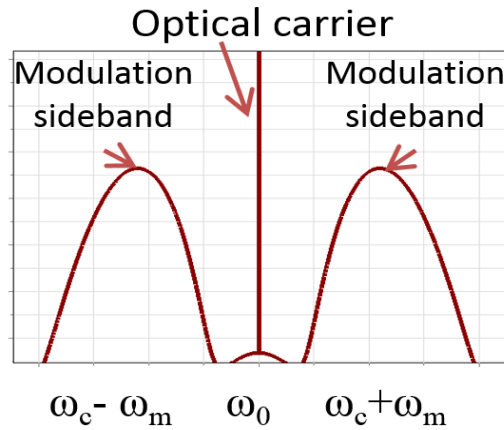
Figure 8. Optical spectrum of the direct/external intensity modulation (IM) technique.

To overcome the direct modulation constraints, external electro-optic modulators (EOM) or external electro-absorption modulators (EAM) are often used due to these can provide high stability, wide frequency modulation bandwidths and zero frequency chirp in high-speed optical communications systems, (Mitchell, 2009, Guillory, 2012). In this kind of intensity modulation technique, the laser diode works in a continuous wave (CW) mode

while the external modulator encodes the RF signal into the optical domain. The external intensity modulation significantly improves overall performance but requires a dedicated external modulator, which introduces extra attenuation and, of course, an additional cost.

Figure 9(a) illustrates the internal structure of a single-drive Mach Zehnder modulator (MZM), which is a simple external EOM. Commonly this device has one input where an incident optical wave is divided by a 50/50 splitter (Y1) into two beams of equal intensity, which are guided in the two arms of the MZM. On one of these arms two electrical electrodes (V_{RF} and V_{DC}) are placed to apply an electrical field that introduces a phase shift on the optical signal, exploiting the Pockels effect of an electro-optic material (e.g. Lithium Niobate-LinbO3), (Guillory, 2012). This optical phase difference is shifted with respect to the unchanged state of the other incident optical wave by an amount $\Delta\varphi(\mathrm{V})= \varphi\mathrm{RF} + \varphi\mathrm{DC}$. At the output of the MZM a second coupler (Y2) allows the recombination of the two beams: the phase shifted and the original optical beam. From here it can be seen that if the light is in phase (i.e. $\Delta\varphi=0$), the output power, P_{out}, is at a maximum point. If the light from the two arms is out of phase (i.e. $\Delta\varphi=\pi$), the output power is at a minimum point. For the case where Y1 and Y2 provide equal splits and the insertion losses are not considered, then

$$P_{out\_mzm} = (1/2)\, P_{in}\,[1 + \cos\,(\Delta\varphi(t))] = P_{in}\,\cos^2(\Delta\varphi(t)/2) \tag{3}$$

and

$$\Delta\varphi(t)= \pi\,(V_{DC} + V_{RF}(t))/V_{\pi} = \pi\,(V_{mod})/V_{\pi} \tag{4}$$

where V_{π}, also known as the half-wave voltage, is the voltage needed to go from maximum to minimum transmission point (see Figure 9b), $V_{RF}(t)$ is the voltage of the RF (Analog) signal and V_{DC} is the bias voltage mainly used to configure the operation point of the MZM. In Figure 9(b) three operating points can be noted: the maximum point giving full transmission, the quadrature (QUAD) point located in the middle of the linear region of the MZM's transfer function and the minimum point giving the full extinction, (Guillory, 2012). It is important to highlight that P_{bias} and QUAD points determine the best operating points

of the DFB laser and MZM's transfer function, respectively. Therefore these points will be used in the practical implementations performed in this thesis work.
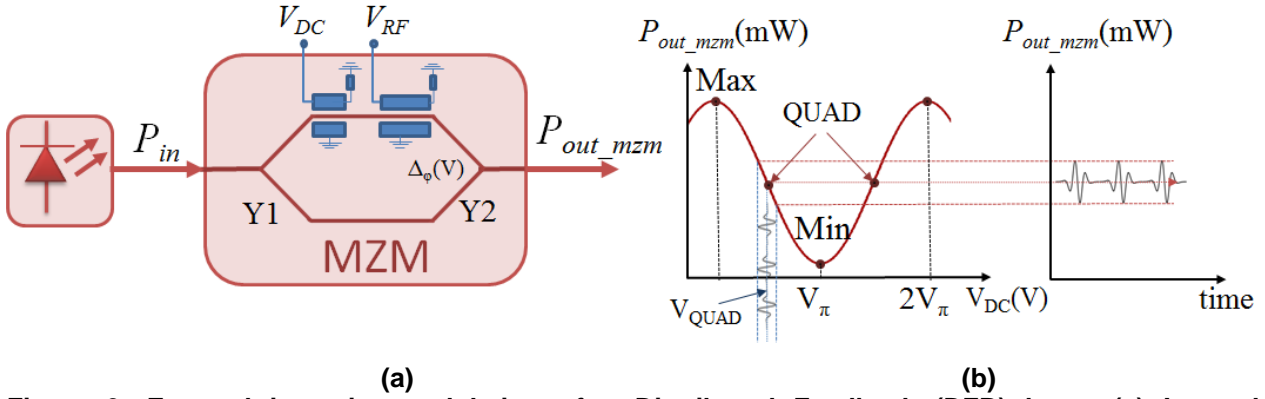
(a) **(b)**
Figure 9. External intensity modulation of a Distributed Feedback (DFB) laser. (a) Internal configuration of a Mach Zehnder modulator (MZM). (b) Transfer function of a MZM.

On the other hand, the IM/DD optical communications systems commonly use spools of optical fiber to transport signals from a source to its destination. For example, long- and short-reach optical communications can be implemented using single-mode fiber (SMF) and multimode fiber (MMF), respectively. Nowadays it would be common to find optical infrastructure for In-Building applications mostly based on MMF. Nevertheless, bandwidth and distance limitations caused by modal dispersion can be a serious problem for next generation Multi-Gigabit optical fiber interconnects. The optical communication systems based on SMF are attractive because of they can provide long-distances Multi-Gigabit communications. For this reason, most new fiber installations include at least one SMF in the cable infrastructure, (Casimer DeCusatics, 2008).

Despite of SMF enables very high-data rate optical communications systems, the Chromatic Dispersion (CD) parameter can limit their information capacity and transmission distance. It is well-known that CD is mainly originated by the frequency-dependent propagation of the light when is transmitted over a dispersive medium such as SMF. This effect can clearly be observed in IM/DD optical systems when transmit high-data rate digital signals over several kilometers of SMF. In a practical sense, the intensity modulated (double side band) optical signal is composed of several spectral components, which travel at different speeds through SMF. These different propagation speeds can be

observed at the output of the fiber as broadening in the transmitted signals, which in some cases can generate intersymbol interference (see Figure 10). In order to remove the spreading of the optical pulses, dispersion compensation techniques such as dispersion compensating fibers, electronic dispersion compensation (EDC) components, Fiber Bragg Gratings (FBG) and digital filters have been implemented, (Kahlon and Kaur, 2014). In addition, it is common to use Erbium-doped fiber amplifiers to compensate fiber attenuation in long-range optical fiber communications. It is important to mention that techniques above mentioned can remarkably improve the system performance against fiber attenuation and chromatic dispersion effects, however the complexity and cost of whole system are also increased.
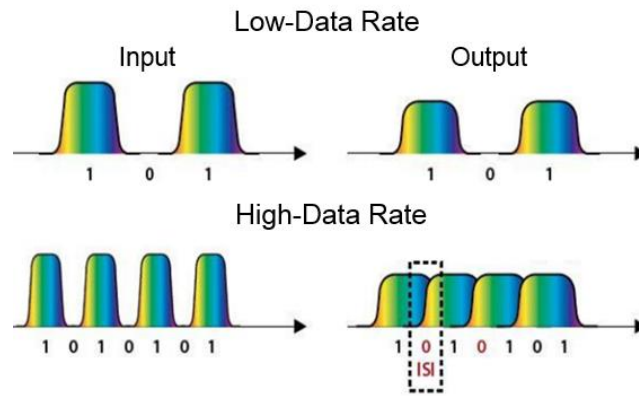
Figure 10. Impact produced by Chromatic Dispersion in digital optical communications systems.

Commonly, transmission analysis of RF intensity-modulated signals over SMF is performed considering only fiber attenuation and chromatic dispersion effects. Thus, a SMF can be modeled by the low-pass equivalent of its optical transfer function given by

$$H(f) = \exp\left(\frac{j\lambda^2 D\pi f^2 L}{c}\right) \times \exp\left(\frac{-\alpha_0 L}{2}\right) \qquad (5)$$

where L is the fiber length, f is the low-pass equivalent frequency, λ is the operating wavelength of the diode laser, D is the dispersion parameter, c is the speed of light in vacuum, and α_0 is the fiber power attenuation coefficient, which can also be expressed in dB using $\alpha_{dB} = 4.34\alpha_0$, (Hui and O'Sullivan, 2009). Figure 11 shows several plots of the

SMF's transfer function obtained by evaluating Equation 5 with typical values of a standard SMF (that is, D=17 ps/km·mm and α_{dB}= 0.2 dB/Km) when the optical source of the IM/DD system is emitting light at λ =1550 nm. All these plots show several link length-dependent nulls at specific frequencies. These "power nulls" show the chromatic dispersion effect, which as mentioned limit the information capacity and transmission distance in the IM/DD systems. For example, in Figure 11(a), the first null for 10-km fiber length plot is located at 19.16 GHz whereas for 40-km this power null appears at 9.58 GHz. These two plots show clearly that there exist a reduction by about 10 GHz in the maximum theoretical bandwidth of the IM/DD system. While this bandwidth reduction would not affect the transmission of RF signals working at 2.4 GHz and 5 GHz, this could limit the distribution of ultra-wideband (UWB) signals, which is an important topic in this thesis work. Furthermore, it can also be seen from Figure 11(b) that signals with frequencies below 10 GHz could be propagated over significant SMF lengths. However, propagation of millimeter waves are severely limited. For example, RF signals at 40 GHz and 60 GHz are restricted at 2-km and less than 1-km respectively. Therefore, it is necessary to consider those alternatives reported by Beltran et al., (2011-A), Guillory, (2012), and Omomukuyo et al., (2013) in order to overcome this issue.
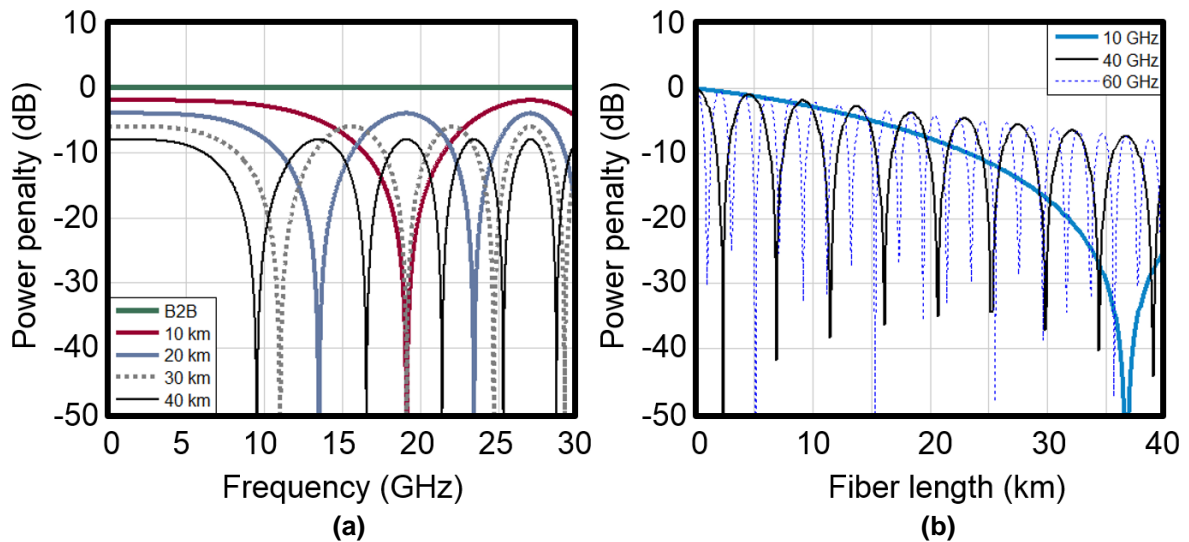
Figure 11. Impact produced by Chromatic Dispersion in analog optical communications systems.

Finally the photoreceiver of an IM/DD optical system has the purpose to convert the optical signal into electrical domain and to recover the transmitted data. The typical optical

receiver configuration can consist of a front-end stage, a linear channel stage, and data recovery stage, (Djordjevic, Ryan, and Vasic, 2010). The interconnection between the three different stages is illustrated in Figure 12.

O/E optical to electrical; AGC automatic gain control.
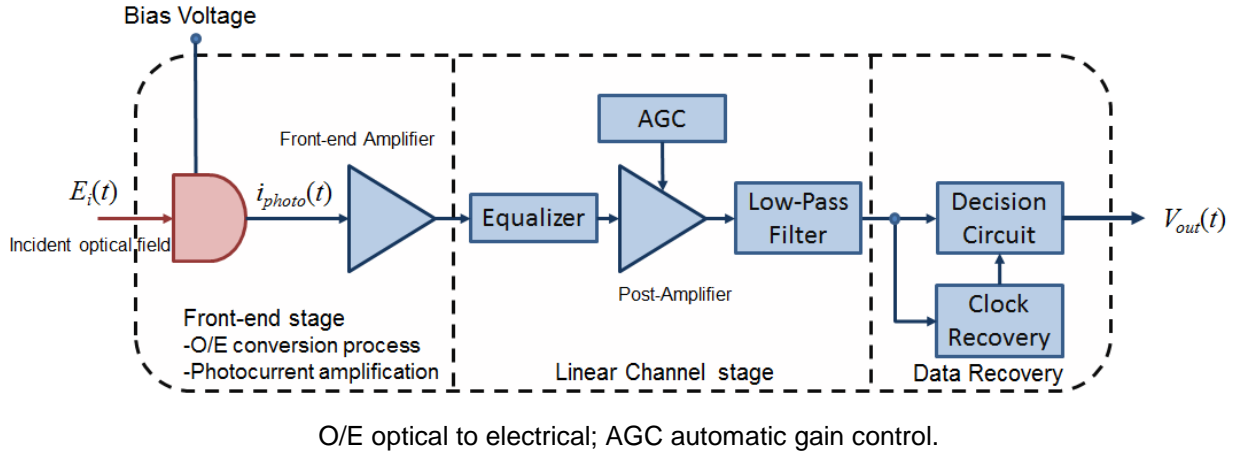
Figure 12. A typical direct detection receiver architecture.

The front-end stage consists of a photodetector and a preamplifier. The photodetector works as a square-law optoelectronic transducer that generates an electrical signal, $i_{photo}(t)$, which is proportional to the square of the instantaneous optical field, $E_i(t)$, impinging on its surface. The preamplifier most commonly used are the high-impedance front-end amplifier and transimpedance front-end amplifier, both are shown in Figure 13. Important characteristics of high-impedance amplifiers are their good receiver sensitivity, however, the bandwidth in this scheme is low because the RC constant is large (this is due to in these schemes a large value of load resistance to reduce the level of thermal noise is used). On the other hand, transimpedance amplifier can provide both high receiver sensitivity and large bandwidth. Even though the load resistance is high, the negative feedback reduces the effective input resistance by a factor of G-1, where G is the front-end amplifier gain, (Djordjevic et al., 2010).

The linear channel in optical receivers consists of a high-gain amplifier and a low-pass filter. An equalizer is sometimes included just before the amplifier to deal with residual intersymbol interference (ISI). The amplifier gain is controlled automatically to limit the average output voltage to a level irrespective of the incident average optical power at the

receiver. The low-pass filter shapes the voltage pulse. Its purpose is the reduction of noise without introducing much intersymbol interference (ISI).

(a)   **(b)**
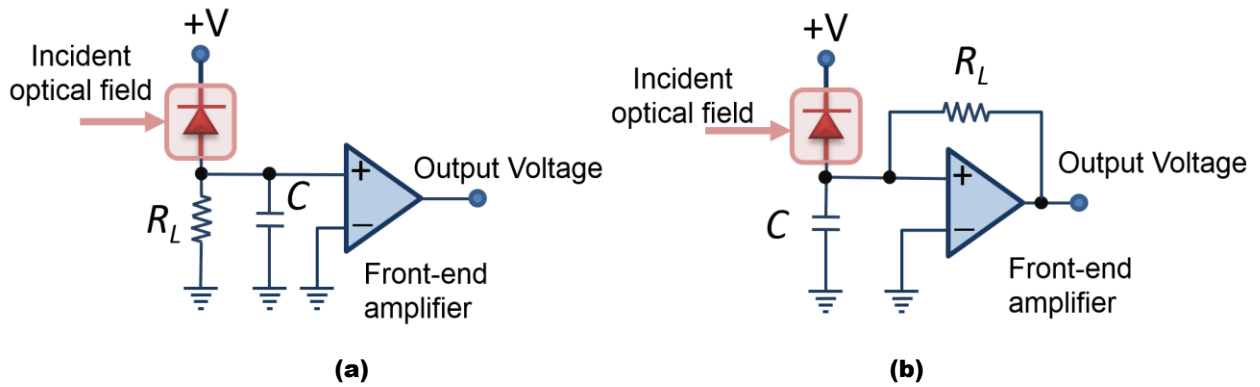
Figure 13. Optical receiver front-end schemes. (a) high-impedance front-end and (b) transimpedance front-end.

The data-recovery stage consists of a decision circuit and a clock recovery circuit. The main purpose of clock recovery circuit is to provide timing for decision circuit by extracting the clock from the received signal. The clock recovery circuit is most commonly implemented using the phase-lock loop (PLL), (Djordjevic et al., 2010). The decision circuit compares the output from the linear channel to a threshold level, at sampling times determined by the clock-recovery circuit, and decides whether the signal corresponds to bit 1 or bit 0. The best sampling time corresponds to the situation in which the signal level difference between 1 and 0 bits is maximum.

For simplicity, the front-end amplifier and the electronic processing (linear channel stage and data recovery stage) is modeled as an ideal, noiseless, unity-gain electronic amplifier that present a load of R_l ohms to the photodetector such is illustrated in Figure 14.
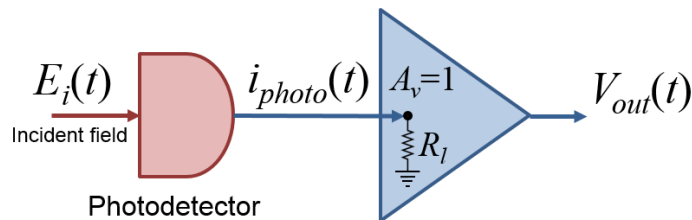
Figure 14. Simplified Direct Detection Receiver (Alexander, 1997).

Considering the analysis performed in (Alexander, 1997) the $i_{photo}(t)$ can be obtained by

$$i_{photo}(t) = \Re E_i(t)^2 = \Re P_{out}(t) \tag{6}$$

where $\Re$ is the photodetector responsivity, which is defined as the photocurrent generated per unit incident optical power (i.e. this parameter determines the photodetector efficiency). With λ in µm, $\Re$ is expressed as

$$\Re = \frac{\lambda q \eta_{qe}}{hc} = \frac{\lambda q \eta_{qe}}{1.24} \tag{7}$$

where h is the Planck's constant, c is the speed of light λ is the wavelength of the emitted light, q is the electronic charge and η_{qe} is the quantum efficiency of the detector's material composition. The responsivity of a PIN photodetector is always less than unity and a graph showing typical responsivity values for different PIN photodetectors is depicted in Figure 8.3(b) of (Senior, 2009). From this figure high responsivity values of 0.9 A/W at signal wavelengths of 1.30 µm and 1.55 µm for InGaAs photodiode can be observed. Therefore photodetectors built with this alloy are preferred for implementing high-speed optical communications systems.

2.2.2 Radio over Fiber architectures

Radio over Fiber (RoF) technology allows RF signals distribution from a Central Office or Central Node (CO/CN) towards Remote Antennas Units (RAUs) using fiber-optic access network architectures. Basically, three architectures (see Figure 15) may be deployed for RoF technology: point-to-point, active star (point-to-multipoint) and passive star (point-to-multipoint), (Koonen, 2006).

In point-to-point architectures, individual fibers are deployed to distribute RF signals from the CO to RAUs. Therefore, many fibers are needed, which entails high first installation costs, however also provides most flexibility to upgrade services for customers individually, (Koonen, 2006). As an example, Figure 16 shows the two-way

communication link (downlink and uplink) antenna remote point-to-point architecture that use the IM/DD technique to transport RF signals. Figure 16(a) shows as the downlink and uplink communications are performed by using two optical fibers for each one. Figure 16(b) shows as one optical fiber can be used in this architecture adding optical circulators and laser diodes with different wavelength.
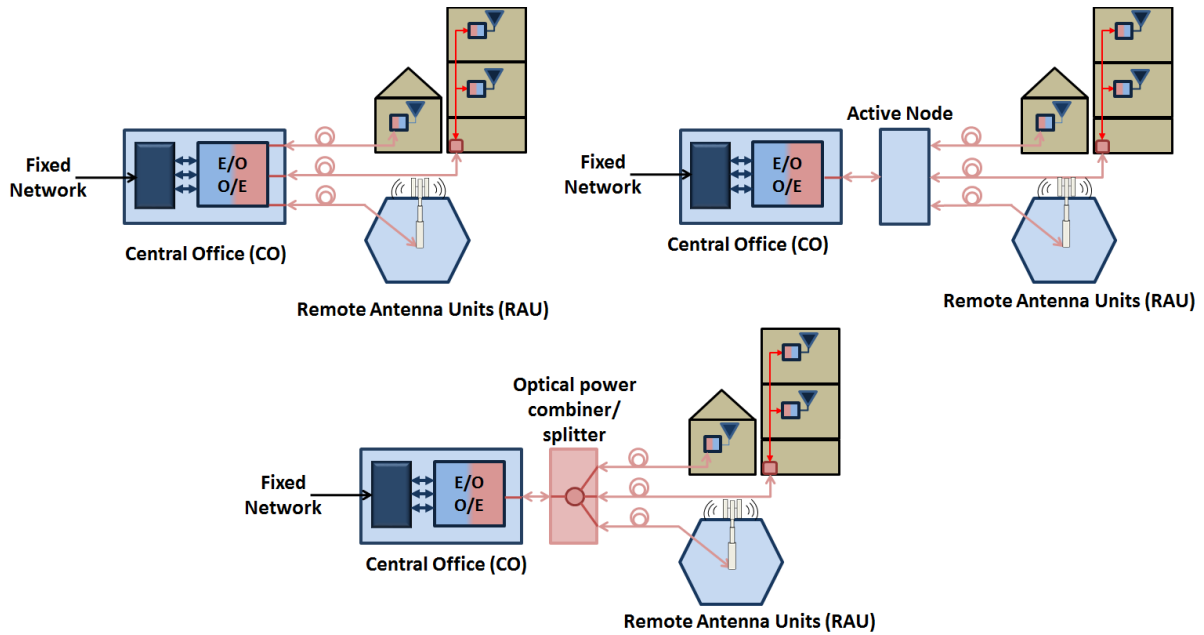
Figure 15. Radio over Fiber architectures. (a) Point-to-Point, (b) Active point-to-multipoint (star) and (c) Passive star.
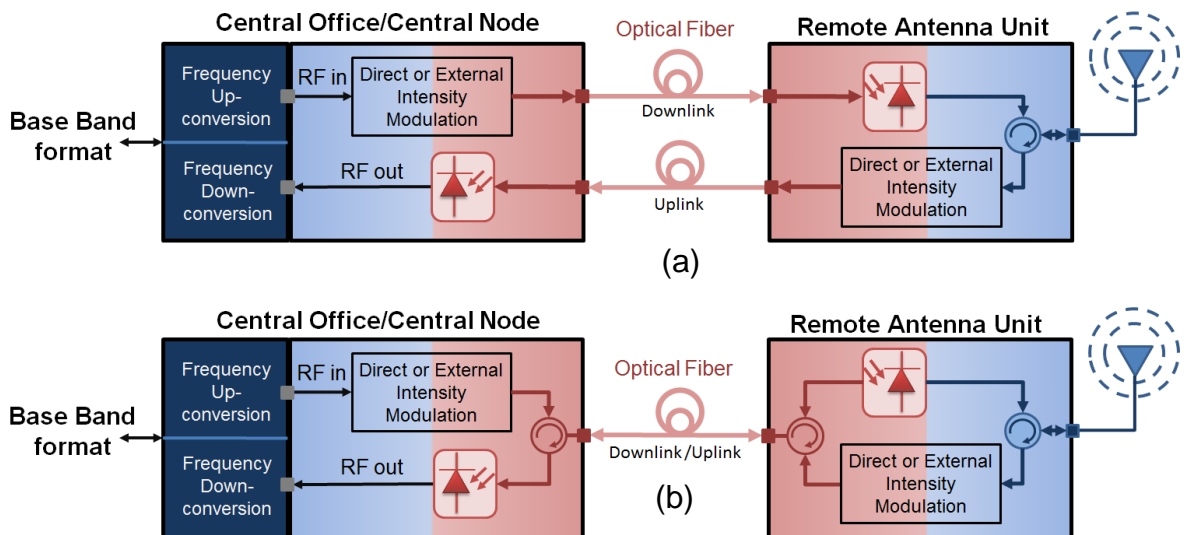
Figure 16. Optical configuration of a point-to point RoF architecture. The optical channel can be formed by (a) two independent optical fibers or (b) by using one fiber, two optical circulators and laser sources with different wavelength.

As previously discussed, chromatic dispersion (CD) is an impairment present in the single mode fiber (SMF) that limits the length of optical fiber links and maximum data rate in the optical communications system. The impact produced by CD is considerably greater for millimeter-wave signals (e.g. 40 GHz and 60 GHz) than signals below of 10 GHz. Therefore, base band (BB) signals and/or intermediate frequency (IF) signals transmitted over SMF schemes are also considered in the literature. Figure 17 shows a BB/IF over fiber system operating in point-to-point architecture. Note as additional components (e.g. mixers and a local oscillator-LO) are implemented within of the RAU in order to set the transmitted signal on the final frequency. The addition of these components increase the cost and power consumption of RAUs. However, long-distances and high data-rates communications could be achieved because of the CD effect is minimum at low frequencies (see Figure 11).
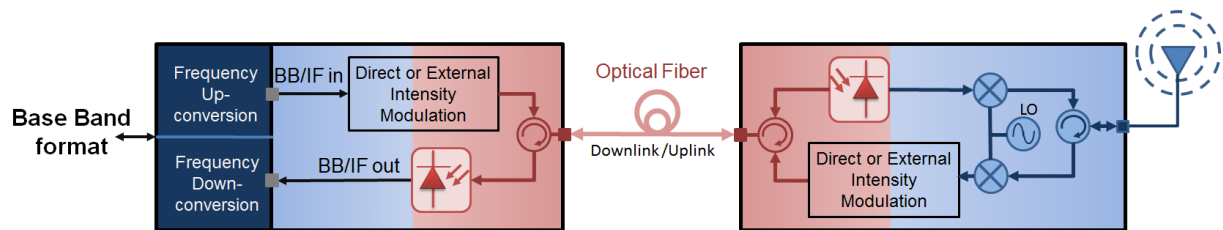
Figure 17. Optical configuration of a point-to-point architecture for transmitting base band (BB) and intermediate frequency (IF) signals.

As an alternative to the scheme presented in Figure 17, works presented by Mitchell (2009), Beltran et al. (2011-A) and Omomukuyo et al. (2013) take advantage of optical heterodyne detection methods to generate and transmit millimeter-wave signals. Basically, this method employs two laser diodes emitting light at different wavelengths over the SMF. One laser diode is modulated with the baseband signal or intermediate frequency signal while the other one, called local oscillator laser or reference laser, emits a continuous optical wave. At the output of the photodetector, the original signal (BB or IF) mounted on a millimeter-wave carrier is obtained. This can be achieved due to the optical beating produced between these two wavelengths. The frequency oscillation of the electrical carrier generated at the output of the photodetector is determined by the frequency difference between both wavelengths. Note that optical heterodyning can remove electrical millimeter-wave oscillators at the RAU. However, implementation costs

can be greater than those schemes represented in Figure 17 because of several optical components such as two lasers, optical power combiners, and a high-bandwidth photodetectors are required, (Guillory, 2012).

In active point-to-multipoint (star) architectures only a single feeder optical fiber is used to carry all traffic from the CO/CN to an active node close to the end users, where a specific number of individual fibers are deployed towards each cabinet/home/building, (Koonen, 2006). This architecture reduces significantly implementation costs. Nevertheless, the active node needs powering and maintenance. The active node may be located in a cabinet at the street curb site, or in the basement of buildings, where the communication traffic is distributed throughout a distributed antenna system (DAS), (Cooper, 1990, Fye, 1990). Typical examples showing this architecture can be observed in Figure 5 and Figure 6. As in the previous case, the transmission of RF signals in these schemes can be performed using IM/DD and/or remote heterodyne detection techniques. On the other hand, in passive star architectures the active node of the active star topology is replaced by a passive optical power splitter/combiner that feeds the individual short branching fibers to the end users. In addition to the reduced installation costs of a single fiber feeder link, the completely passive nature of the architecture avoids the powering and maintaining active equipment costs, (Koonen, 2006). In recent years, this architecture has become very popular because of the introduction of passive optical networks (PON).

In this thesis work are considered point-to-point architectures such those shown in Figure 16 and Figure 17 due to its simplicity and easy integration with next generation fiber-optic access networks.

2.2.3 Radio over Fiber application areas

As previously mentioned, two of the first applications of Radio over Fiber (RoF) technology were analog CATV signal distribution and cellular antenna remoting for outdoor service, (Cooper, 1990, Fye, 1990, Chiddix et al., 1990). In the latter case, cellular radio systems based on RoF systems for in-building (indoor) applications have been widely studied and commercially implemented over the last decade, (Wake, Nkansah, and Gomes, 2010,

FierceWirelessTech, 2013). Nowadays, it is common to find commercial distributed antennas system (DAS) solutions deployed by carriers, neutral-host third-party providers and building owners supporting multiple wireless services, such as 2G, 3G, Long Terminal Evolution (LTE) and WiFi standards (e.g. IEEE 802.11 a/b/g/n) on a single DAS platform, (FierceWirelessTech, 2013). This ability to transmit different wireless signals over the same optical link is attractive for network operators because of they can increase considerably the network capacity and to reduce the cost per bit delivered. By these important reasons, distributed antenna systems have also been installed in shopping malls, city centers, airports, convention centers, sports venues, warehouses, factories, hospitals, underground subway stations, and other places where traditional radio cellular systems have not been successful because of difficult zoning, cost constraints or other barriers to entry, (Wake et al., 2004, Mitchell, 2009, Wang et al., 2012).

The passenger rail transport (high-speed, regional and commuter) and heavy rail freight transportation are other two promising applications areas where RoF-DAS would be able to provide broadband Internet access to passengers, (Wang et al., 2012), and precise train location to LOCOTROL systems, (Yuan and Wu, 2014). For example, a commercial solution proposed by ViaLite communications can provide wireless services such as TETRA, GSM-Rail, VHF/UHF and GPS along several kilometers of the railway track, even when the train travels across tunnels and urban canyons, (ViaLite, 2016). On the other hand, broadband wireless communications for High Speed Train (HST) systems using RoF-DAS is an open research area because of some of the important issues such as delay spread, delay effect on Medium Access Control protocols, RoF link performance, RoF for in-train communications and the system's ability to respond to fast hand-over rates (e.g. times less than 1 second) have not been completely addressed, (Wang et al., 2012).

Furthermore, wireless personal area networks (WPANs) is an important application area where RoF technology will be able to provide both narrowband and broadband wireless services to fixed and mobile end-users. For example, clouds of low data rate (LDR) wireless sensor networks (WSNs) interconnected by RoF architectures (RoF-WSNs) will play a leading role within of the called "smart cities" covering several applications areas such as water distribution systems, electricity distribution systems, intelligent

transportation systems (ITS), health-care systems, smart buildings, monitoring bridges and seismic, environmental monitoring, among others (Trevor, et al., 2013, Hancke, Silva, and Hancke, 2013). From here, it is worth mentioning that because of properties such as low complexity, low cost, ultra-low power consumption, robustness against severe multipath fading, and very good time-domain resolution, impulse radio ultra-wideband (IR-UWB) technology will be a key enabler for LDR-WSN deployments, (Zhang et al., 2009-A). On the other hand, it is expected that high data rate (HDR) RoF-WPANs will be working like broadband wireless service providers where a RAUs would be installed. For example, in new generation Home Area Networks, RoF architectures deployed inside of a house will enable very high throughput (VHT) wireless services (e.g. broadband internet, uncompressed/lightly compressed multimedia wireless streaming, sync data/file transfer, etc.) to any wireless smart-device located in any room using MB-OFDM UWB or 60 GHz wireless technologies, (Guillory, 2012). In this context, several research works have recently considered the transmission of IR-UWB signals extended by RoF architectures in order to provide a cost-effective technological solution to address the ever-growing demand of broadband wireless services for indoor applications, (Yao, 2009). As noted, RoF is a highly promising technology that will be used as optical backhaul network for transporting enormous quantities of data generated in the next generation (5G) wireless broadband connections, (Lannoo, et al., 2015).

2.3 Impulse-Radio Ultra-Wideband (IR-UWB) systems

As mentioned in previous subsection, ultra-wideband (UWB) radio has recently been considered as a promising candidate to meet the ever-growing demand for wide bandwidth and high data rate in the future wireless personal-area networks (WPANs), (Yao, 2009). Furthermore, due to inherent properties such as low cost, ultra-low power consumption, robustness against severe multipath fading, and very good time-domain resolution, UWB technology has also been considered as a key enabler for low data rate (LDR) wireless sensor networks (WSN) deployments, (Zhang et al., 2009-A).

At early of last decade, the Federal Communications Commission (FCC) in its 2002 Report and Order, defined as UWB signal to any radio frequency energy intentionally radiated having a bandwidth (BW) wider than 500 MHz measured at -10 dB in the power

spectral density (PSD) of the UWB signal. Furthermore, UWB signals can also be defined by its fractional bandwidth (FBW) which must be larger than 20%. The FBW is obtained by

$$FBW = 2\frac{(f_H - f_L)}{(f_H + f_L)} \tag{8}$$

with f_H and f_L pointing out the upper and lower emission points, respectively. Note that due to the FCC definition is based upon spectrum occupancy and is not linked to a particular transmission technology, different kind of UWB signals could be achieved. However, as defined in Chapter 1, *this work is focused on the Impulse Radio (IR) UWB deployments*.

Traditionally, the IR-UWB systems use low power and ultra-short time pulses Gaussian shape (on the order of hundreds of picoseconds) to convey information, (Win and Scholtz, 1998, Win and Scholtz, 2000, Aiello and Rogerson, 2003, Di Benedetto and Giancola, 2004, Roy et al., 2004, Di Benedetto et al., 2006, Arslan et al., 2006, Ghavami et al., 2007). These pulse width times result in very wideband transmission bandwidths allowing the implementation of high-data rate IR-UWB systems. For example, a pulse duration of 250 ps can generate a pulse repetition frequency (PRF) of 4 Giga pulses per second (Gpps).

In most of the IR-UWB approaches reported in the literature indicate that several consecutive pulses are normally used to transmit one data symbol. This pulse repetition scheme (which can also be interpreted as a simple repetition block code) increases the total symbol power and also improves the bit error rate (BER) performance of the system. Nevertheless, the use of this scheme can imply decreasing the system's data rate. In addition, from the coding theory point of view, the repetition block code (RBC) is not as good as other coding schemes such as the convolutional codes (CC), (Lin and Costello, 1983, Proakis, 1995). Therefore, in several works have proposed these CC for IR-UWB systems, instead of the "RBC", mainly to improve the system's BER without increasing the transmit power, (Forouzan and Abtahi, 2003, Nasiri-Kenari and Shayesteh, 2005, Pietrzyk and Weber, 2005). In addition, as it has been demonstrated by Villarreal-Reyes (2007) a specific set of these CC can suppress spectral lines in the PSD of IR-UWB

signals. For that reason this research work also considers the analysis of the **convolutionally coded** IR-UWB signals. This analysis is well explained in (Villarreal-Reyes, 2007). Furthermore, in the following discussion and chapters the terms "**non-coded**" and "**non-convolutionally coded**" will be used for IR-UWB systems employing the pulse repetition/RBC.

a) Binary phase shift keying (BPSK)

b) Binary pulse position modulation (BPPM)

c) Quaternary biorthogonal pulse position modulation (BOPPM) with Gray mapping
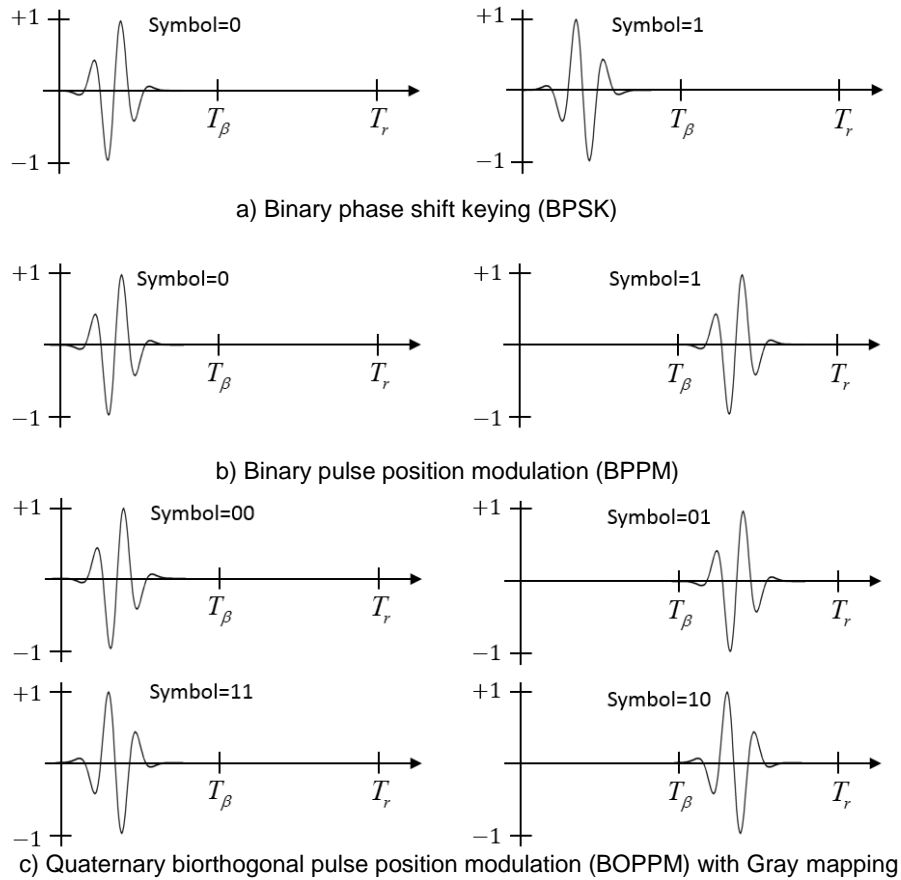
Figure 18. Several modulation schemes for an IR-UWB signal using the 5th **order derivative of a Gaussian pulse.** T_β **is the PPM modulation index and** T_r **is the mean repetition time between pulses.**

The non-coded and convolutionally coded pulses normally are modulated by some of the several modulation schemes proposed for IR-UWB systems such as pulse position modulation (PPM), pulse amplitude modulation (PAM), binary phase shift keying (BPSK), biorthogonal PPM (BOPPM) and pulse shape modulation (PSM). As an example, Figure 18 shows the modulation schemes that will be used in this thesis work: binary PPM (BPPM), BPSK, and quaternary BOPPM (Q-BOPPM) with Gray mapping. These modulations schemes offer advantages and disadvantages in terms of BER performance, complexity and PSD characteristics of the signal, (Villarreal-Reyes, 2007).

Finally, the modulated IR-UWB pulses can be multiplied by periodic or random Time-Hopping (TH) and/or Direct sequence (DS) spreading codes in order to shape spectrally the IR-UWB signals and/or to provide multiple access characteristics for UWB transmissions, (Win and Scholtz, 1998, Win and Scholtz, 2000, Aiello and Rogerson, 2003, Di Benedetto and Giancola, 2004, Roy et al., 2004, Di Benedetto et al., 2006, Arslan et al., 2006, Ghavami et al., 2007). A block diagram of a typical implementation for a non-coded and convolutionally coded IR-UWB system is shown in Figure 19.
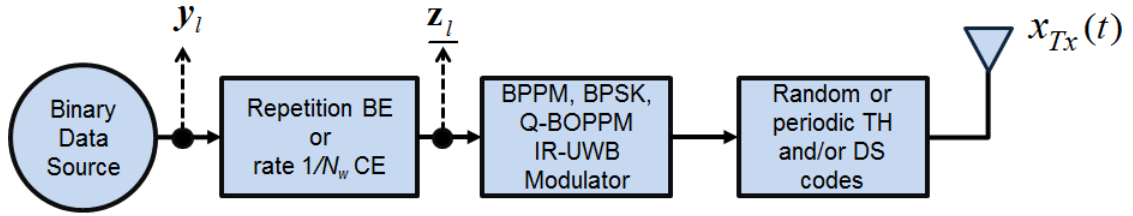
Figure 19. Block diagram of a non-coded and convolutionally-coded IR-UWB transmitter. y_l **is the binary data stream introduced to the repetition block encoder (RBE) or the convolutional encoder (CE);** z_l **is a code vector with** N_w **elements all equal to** y_l **for the RBE case and not necessarily equal to** y_l **when a CE is used.**

2.3.1 Non-coded Time Hopping IR-UWB signal model

A generic signal model for a typical non-coded IR-UWB system including orthogonal, antipodal and biorthogonal modulation formats with TH and DS mechanisms was described by (Villarreal-Reyes, 2007)

$$
\begin{aligned}
x_{Tx} &= \sum_{l=-\infty}^{\infty} \sum_{k=0}^{N_w-1} \alpha_l w_{Tx}(t - lT_s - kT_r - c_{lN_w+k}T_c - \beta_l T_\beta) \\
x_{Rx} &= \sum_{l=-\infty}^{\infty} \sum_{k=0}^{N_w-1} \alpha_l w_{Rx}(t - lT_s - kT_r - c_{lN_w+k}T_c - \beta_l T_\beta - \tau) + n(t)
\end{aligned}
\tag{9}
$$

where $w_{Tx}(t)$ and $w_{Rx}(t)$ are the transmitted and received pulses respectively, $\{\alpha_l\}$ and $\{\beta_l\}$ are the PAM and PPM data streams and N_w is the number of transmitted pulses per data symbol. The pseudo-random (PR) TH sequence $\{c_{lN_w+k}\}$ takes values on the set $\{0,1,2,\ldots,N_c-1\}$ with period χ_c. The T_{wTx} and T_{wRx} are the pulse duration of the transmitted and received pulses, respectively. T_r is the mean repetition time between pulses, T_s is the symbol time ($T_s = N_w T_r$), T_β is the PPM modulation index and T_c is the nominal shift caused

by the PR-TH sequence. In order to take into account the impact of the wireless transmission in the signal model, τ represent the propagation delay and $n(t)$ the additive noise.
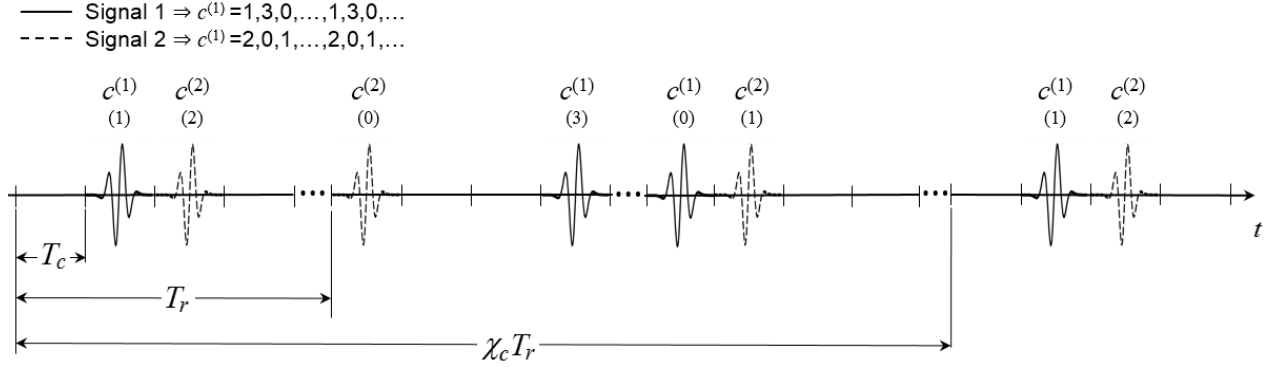
Figure 20. Pulse positions for two TH-IR sequences. $c^{(1)}$ and $c^{(2)}$ are two different PR-TH sequences. T_r is the mean repetition time between pulses, T_c is the nominal shift caused by the PR-TH sequence and χ_c is the period of the PR-TH sequence.

Figure 20 shows the data transmission of two IR-UWB users using different TH codes. It can be seen as different time slots are chosen according to the TH code to convey information. This latter fact allows the reduction of the multiple access (MA) interference in a multiuser scenario. Note that several modulation schemes such as PPM, pulse amplitude modulation (PAM), On-Off Keying (OOK) and PAM/PPM can be modelled using Equation (9). This can be achieved by setting α and β parameters. For example, if M-ary PPM is considered, then $\alpha=1$ and β will take values on the set $\{0,1,2,\ldots,M-1\}$. It is important to mention that in this research only orthogonal M-*ary* PPM will be considered. For that reason, in order to avoid intersymbol interference (ISI), $T_\beta \geq \max(T_{wTx}, T_{wRx})$, $T_c \geq T_\beta$, and $T_r \geq N_c T_c$ will be assumed. On the other hand, if BPSK is considered then $\alpha_l \in \{-1,+1\}$ and $\beta_l=0$ in contrast for M-*ary* BOPPM will be used $\alpha_l \in \{-1,+1\}$ and $\beta_l \in \{0,1,\ldots,(M/2)-1\}$, (Zhang and Gulliver, 2005).

2.3.2 Non-coded Direct Sequence IR-UWB signal model and non-coded Mixed TH/DS IR-UWB signal model

In the direct sequence (DS) IR-UWB systems the pulse amplitude is multiplied by a pseudo-random (PR) sequence which is linked to each user in the network, (Foerster,

2002, Boubaker and Letaief, 2003, Di Benedetto and Giancola, 2004). Thus, a typical non-coded DS-IR-UWB signal can be described by

$$
\begin{aligned}
x_{Tx} &= \sum_{l=-\infty}^{\infty} \sum_{k=0}^{N_w-1} a_{lN_w+k}\alpha_l w_{Tx}(t-lT_s-kT_r) \\
x_{Rx} &= \sum_{l=-\infty}^{\infty} \sum_{k=0}^{N_w-1} a_{lN_w+k}\alpha_l w_{Rx}(t-lT_s-kT_r-\tau)+n(t)
\end{aligned}
\tag{10}
$$

where $\{a_{lN_w+k}\}$ is a PR-DS sequence with period χ_a, which usually takes values within the set $\{-1,+1\}$. The sequence $\{a_{lN_w+k}\}$ is normally used for multiple access purposes as in traditional code division multiple access (CDMA), (Villarreal-Reyes, 2007). However, it can also be used to improve the spectral properties of the transmit signal, (Nakache and Molisch, 2006). It is important to mention that DS-IR UWB systems could provide data rates greater than TH-IR UWB systems. This is due to T_r can be set just slightly larger than $\max(T_{wTx}, T_{wRx})$, unlike of TH-IR UWB systems, which entirely depends on $T_r \geq N_c T_c$. A typical DS-IR-UWB signal is shown in Figure 21.
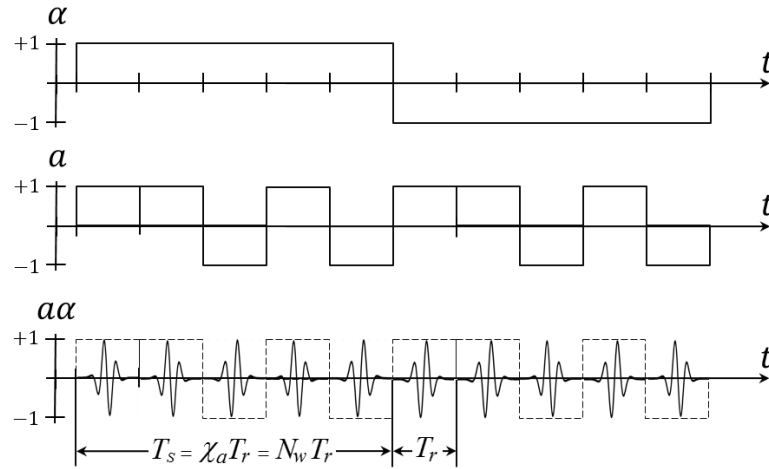
Figure 21. Typical Direct Sequence (DS) IR-UWB signal. $\{\alpha_l\}$ **is the PAM data stream,** $\{N_w\}$ **is the number of transmitted pulses per data symbol,** T_r **is the mean repetition time between pulses,** T_s **is the symbol time and** χ_a **is the period of the PR-DS code** $\{a_{lNw+k}\}$**.**

On the other hand, a mixed TH-DS IR-UWB signal can be defined as

$$x_{Tx} = \sum_{l=-\infty}^{\infty} \sum_{k=0}^{N_w-1} a_{lN_w+k} \alpha_l w_{Tx}(t - lT_s - kT_r - c_{lN_w+k}T_c - \beta_l T_\beta)$$

$$x_{Rx} = \sum_{l=-\infty}^{\infty} \sum_{k=0}^{N_w-1} a_{lN_w+k} \alpha_l w_{Rx}(t - lT_s - kT_r - c_{lN_w+k}T_c - \beta_l T_\beta - \tau) + n(t)$$

(11)

In this case each parameter in Equation (11) can be set to fulfil a specific design requirement. For example, Gezici, Kobayashi, Poor, and Molisch (2005), have reported the use of TH sequence for multiple access purposes whereas the DS code is used to smooth the signal's PSD.

2.3.3 Convolutionally coded TH/DS-IR UWB signal model

Convolutional codes are widely used in digital communication systems to improve bit error rates, (Lin and Costello, 1983, Proakis, 1995). In fact, they are used to protect the transmitted digital data from channel induced impairments. Therefore, it is likely that several practical UWB systems will include some sort of convolutional coding for forward error correction (FEC) purposes, (Forouzan, Nasiri-kenari, and Salehi, 2002, Forouzan and Abtahi, 2003, Nasiri-Kenari and Shayesteh, 2005, Reggiani and Maggio, 2006, Zeinalpour-Yazdi and Nasiri-Kenari, 2006, Villarreal-Reyes, 2007). As an example, the IEEE802.15.4-2011 standard, which implements UWB technology in one of its PHY layers, also includes FEC mechanisms based on a Reed Solomon (RS) encoder concatenated to a rate $1/2$ convolutional encoder.

The signal model for convolutionally coded TH/DS-IR UWB systems analyzed in this thesis work can be represented as (Villarreal-Reyes, 2007)

$$x_{Tx} = \sum_{l=-\infty}^{\infty} \sum_{k=0}^{N_w-1} a_{lN_w+k} \alpha_{\sigma_{l,k}} w_{Tx}(t - lT_s - kT_r - c_{lN_w+k}T_c - \beta_{\sigma_{l,k}} T_\beta)$$

$$x_{Rx} = \sum_{l=-\infty}^{\infty} \sum_{k=0}^{N_w-1} a_{lN_w+k} \alpha_{\sigma_{l,k}} w_{Rx}(t - lT_s - kT_r - c_{lN_w+k}T_c - \beta_{\sigma_{l,k}} T_\beta - \tau) + n(t)$$

(12)

where σ_l include all possible states of the joint source-encoder (SE) pair stochastics process proposed by Villarreal-Reyes (2007), which can be classified as Moore type (within the definition adopted for finite state sequential machines); N_σ is the total number of states of this joint SE pair, which can be determined by both the number of memory elements, v, of the binary convolutional encoder (CE) and the data source implemented in the IR-UWB system. As an example, $N_\sigma = 2N_q=2(2^4)=32$ states can be generated if a binary data source (BDS) and a CE with $v=4$ are implemented. Furthermore, $\alpha_{\sigma l,k}$ and $\beta_{\sigma l,k}$ are, respectively, the kth PAM and PPM variables used for the transmission of the lth joint SE pair output vector, $\mathbf{z}_l=[z_l^{(0)}, z_l^{(1)},\ldots, z_l^{(\kappa-1)}]$, where κ indicates the number of binary CE outputs. As noted, if $\underline{z}_l$ is suitably mapped to $\alpha_{\sigma l,k}$ and $\beta_{\sigma l,k}$ several modulation schemes could be represented. As an example, the output vector, $\underline{z}_l=[z_l^{(0)}, z_l^{(1)}]$, generated by a rate $1/\kappa=1/2$ CE could drive a Q-BOPPM modulator using $\alpha_{\sigma l,k}=2z_l^{(0)}-1$ and $\beta_{\sigma l,k}=z_l^{(1)}$ to change the pulse polarity and pulse position, respectively.

On the other hand, a signal model for convolutionally coded M-PPM IR-UWB systems can be represented as

$$x_{Tx} = \sum_{l=-\infty}^{\infty} \sum_{k=0}^{N_w-1} w_{Tx}(t - lT_s - kT_r - \beta_{\sigma_{l,k}} T_\beta)$$

$$x_{Rx} = \sum_{l=-\infty}^{\infty} \sum_{k=0}^{N_w-1} w_{Rx}(t - lT_s - kT_r - \beta_{\sigma_{l,k}} T_\beta - \tau) + n(t)$$

(13)

where $\beta_{\sigma l,k} \in \{0,1,\ldots,M-1\}$ is the kth M-*ary* transmitted symbol when the encoder is in state σ_l. In this scheme, if the same rate $1/2$ CE is used, a Quaternary PPM modulator could be employed. That is, the value of $\beta_{\sigma l,k}=\{z_l^{(0)}, z_l^{(1)}\}$ would determine one of the 4 time slots, $\{0,1,2,3\}$, of a Quaternary-PPM symbol.

2.4 Spectral masks and the importance of spectral shaping in IR-UWB systems

As mentioned the UWB signals occupy a very large part of the limited radio spectrum ($\geq$ 500 MHz). Therefore the FCC in its 2002 Report and Order has also established power

limits in form of spectral masks. The aim of these spectral masks is to enable the harmonious coexistence between UWB systems and traditional wireless systems such as Global Position Systems (GPS), digital TV, WiFi, Bluetooth, Zigbee, WiMax, 2G/3G/LTE mobile communications systems, satellite communication, and various systems deployed for government applications, such as digital broadband radio working in the public safety band, (Wong and Lau, 2008). We term all these typical wireless systems as narrowband (NB) systems referring to their bandwidth compared to that of UWB. In Table 1 and Figure 22 the average emission limits for UWB signals as specified by the U.S. FCC for indoor and outdoor applications are presented, (FCC, 2002). These average emission limits are given in terms of effective isotropic radiated power (EIRP) in dBm considering 1 MHz resolution bandwidth (RBW), root mean square (RMS) average detector and average time of 1 ms or less.
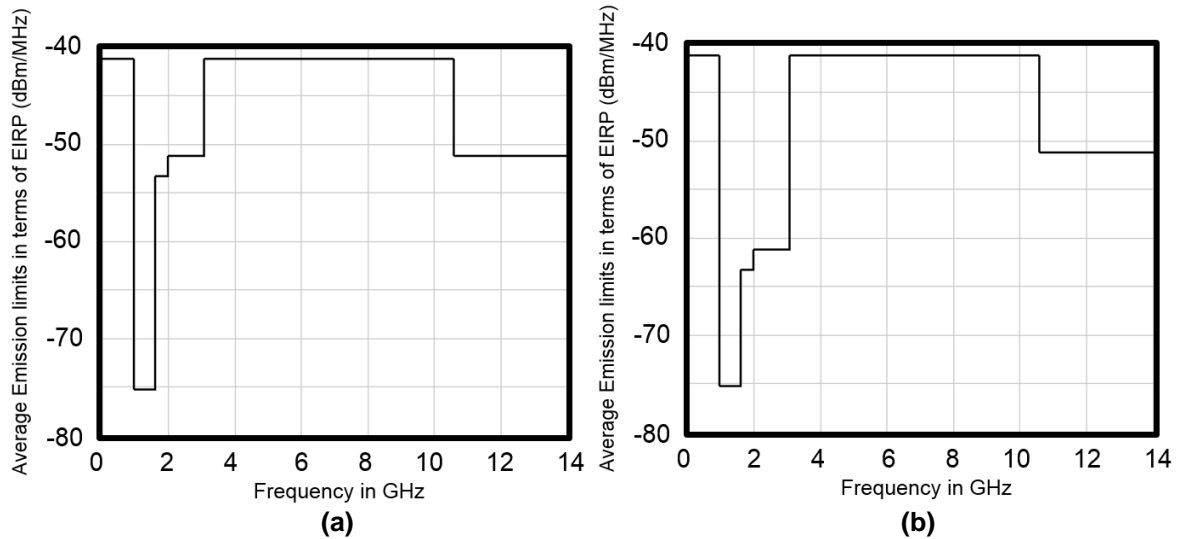
Figure 22. FCC UWB spectral masks for (a) indoor and (b) outdoor applications.

Table 1: Spectral masks for UWB average emission limits in terms of EIRP in dBm/MHz established by the Federal Communications Commission (FCC).

Frequency band (GHZ)	Power levels in terms of EIRP (dBM/MHz)	
	Devices for indoor applications	Devices for indoor applications
0.000009-.960	-41.3	-41.3
0.960-1.610	-75.3	-75.3
1.610-1.990	-53.3	-63.3
1.990-3.100	-51.3	-61.3
3.100-10.600	-41.3	-41.3
10.600-22.000	-51.3	-61.3
22.000-31.000	Vehicular spectral mask	
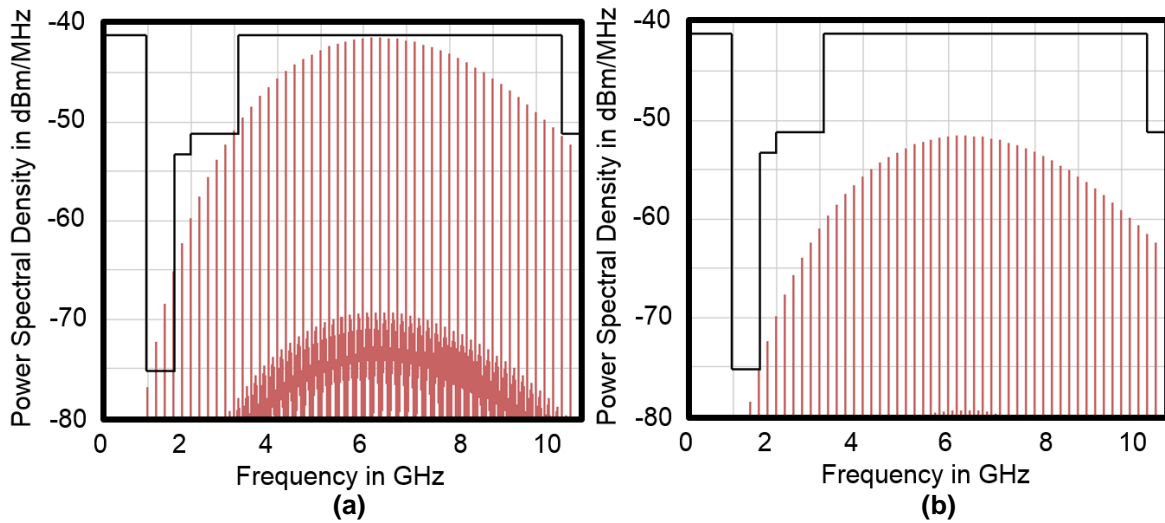
Figure 23. Comparison between the FCC UWB spectral mask for indoor communications systems and simulated PSD of a binary PPM IR-UWB signal. The 3rd derivative Gaussian pulse was used with pulse duration $T_w \approx 0.4$ ns. The transmit power of the PSD signal plotted in (b) was reduced 10 dB to meet with the spectral mask. No TH was used in both signals.
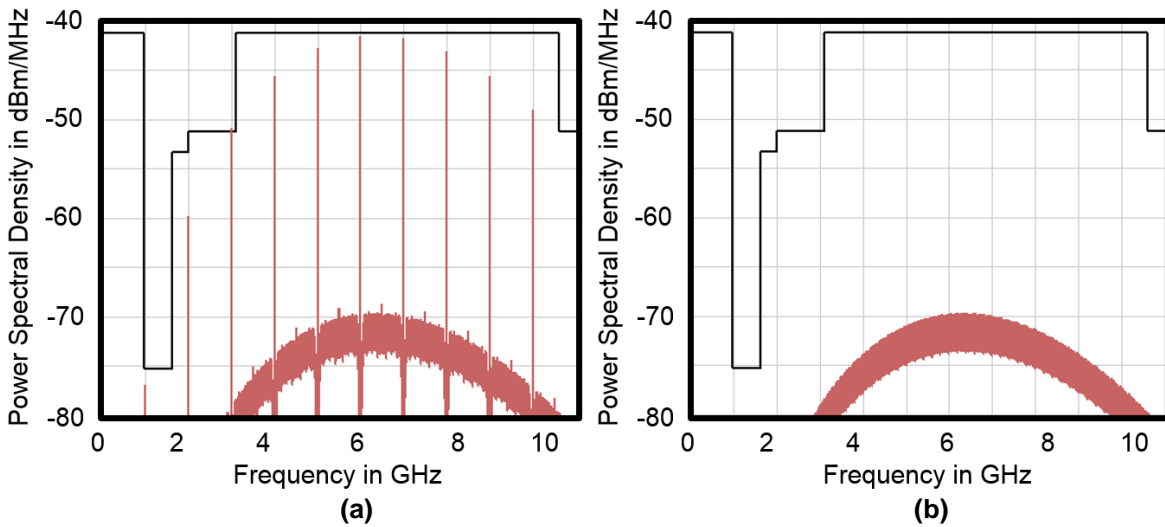
Figure 24. Comparison between the FCC UWB spectral masks for indoor communications systems and the simulated PSD of a binary PPM IR-UWB signal using: (a) an ideal (perfectly random) TH code distributed over the set {0, 1, 2, 3, 4} and (b) an ideal (perfectly random) DS code taking values of the set {+1,-1}.The signals have the same base parameters (e.g. transmit power and data rate) as the signal used to obtain Figure 23(a).

As it can be seen in Figure 22, both indoor and outdoor FCC spectral masks allow the transmission of IR-UWB signals with a maximum power spectral density (PSD) of -41.3 dBm/MHz over the frequency interval 3.1-10.6 GHz. On one hand, the available 7.5 GHz bandwidth enable the implementation of High Data Rate (HDR) IR-UWB systems using affordable microwave wireless technology rather than expensive millimeter-wave

components (e.g. amplifiers and local oscillators) commonly used for implementing 60 GHz UWB systems. On the other hand, the very low PSD levels implies a tradeoff in terms of transmission distance and HDR communications. Therefore, in order to maximize the spectrum usage of these FCC spectral masks in terms of both bandwidth and power allowed, whilst the interference effect from/to narrowband users is minimized, the IR-UWB systems shall implement spectral shaping methods.

In order to see the importance of these spectral shaping methods, let us consider a simulated PSD of an IR-UWB signal using binary pulse position modulation (BPPM) without time hopping (TH) or DS multiplication multiple access formats. This signal and the FCC spectral mask for indoor environments (see Figure 22a) are plotted in Figure 23. It can be seen in Figure 23(a) that this signal does not comply with the spectral mask because of strong spectral lines spaced at 200 MHz intervals infringes the region of the GPS and aeronautical radio navigation systems (i.e. from 0.960 GHz to 1.610 GHz). As it is well-known, the spectral lines that appear in the PSD of a baseband signal are due to deterministic elements present in the signal; the modulation format used, or/and the statistics of the data stream. Thus, in order to adjust this PSD under the indoor FCC spectral mask, spectral shaping methods based on TH codes and/or DS codes could be implemented. The comparison between the simulated PSD of the BPPM IR-UWB signal using an ideal TH sequence uniformly distributed over the set $\{0, 1, 2, 3, 4\}$ and the indoor spectral mask are shown in Figure 24(a). It can be seen that the inclusion of this ideal time hopping sequence enables the compliance with the FCC regulation without reducing the signal's transmit power. If this TH sequence is not used, a reduction of more than 10 dBm/MHz must be done in order to meet with the spectral mask (see Figure 23-b). In addition, note how the inclusion of the TH sequence also reduces the number of spectral lines, as they now appear spaced at 1 GHz intervals. On the other hand, when a DS code based spectral shaping method is included in the signal, a spectral line free (SLF) PSD could be achieved. The comparison between the simulated PSD of the BPPM IR-UWB signal using an ideal (perfectly random) DS multiplication taking values within the set $\{+1,-1\}$ and the indoor FCC spectral mask are shown in Figure 24(b). It can be seen that this SLF PSD fits completely under the spectral mask, even the transmit power could be increased in order to improve the system's BER. Comparing both spectral shaping

methods, it is clear that the inclusion of a DS spreading code for randomizing the pulse polarity in the BPPM IR-UWB signal offer better performance than the inclusion of the TH sequence. According to the spectral analysis performed by Villarreal-Reyes (2007), the complete elimination of the discrete part of the PSD can only be achieved when the expected value of the DS code becomes zero, which occurs if this sequence is perfectly random (that is, independent identically distributed with uniform distribution). Nevertheless, the use of perfectly random TH and/or DS codes is only an idealization that in practical implementations is addressed by generating a pseudo-random (PR) TH sequence with extremely long period. The use of extremely long period increases the transmitter and receiver complexity without provide significant BER performance improvements (when comparing systems with the same transmit power). Therefore, the inclusion of any of these two spectral shaping methods in IR-UWB systems would require a compromise between complexity and number of spectral lines eliminated in the PSD.

On the other hand, it is important to mention that there exist other spectral masks established by international frequency body regulators around the world. For example, in Europe the European Conference of Postal and Telecommunications Administrations/Electronic Communications Committee (CEPT/ECC) and in Asia the Ministry of Internal Affairs and Communications (MIC) of Japan, the Ministry of Industry and Information Technology of China, Infocomm Development Authority of Singapore (IDA) and the ministry of information and communication of Korea have issued spectral masks more restrictive than those established in North America countries (e.g. the in U.S. FCC and the Spectrum Management and Telecommunications program in Canada), (Kim, Leem, Kang, and Lee, 2008, Rahim, 2010, Fernandes and Wentzloff, 2010). Even additional mitigation methods such as detect and avoid (DAA) and Low Duty Cycle (LDC) must be implemented in order to provide extra protection for aeronautical radio communication systems, satellite (downlink) communications services and radiolocation systems, (Zhang et al., 2009-A, Fernandes and Wentzloff, 2010). Figure 25 summarizes the frequency bands for different countries in which UWB wireless communication is allowed at a level of -41.3 dBm/MHz. From these regulations, it can see that the frequency interval 7.25 GHz to 8.5 GHz is the only common spectrum. It should be noted that this could be one of the main obstacles for successful deployment of UWB devices in the mass

market. Bearing this in mind, some of the important standardization organizations such as the IEEE LAN/MAN Standards Committee and the ECMA International have established frequency band plans in order to support the transmission of UWB signals within worldwide spectrum regulations. For example the IR-UWB-PHY of the LDR-WPAN standard, (IEEE Std. 802.15.4-2011, 2011), supports sixteen UWB channels with a bandwidth from 499.2 MHz to 1354.97 MHz defined in three sub bands below 10.2 GHz. Figure 26(a) shows a graphical representation of all these channels. As it can be seen, the channels 4, 8 and 9 could be worldwide accepted. For the case of standardized HDR-WPANs working within the FCC UWB frequency band (from 3.1 GHz to 10.6 GHz), the ECMA-368 standard, (ECMA-368, 2008), which is based on in the MB-OFDM UWB PHY layer proposed in the IEEE802.15.3a standard (now disbanded), divide the UWB spectrum into fourteen channels with a bandwidth per channel equal to 528 MHz. Note in Figure 26(b) as the first 12 channels are grouped into 4 band groups consisting of 3 channels each one. The last two channels are grouped into a fifth band group. A sixth band group is also defined within the spectrum of the third and four band group. As it can be seen, both frequency division approaches can ensure that at least one of the channels shall be supported within the worldwide UWB spectrum regulations.

Legend: Detect and Avoid (dashed red outline); Low Duty Cycle (yellow)

Countries	Max mean EIRP density: -41.3 dBm/MHz	Year
New Zeeland	4.8 (Low Duty Cycle); 6.0 – 8.5	2015
Singapore	3.4, 4.2 (Detect and Avoid); 4.8; 6.0 – 9.0	2011
China	4.2, 4.8 (Detect and Avoid); 6.0 – 9.0	2011
Canada	4.75 (onward)	2009
Europe	4.2 (Low Duty Cycle), 4.8 (Detect and Avoid); 6.0 – 8.5, 9.0 (Detect and Avoid)	2008
S. Korea	4.8 (Detect and Avoid); 7.20 – 10.20	2006
Japan	3.4, 4.8 (Detect and Avoid); 7.25 – 10.25	2006
U.S./FCC	(full band 3.1 – 10.6)	2002

Frequency axis (GHz): 3.1 3.6 4.6 5.6 6.6 7.6 8.6 9.6 10.6

Figure 25. UWB intended bands for communication in different regions.
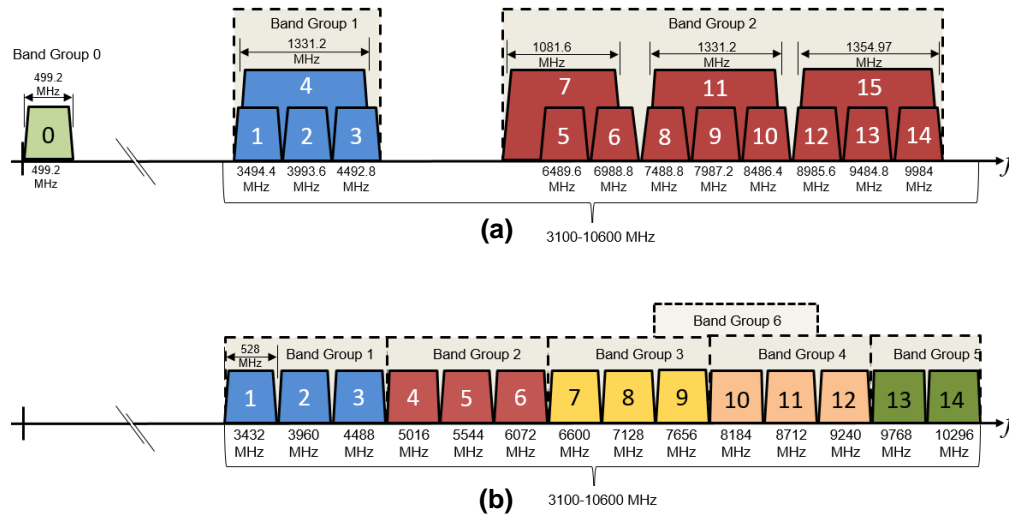
Figure 26. (a) Band plan for IEEE802.15.4-2011 and (b) band plan for ECMA-368.

In addition, it is important mentioning that worldwide compliant HDR-WPANs based on ultra-short time pulses can also be achieved by mixing rectangular or Gaussian UWB pulses with a sine wave (local oscillator) set to the central frequency of interest such as is reported by (Fernandes and Wentzloff, 2010, Colli-Vignarelli and Dehollain, 2011-A, Thotahewa, Redoute, and Yuce, 2014).

2.5 Spectral shaping of IR-UWB signals by convolutional codes.

As mentioned in the previous section, for appropriate spectrum overlay, the local regulators impose spectral masks that strictly constrain the power spectral density (PSD) of a UWB signal, (FCC, 2002, Arslan et al., 2006, Kim et al., 2008, Rahim, 2010, Fernandes and Wentzloff, 2010). Thus, in order to maximize the usage of these spectral masks in terms of both bandwidth and power allowed, whilst the interference effect from/to narrowband users is minimized, the IR-UWB systems shall implement spectral shaping methods such as those provided in Table 2. Most of the information provided in this table, which shows a summary of the advantages and disadvantages of each proposed spectral shaping method for IR-UWB systems, was brought from subsection 2.5.5 of Villarreal-Reyes (2007). The comments regarding the spectral line elimination capabilities of each scheme were made taking as reference the spectral line content of a periodic signal like that shown in Section 2.4 of the same reference.

As it can be seen in Table 2, the spectral shaping method based on Convolutional Codes (CC) with convenient PSD characteristics provide both good bit error rate (BER) performance and improved PSD characteristics, (Villarreal-Reyes, 2007). This method can eliminate a significant numbers of spectral lines in time hopping (TH) pulse position modulated (PPM) IR-UWB systems using the namely spectral line suppressive (SLS)-CC. On the other hand, total spectral line elimination in the PSD can be achieved by using the spectral line free (SLF)-CC with binary phase shift keying (BPSK) or biorthogonal PPM (BOPPM) IR-UWB systems. Furthermore, these important characteristics are kept even when the binary data stream at the encoder input is generated by an unbalanced binary data source (that is, the data stream does not consists of uniformly distributed i.i.d. binary random symbols). This is an important advantage because of not all the data sources or compression algorithms found in practical systems generate perfectly random binary data streams which certainly would generate spectral lines in the PSD. Thus, the inclusion of a spectral shaping method for suppressing spectral lines generated by periodic components present in the signal is more attractive than those methods requiring extremely long period scrambling sequences to design compliant IR-UWB systems.

Table 2. A comparison of spectral shaping mechanisms for IR-UWB signals.

Spectral Shaping method	Main Characteristic	Advantages	Disadvantages
Pulse Shape Based Spectral Shaping	The pulse energy density spectrum (EDS) determines the overall PSD shape.	• The pulse EDS can be designed for maximum spectral mask utilization. • Can be used to implement orthogonal signaling. • Can be used to produce notches in the PSD.	• The pulse shape may be distorted by the antenna and channel. Thus the EDS of the radiated pulse may differ from the intended EDS. • Can not be effectively used to eliminate spectral lines in the PSD.
TH Code Based Spectral Shaping	The TH sequence can be used to eliminate spectral lines or generate notches in the PSD. The TH sequence can be used to eliminate spectral lines or generate notches in the PSD.	• If the TH sequence is assumed to be perfectly random, then a significant number of spectral lines can be eliminated in the PSD. • Can be used to generate several notches in the PSD simultaneously	• To maximize the amount of spectral lines eliminated the TH sequence must be perfectly random. • The generation of a TH code with extremely long period (such that it approaches a perfectly random sequence) complicates the transmitter and receiver design. • For most practical implementations some spectral lines remain in the PSD.

Table 2. Continuation…

Spectral Shaping method	Main Characteristic	Advantages	Disadvantages
TH Code Based Spectral Shaping			• The effectiveness to generate spectral notches in the PSD is adversely affected by timing jitter
DS Code Based Spectral Shaping	The DS code can be used to eliminate spectral lines.	• Can be used to generate several notches in the PSD simultaneously • If the DS sequence is assumed to be perfectly random, then a spectral line-free PSD can be achieved	• If the DS sequence is not perfectly random, then spectral lines will appear in the PSD. • The generation of a DS code with extremely long period (such that it approaches a perfectly random sequence) complicates the transmitter and receiver design. • If the period of the DS code is relatively short, then the number of spectral lines in the PSD is increased.
Pseudo Chaotic TH	Generates random-like TH sequences using a pseudo-chaotic encoder.	• Generates aperiodic random-like TH sequences that eliminate a significant number of spectral lines in the PSD. • If Viterbi decoding is implemented in the receiver, then a significant BER improvement over non-coded binary PPM can be achieved.	• In order to generate the random like TH sequence, the PCTH encoder must be fed with i.i.d. binary symbols with uniform distribution (e.g. perfectly random data stream). • In order obtain i.i.d. binary symbols with uniform distribution, a compression and scrambling block may be needed between the data. • If the PCTH encoder is not fed with i.i.d. binary symbols with uniform distribution, then the number of spectral lines eliminated is reduced.
Convolutional Codes (CC) with convenient PSD characteristics	Convolutional codes are used to provide both maximum spectral line mitigation in the PSD and BER improvement.	• Can be used to eliminate as many spectral lines as the PCTH scheme for TH-PPM signals or to generate spectral line free PSD for BPSK/BOPPM signals, even when the binary data stream at the encoder input is generated by an unbalanced Binary Markov Source (i.e. these are not perfectly random data stream .	• Spectral shaping capabilities limited to data streams generated by an unbalanced/balanced Binary Markov Source. • Medium complexity in the transmitter and receiver.

In addition, as previously mentioned, convolutional codes (CC) for forward error correction (FEC) purposes were considered in several works for IR-UWB systems over the last decade, (Forouzan et al., 2002, Forouzan and Abtahi, 2003, Nasiri-Kenari and Shayesteh, 2005, Reggiani and Maggio, 2006, Zeinalpour-Yazdi and Nasiri-Kenari, 2006, Villarreal-Reyes, 2007), even standards for LDR-WPANs (IEEE 802.15.4-2011) and HDR-WPANs (ECMA-368, 2008) have proposed them in their FEC layer. This latter fact shows that the inclusion of error correction mechanisms has become standard in actual UWB communication systems. In this context a system using traditional convolutional encoders or no convolutional coding will need extra mechanisms to effectively shape the PSD and achieve compliance with the current regulations. Therefore, in terms of implementation, an IR-UWB system employing some of the convolutional codes reported by (Villarreal-Reyes, 2007) may be less complex than a system employing traditional convolutional encoders.

2.6 IR-UWB over Fiber systems

As discussed in subsection 2.4, the Federal Communications Commission (FCC) in the United States and other radio-spectrum international regulators around of the world have issued power limits to regulate the UWB signal transmissions. The maximum power spectral density (PSD) allowed by this regulations is -41.3 dBm/MHz over specific frequency intervals (see Figure 22). Due to this very low PSD, the UWB communications outline a personal coverage area (that is, less than 10 meters). As consequence, the UWB-WPAN would operate mainly in stand-alone mode, with nearly nonexistent integration into the fixed wired and wireless wide-area infrastructures, (Pan and Yao, 2010-A). Therefore, in order to overcome this coverage limitation providing availability of undisrupted UWB service across different networks, (Pan and Yao, 2011-A), the relatively new concept of IR-UWB "plus" radio over fiber (IR-UWB + RoF) or simply IR-UWB over fiber (IR-UWBoF) was proposed, (Yao et al., 2007, Yao, 2009).

The state of the art of the IR-UWBoF systems is focused on two main topics: the photonics UWB pulse generation methods and their distribution over different RoF architectures. In next paragraphs will be given an overview of these topics.

2.6.1 Overview of photonics UWB pulse generation

As mentioned in subsection 1.4, several works showing theoretical analysis and experimental performance evaluations of IR-UWBoF systems operating within the 3.1 GHz to 10.6 GHz frequency band have been widely addressed in the literature. Most of these publications have been focused on photonics UWB signal generation techniques. According to Xianbin Yu et al., (2013), these techniques can be divided into two broad classes: time delay and nonlinear signal processing. In the first class, Gaussian pulses with phase difference are combined at the receiver side by controlling the delay time between them. In this context, different methods for implementing this optical delay lines have been exploited. For example Yao et al., (2007) classify this method in three main categories:

1. **UWB pulse generation based on phase-modulation-to-intensity-modulation (PM–IM) conversion.** This technique was proposed to recover the information of phase modulated signals without using complex and costly coherent detection techniques. In general, two methods are used: 1) chromatic-dispersion-based PM–IM conversion (see Figure 27) and 2) optical filter-based PM–IM conversion (see Figure 28), (Yao et al., 2007). In the first method, the phase modulated optical signal is transmitted through a single-mode fiber (SMF) in order to rotate the phase of both sidebands (that is, a delay between both sidebands is produced) to be totally or partially in phase. This rotation can be achieved thanks to the dispersion induced by the SMF (Zeng and Yao, 2004), which allows to recover the modulating signal using direct detection technique. It is important to mention that the frequency response of this method has a transfer function equivalent to a microwave bandpass filter, by which input modulating signal with a Gaussian pulse could be converted to UWB monocycle or UWB doublet pulses such as is shown in (Yao et al., 2007, Zeng and Yao, 2006-A).

   In the second method an optical filter is used to act as an optical frequency discriminator, (Zeng and Yao, 2005). The elimination of either one sideband or the carrier would lead to the PM–IM conversion. Therefore, if a phase-modulated

Gaussian pulse is sent to an optical frequency discriminator, depending on the location of the optical carrier at its linear or quadrature slope, a Gaussian monocycle or doublet could be generated, (Yao et al., 2007). In addition, the location of the optical carrier at the positive or negative slope would lead to the generation of UWB pulses with opposite polarity, (Zeng and Yao, 2006-B, Chengliang Yang et al., 2014-A).

2. **UWB pulse generation using a photonic microwave delay-line filter**. Most of the photonic microwave filters proposed in the literature have a structure with a finite impulse response (FIR), (Dai and Yao, 2010). Furthermore, in order to avoid optical interference, these filters are usually designed to operate in the incoherent regime employing direct detection technique. It is well-known that regular photonic microwave delay-line filters based on incoherent detection have all-positive coefficients, which make them working as a low-pass filters, (Dai and Yao, 2010). However, as mentioned before, bandpass characteristics are desired because of UWB pulses without baseband resonance around dc (that is, derivatives of the pulse) can be generated. Therefore, microwave delay-line filters need to have both positive and negative coefficients to produce bandpass characteristics. Bearing this in mind, some practical implementation of microwave delay-line filters used to generate UWB monocycles and UWB doublets are based on the cross-gain modulation (XGM) effect in a semiconductor optical amplifier (see Figure 29), (Yao et al. 2007, Zeng, Wang, and Yao, 2007, Qing Wang, et al, 2006), polarization modulator (see Figure 30), (Yao et al. 2007, Qing Wang and Yao, 2007), the interaction between two electro-optic Mach Zehnder modulators (EO-MZM) biased at complementary slopes (Bolea et al., 2010), the EO-MZM's transfer function response at different working wavelengths (Jianqiang Li, et al., 2008) or others methods, (Chengliang Yang et al., 2014-B).

3. **UWB pulse generation based on optical spectral shaping and dispersion-induced frequency-to-time conversion.** This technique takes advantage of the so-called frequency-to-time mapping phenomenon, (Torres-Company, Leaird, and Weiner, 2011), which relies on the fact that after linear propagation through a

dispersive medium (e.g. SMF), the temporal intensity profile (time-domain shape) of an ultrashort optical pulse generated by a broadband coherent optical source (e.g. a mode-locked laser), becomes a scaled version of its optical spectrum shape, (Tong, Chan, and Tsang, 1997, Torres-Company et al., 2011). In this sense, the photonic UWB pulse generator based on this technique (see Figure 31), first shapes the spectrum of a broadband coherent optical source according to the desired time-domain UWB waveform by using an optical spectral shaper (e.g. optical discriminators and variable delay lines). Afterwards, the shaped spectrum is converted to a time-domain shape by passing it through a dispersive medium such as dispersive fiber or a reflection chirped fiber Bragg grating (FBG), (McKinney, Lin, and Weiner, 2006, Wang et al., 2007).
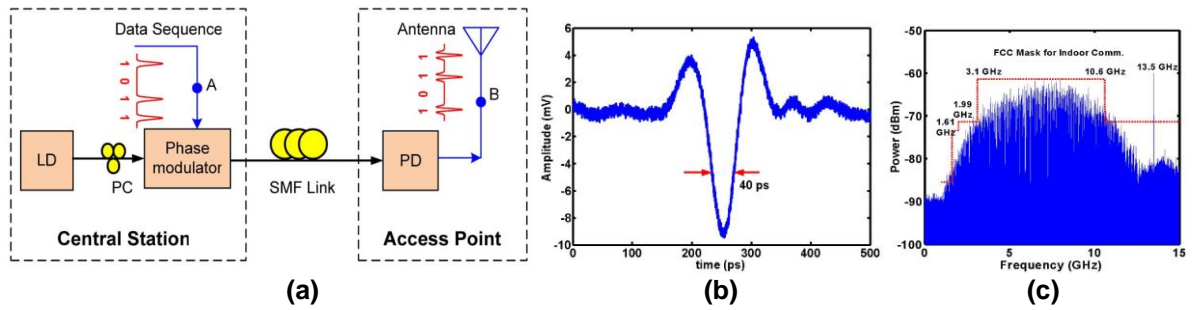
Figure 27. (a) Schematic of a UWB pulse generator based on PM–IM conversion method (chromatic dispersion induced). (b) Waveform of the generated Gaussian doublet and (c) the corresponding power spectrum (Yao, Zeng and Wang, 2007, Zeng and Yao, 2006-A). Note that the waveform and the power spectrum were measured in the test point B of the system.
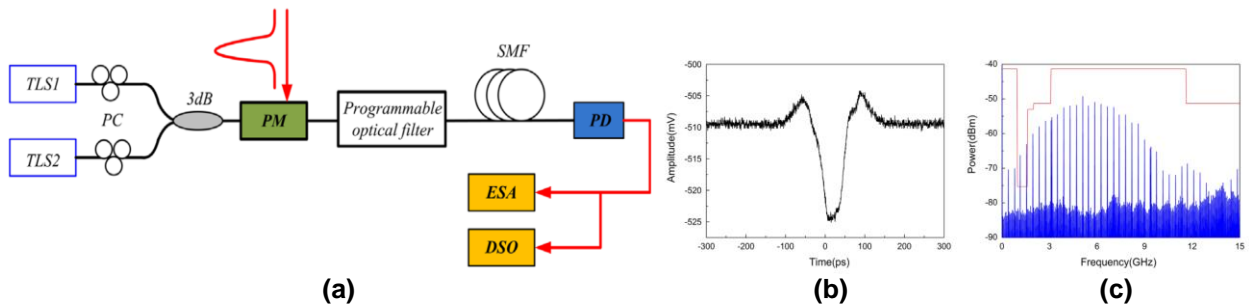
TLS: Tunable laser source; PM: Phase Modulator; SMF: Single mode fiber; PD: photodetector; ESA: Electrical spectrum analyzer; DSO: Digital Signal Oscilloscope.

Figure 28. (a) Schematic of a UWB pulse generator based on PM–IM conversion method (optical frequency discriminator). (b) Waveform of the generated positive Gaussian doublet pulse and (c) the PSD of a pulse train with repetition rate of 390.625 MHz is shown, (Chengliang Yang, Li Xia, Songnian Fu and Deming Liu, 2014-A).
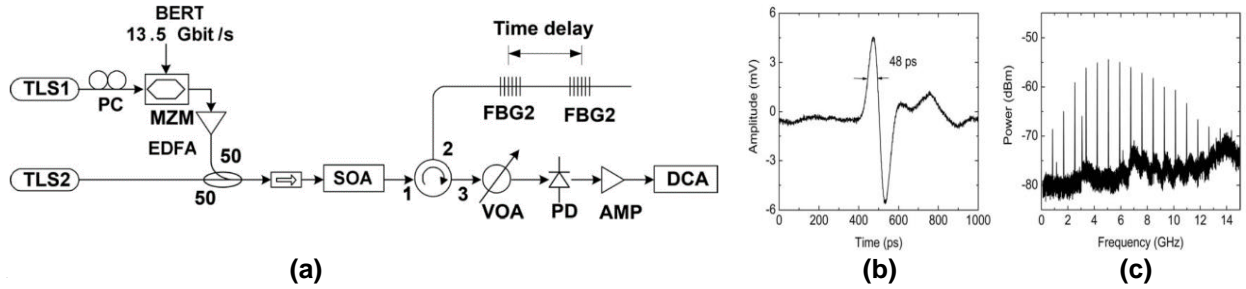
TLS: Tunable laser source; MZM: Mach Zehnder Modulator; BERT: Bit error rate tester; EDFA: Erbium Doped Fiber Amplifier; SOA: Semiconductor optical amplifier; FBG: Fiber Bragg grating; VOA: Variable optical attenuator; PD: Photodetector; AMP: Electrical amplifier; DCA: Digital communication.

Figure 29. (a) Schematic of a UWB pulse generator based on the XGM in a SOA. (b) Waveform of the generated positive Gaussian monocycle pulse and (c) the PSD of a pulse train with repetition rate of 0.84 GHz (Qing Wang, Fei Zeng, Blais, and Yao, 2006).
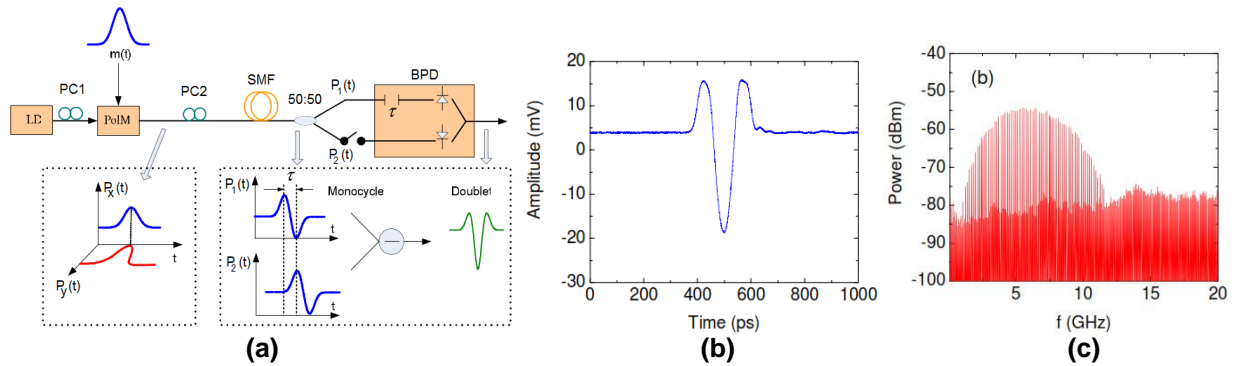
LD: Laser diode; PC: Polarization Controller; SMF: Single mode fiber; BPD: Balanced photo-detector.

Figure 30. (a) Schematic of a UWB pulse generator based on the polarization-to-intensity (Pol-to-IM) conversion and a length of SMF. (b) Waveform of the generated positive Gaussian doublet pulse and (c) the PSD of a pulse train with repetition rate of 156 MHz, (Qing Wang and Yao, 2007).
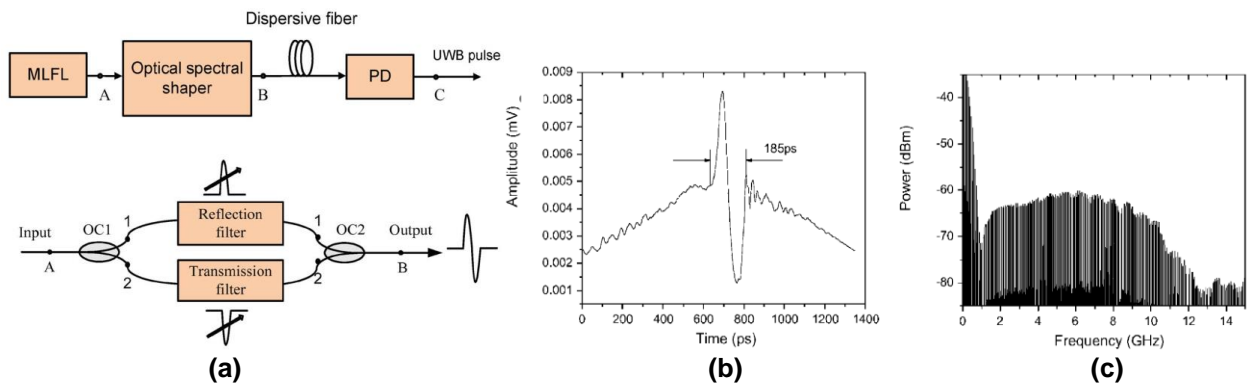
OC: Optical coupler; PD: photodetector; MLFL: mode-locked fiber laser.

Figure 31. (a) Schematic of a UWB pulse generator based on spectral shaping and frequency-to-time conversion and optical spectrum shaper configuration. (b) Waveform of the generated positive Gaussian monocycle pulse and (c) the power spectrum of the generated monocycle (Wang, Zeng, and Yao, 2007).

On the other hand, the second class is based on the nonlinear processing capability of some electrical or photonic components, after which the derivative of a pulse is achieved. For example, Wang and Yao (2006) take advantage of non-linear properties of an electro-optic Mach Zehnder Modulator (EO-MZM) to generate UWB doublets (see Figure 32). The non-linearities of semiconductor optical amplifiers (see Figure 33) such as the gain saturation effect (Dong et al., 2007, Weiwei Zhang, Sun Junqiang, Jian Wang, Cheng Cheng, and Xinliang Zhang, 2009, Gang Chen and Shilong Pan, 2012), four-wave-mixing (FWM), (Dong et al., 2008), cross-gain modulation (XGM), (Qing Wang, et al, 2006), and cross-phase modulation (XPM), (Jianji Dong, et al., 2007), have been also used to generate UWB monocycles and UWB doublets. Furthermore, various effects in highly nonlinear fiber (HNLF) such as pulse shaping with a nonlinear optical loop mirror (NOLM), (Huang, et al., 2008) (see Figure 34), nonlinear polarization rotation (NPR), (You Min Chang et al., 2010), optical parametric amplification (OPA), (Li, et al., 2009), and combined use of these techniques, (Chang et al., 2011), have also been investigated to generate the first and second derivative of a Gaussian pulse.
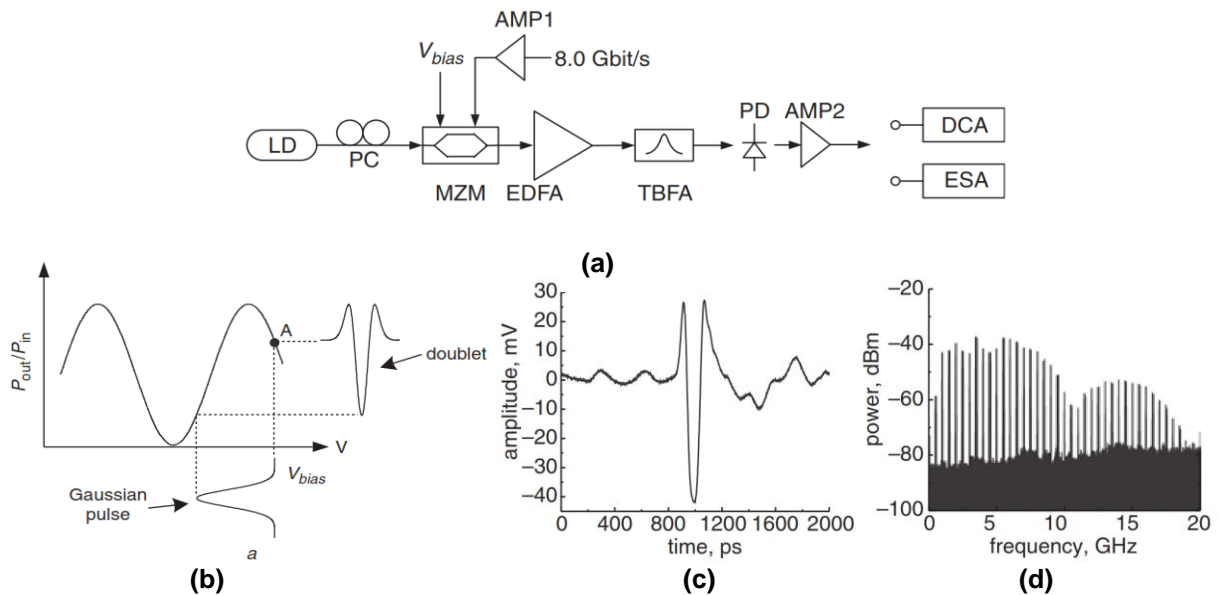
Figure 32. (a) Schematic of a UWB pulse generator based on the use of the nonlinear region of a Mach Zehnder modulator's transfer function. (b) Principle of operation to generate a positive Gaussian doublet pulse. (c) Waveform of the generated positive Gaussian doublet pulse and (d) the PSD of a pulse train with repetition rate of 500 MHz (Wang and Yao, 2006).

(a) ... **(b)** **(c)** **(d)** **(d)**
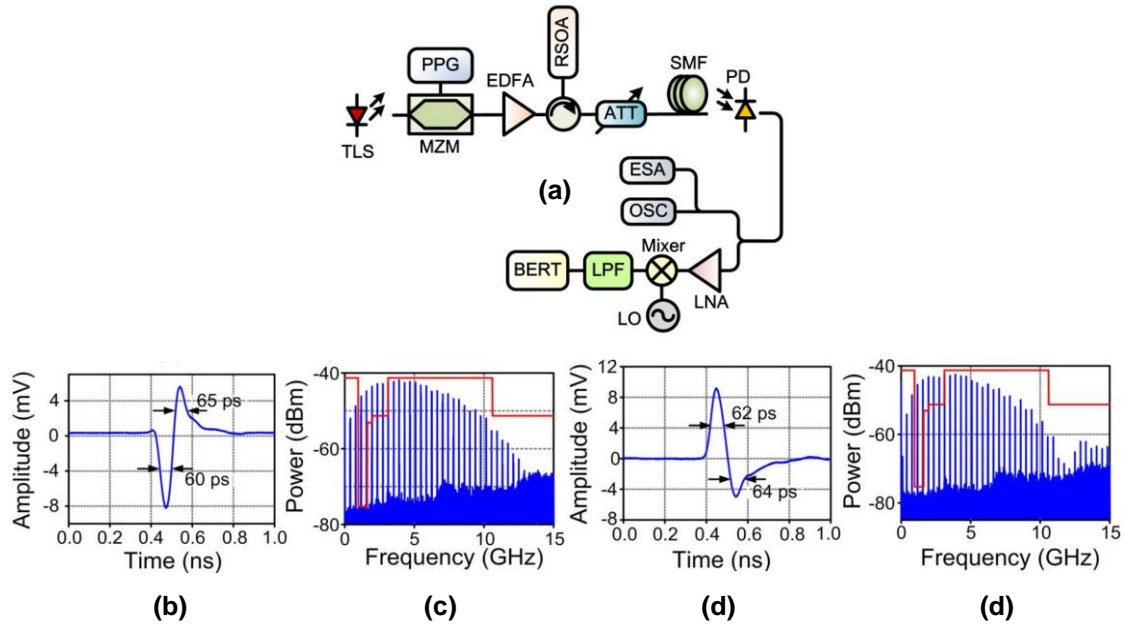
PPG: Pulse pattern generator; EDFA: Erbium Doped Fiber Amplifier; ATT: Optical attenuator; LPF: Low-pass filter.

Figure 33. (a) Schematic of a UWB pulse generator based on frequency-dependent gain saturation in a reflective semiconductor optical amplifier (RSOA). (b) and (d) are the waveforms generated by the optical configuration and (c) and (e) are the power spectrum, respectively (Gang Chen and Shilong Pan, 2012).
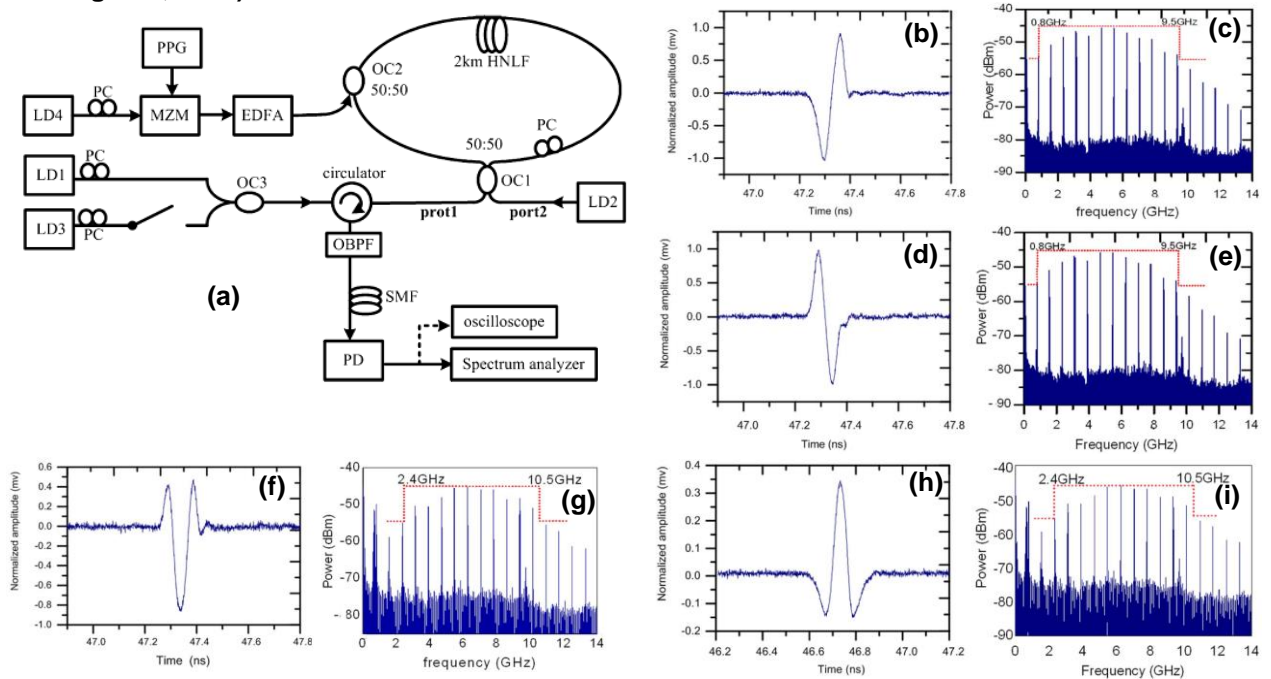
OC: optical coupler; LD: laser diode; PPG: pulse pattern generator; MZM: Mach–Zehnder modulator; PC: polarity controller; HNLF: high nonlinear fiber; PD: photo detector; OBPF: optical band-pass filter; SMF: single mode fiber.

Figure 34. (a) Schematic of a UWB pulse generator based on cross-phase modulation (XPM) effects in nonlinear optical loop mirror (NOLM). (b) and (d) are the generated positive and negative Gaussian monocycle pulses, respectively. (f) and (h) are the generated positive and negative Gaussian doublet pulses, respectively. The PSD of a pulse train with repetition rate of 780 MHz is shown for each waveform in (c), (e), (g) and (i), (Huang, et al., 2008).

As it can be seen, all techniques previously mentioned have been mainly proposed to generate UWB monocycles and UWB doublets. The authors of these works have chosen these kind of waveforms because of the simplicity for generating them, (Ghavami et al., 2007). Moreover, the IR-UWBoF systems using monocycles and doublets can achieve lower bit error rates (BER) and robust multipath resilience. However, the studies presented in (Villarreal-Reyes, 2007, Abraha et al., 2012, Zhu, et al., 2013) and several experimental demonstrations reported above show that these pulse shapes poorly exploit the permissible power under the FCC spectral mask without additional processing, resulting in limited wireless coverage. Thus, in order to overcome this limitation, higher-order derivatives of UWB pulses must be implemented. In this context, photonics techniques to generate triplets, quadruplets, quintuplets and complex signals compliant with the FCC spectral masks have been recently presented in the literature. For example, the work presented in (Xianbin Yu et al., 2009) shows a pair of methods based on the relaxation oscillations of a semiconductor laser (direct modulation laser and external injection of a laser) to generate complex signals whose PSD fit under the FCC indoor spectral masks (see Figure 35 and Figure 36). In (Bolea et al., 2009) the design of a reconfigurable and tunable N-tap photonic microwave filter that provide both positive and negative coefficients through a proper biasing of two EOM is presented. By using this scheme is possible to generate a 4-coefficients UWB pulse (triplet) complying with the requirements of the FCC spectral mask. Feng et al., (2014-A) have shown the generation of doublets and triplets by means of a reconfigurable orders UWB signals generation scheme based on the modification of the gain saturation effect of two cascade-connected reflective semiconductor optical amplifiers (RSOAs). The concept of PM-IM conversion with a dispersive device, (Zeng and Yao, 2006-A), and a fiber Bragg grating (FBG) operating as a frequency discriminator, (Zeng and Yao, 2005), is expanded by introducing an optical processor unit (OPU) presented by Moreno et al., (2014) and a FBG superstructure proposed by Moreno et al., (2015), respectively. Both optical configurations can generate triplets and quadruplets compliant with the indoor FCC spectral mask (see Figure 37 and Figure 38). Furthermore, some other works use the optical spectral shaping and frequency-to-time conversion concept to generate FCC compliant UWB pulses by using programmable optical spectral shapers as those reported by Abtahi et al., (2008-B), (2009) and Abtahi and Rusch, 2011 (see Figure 39 and Figure 40). In addition, linear sum

of modified doublet pulses, Abraha et al., (2011) (see Figure 41), chirp-to-intensity conversion, (Quang Trung Le t al., 2014), polarization-to-intensity conversion, (Zheng, et al., 2013), non-linear effects of optical components, (Dong et al., 2010), the chaotic dynamics of the optical feedback laser diode (OFLD), (Jian-Yu Zheng et al., 2010), the chaotic dynamics of an optically injected semiconductor laser with optical feedback, (Ming-Jiang Zhang, et al., 2011), and combination of different techniques previously mentioned are concepts also used to generate compliant FCC UWB signals. It can be seen that the photonics UWB pulse generation is an area widely studied due to optical technologies offer a viable alternative with several advantageous features such as light weight, small size, huge bandwidth, and the immunity to electromagnetic interference, (Yao, 2009). Despite of these advantages, it is important to mention that almost all of these methods require numerous optical components, their stability is very-dependent on environment factors, and most important, some of these methods can generate strong spectral lines in the PSD of signals modulated by modulation formats in which theoretically should not present any. As mentioned in Chapter 1, this spectral lines can deteriorate the system performance, since the transmit power is reduced in order to meet with the spectral masks. *Therefore, the design and implementation of low complex IR-UWBoF systems that simultaneously provide improved BER performance and convenient PSD characteristics is the main objective of this thesis work.*
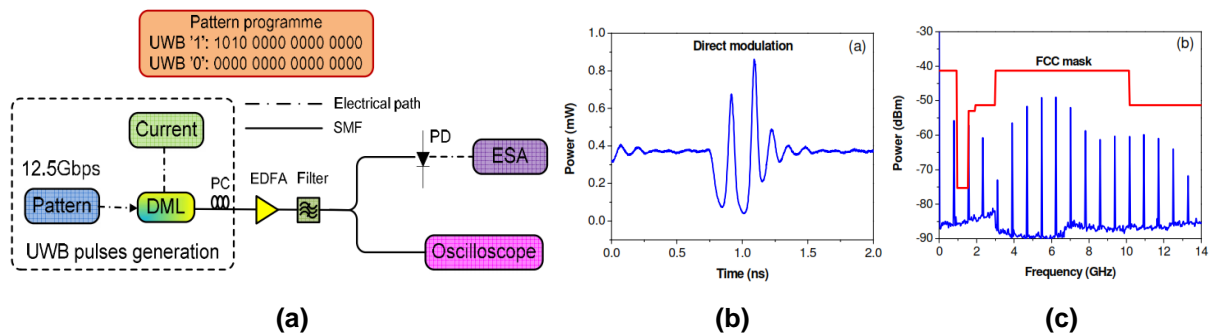
Figure 35. (a) Schematic of a UWB pulse generator based on the relaxation oscillations of a semiconductor laser (direct modulation laser method). (b) Waveform generated and (c) the corresponding PSD of an OOK signal, (Xianbin Yu, Gibbon, Pawlik, Blaaberg and Tafur Monroy, 2009).
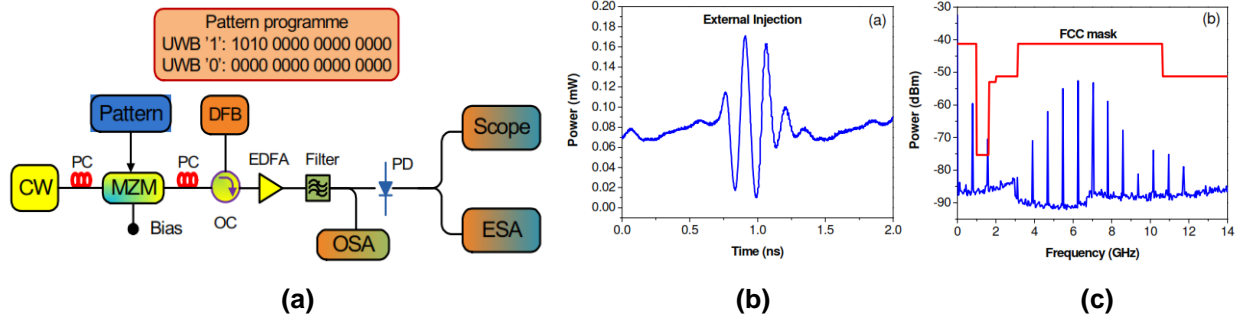
Figure 36. (a) Schematic of a UWB pulse generator based on the relaxation oscillations of a semiconductor laser (external injection of a laser method). (b) Waveform generated and (c) the corresponding PSD of an OOK signal, (Xianbin Yu, et al., 2009).
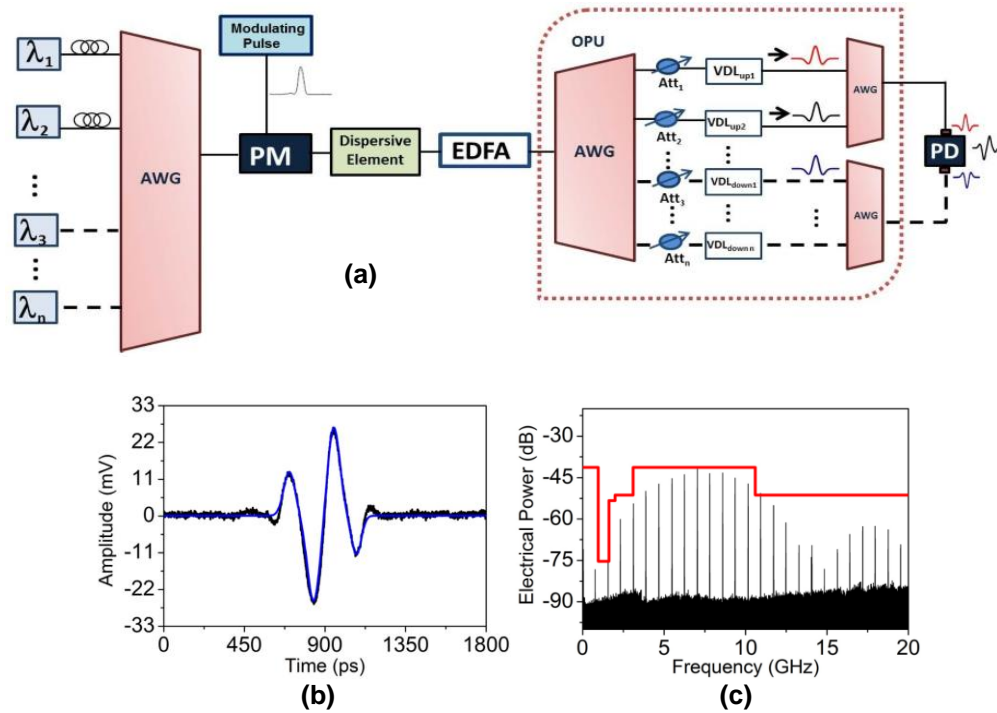
AWG: Array waveguide grating; PM: Electro-optic phase modulator; EDFA: Erbium doped fiber amplifier; Att: Optical attenuator; VDL: Variable delay line.

Figure 37. (a) Schematic of a scalable UWB pulse generator based on the combination of doublet pulses by using an optical processor unit (OPU). (b) Waveform of the generated Gaussian fifth-order derivative and (c) the PSD when OOK modulation format is used, (Moreno, Rius, Mora, Muriel and Capmany, 2014).
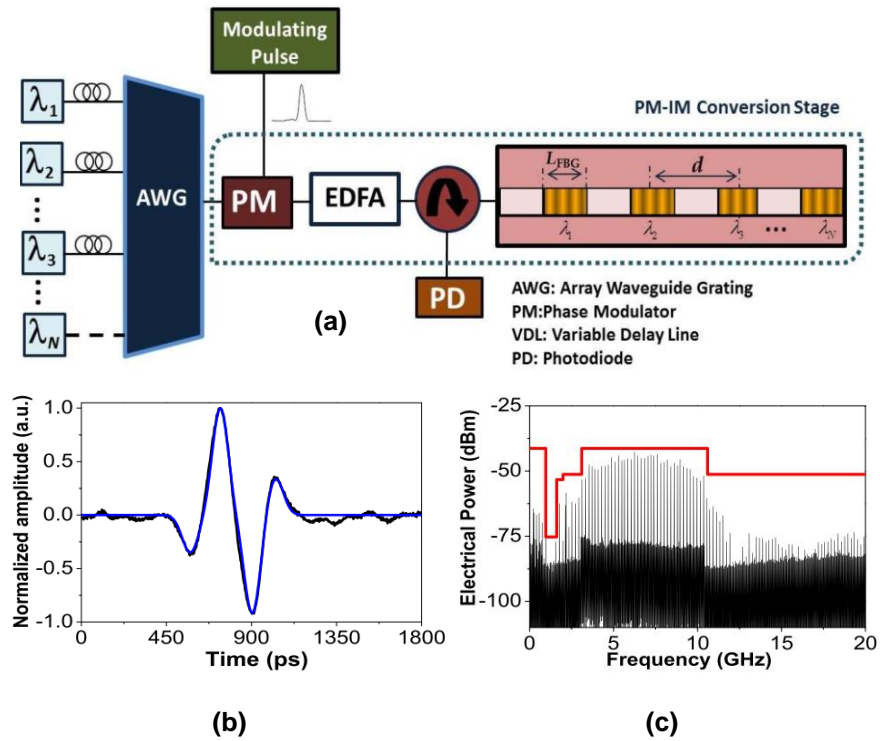
Figure 38. (a) Schematic of a scalable high-order UWB pulse generator employing a FBG-based photonic superstructure. (b) Waveform of the generated Gaussian triplet pulse and (c) the PSD of a periodic pulse train, (Moreno, Mora, and Capmany, 2015).

MLFL: Mode locked fiber laser; ISO: Optical isolator; ATT: Variable optical attenuator; DL: Optical delay line; BPD: Balanced photodetector.
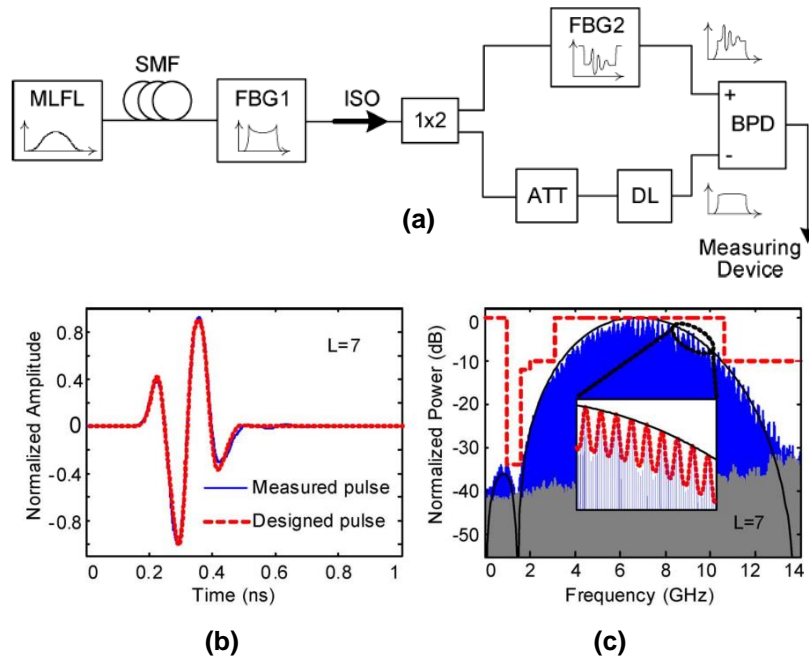
Figure 39. (a) Schematic of a UWB pulse generator based on fiber Bragg gratings (FBGS) and frequency-to-time conversion. (b) Measured UWB pulse and (c) the PSD of a periodic signal, (Abtahi, Magne, Mirshafiei, Rusch, and LaRochelle, 2008-B). The enlarged part shows the sinusoidal variations due to multiple reflections.
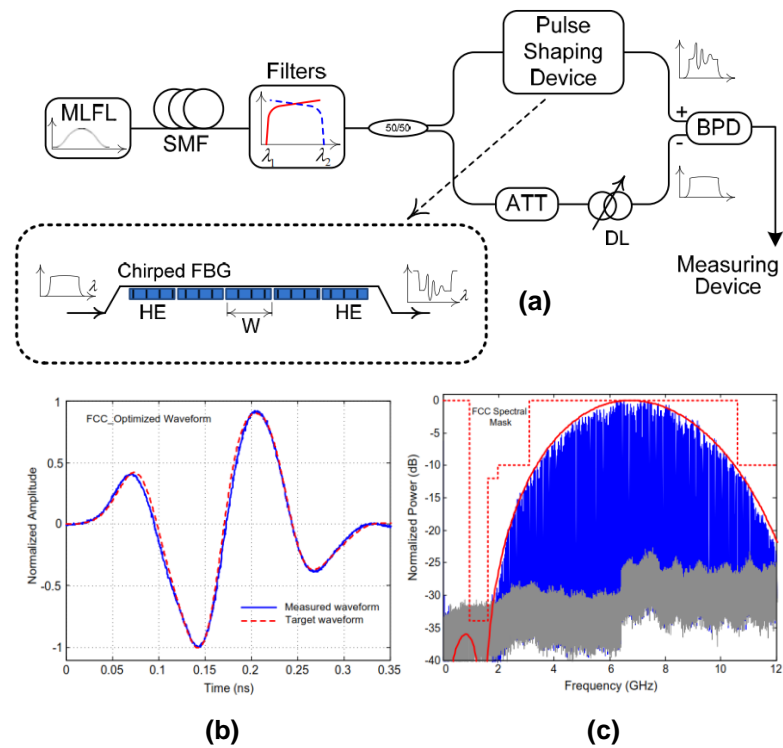
Figure 40. **(a) Schematic of a UWB pulse generator based on spectral pulse shaping using a FBG with temperature controlled apodization and frequency-to-time conversion, (Abtahi, Dastmalchi, LaRochelle and Rusch, 2009). (b) Measured UWB pulse and (c) the PSD of a periodic signal.**
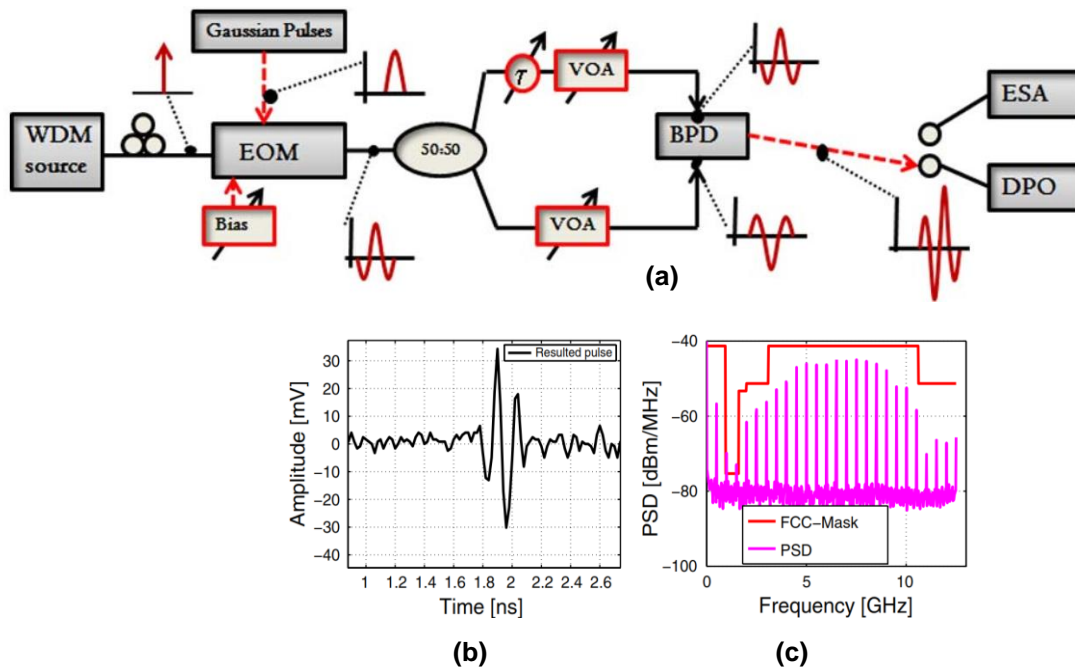
EOM: Electro-optic modulator; VOA: Variable optical attenuator; BPD: Balanced photodetector; ESA: Electrical spectrum analyzer. DPO: Digital phosphor oscilloscope

Figure 41. (a) Schematic of a UWB pulse generator based on the linear sum of modified doublet pulses. (b) Waveform of the generated pulse and (c) the PSD of a periodic pulse train with pulse repetition rate of 500 MHz, (Abraha, Okonkwo, Tangdiongga and Koonen, 2011).
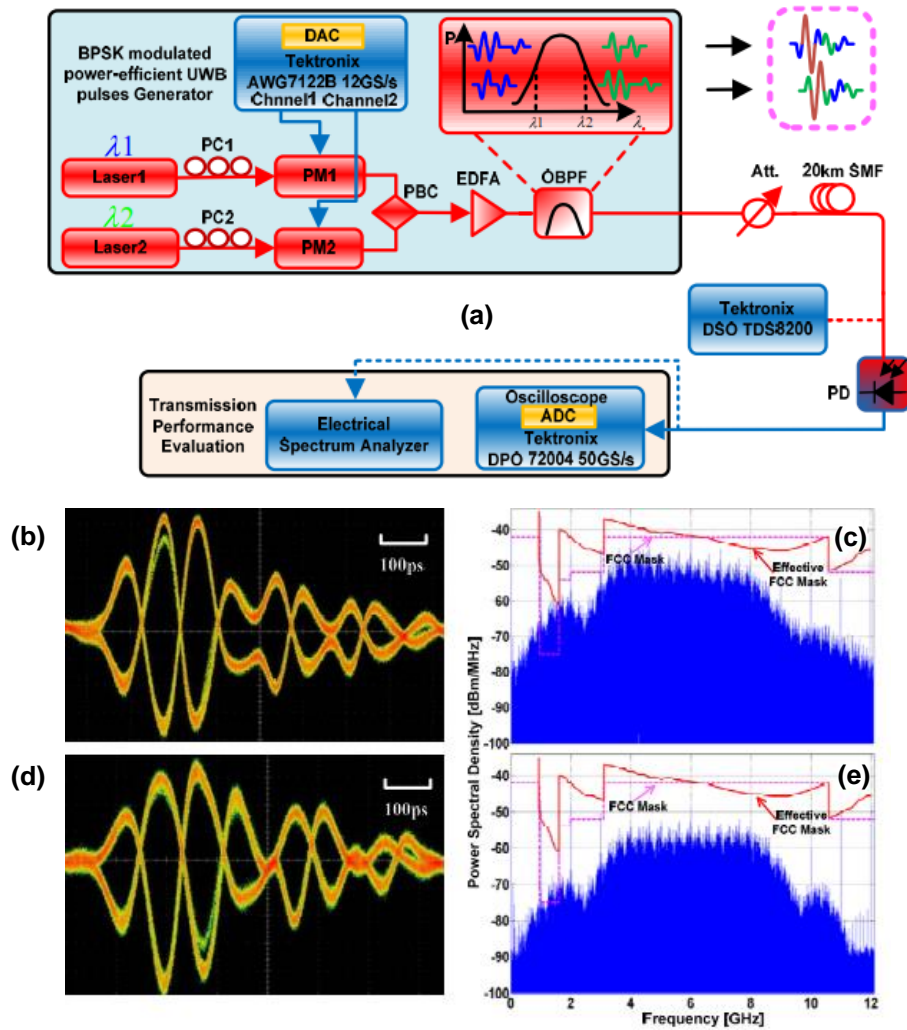
Figure 42. (a) Schematic of a UWB pulse generator based on the symmetric phase modulation to intensity modulation (PM-IM) conversion by incoherent summation of monocycle pulses with inverted polarities, proper time delays and adjustable absolute amplitude. (a) Eye diagrams and (b) electrical spectra of BPSK modulated UWB signals for L=5 in back-to-back; (d), (e) after 20-km SMF transmission, (Li, Chen, Chen and Xie, 2011).

2.6.2 Overview of photonics UWB signals transmission

As mentioned, the IR-UWBoF is a new cost-effective technique used to extend the range, to interconnect isolated UWB networks, and integrate UWB services into fixed wired or wireless communications networks, (Pan and Yao, 2010-A). The distribution of IR-UWB signals over fiber-wireless channels (that is, a channel formed of a length of optical fiber and a wireless link) has been considered for two main applications. One of these

applications are the distributed antenna systems (DAS), which can be implemented in buildings to extend the reach of UWB signals, (Abtahi and Rush, 2011). The fiber lengths used in these DAS are relatively short (tens of meters). The fiber lengths used in these DAS are relatively short (tens of meters). In the second application, the UWB signals are distributed from a central office (CO) to end-users using optical fiber transmission followed by wireless UWB transmission (Pan and Yao, 2011-A). The distances can be several kilometers (20-km and 30-km can be the distance from the local exchange to wireless user in households).

Table 3 provides an overview of the most representative practical implementations of high-data rate (HDR) IR-UWBoF systems mainly designed for distributing IR-UWB signals from a Central Office (CO) to remote antenna units (RAUs) separated by several kilometers of distance. As it can be seen in this table, the systems can offer variable data rates (from 500 Mbps to 3.125 Gbps) over fiber-wireless channels formed of different fiber lengths (5.6-km, 10-km, 20-km, 25-km and 59-km) of single-mode fiber (SMF), and typical wireless links implemented in WPAN scenarios (from 5-cm to 8-m). As noted, these IR-UWBoF implementations may cover the distribution of next generation multi-gigabit WPAN services discussed in previous subsections.

Furthermore, the information inputted in Table 3 indicates how the system performance of IR-UWBoF systems varies in terms of some important factors such as UWB pulse generation method, pulse shape, modulation format, wireless range, channel codification, and spectral shaping techniques. It can be noted from this table that monocycle and doublet generation methods have limited wireless coverage (from 5 cm to 45 cm) @ data rates greater than 1 Gbps. On the other hand, IR-UWBoF systems employing the fifth derivative of a Gaussian pulse, (Rodes, et al., 2010-A, Rodes, et al., 2010-B), or non-conventional pulses (NCP), (Lopez, et al., 2010), which are similar to this high-order derivative (see Figure 43a), can extend their wireless coverage up to 8 meters. In addition, it can be observed in Table 3 that photonics pulse generation methods can provide higher bandwidth (see Figure 43b) and better system performance (see Figure 43c) than methods based on electrical pulse generation with electrical to optical conversion (also compare the BER of the system presented by Pham et al., (2011) with those presented

by Li et al., 2012, for OOK modulation format). This fact can be attributed to bandwidth limitations of electrical components (e.g. arbitrary waveform generator, electro-optic modulator, coaxial cables) used to generate the UWB signal, (Lopez, et al., 2010). Despite the bandwidth limitation of electrical components, it is important to mention that the combination of the electrical UWB pulse generation method with direct intensity modulation (DIM) technique can potentially offer a less complex system than those all-optical IR-UWBoF systems, which it turns out more attractive for implementing low cost LDR-IR-UWB-WPANs. In addition, it should be noted that modulation formats play an important role in the system performance. In this context, it is well-known that the OOK modulation format generates pronounced spectral lines on the power spectral density (PSD) of IR-UWB signals, even when perfectly random (that is, an independent and identically distributed sequence of binary random variables with uniform distribution) data streams are used. This leads to lower efficiency of FCC spectral masks usage due to in most cases the transmit power must be decreased in order to comply with the spectral masks. Comparably, BPSK modulation format can provide an inherent modulation gain to communications, (Proakis, 1995), and a spectral line free (SLF) PSD when the transmitted data streams are perfectly random (Villarreal-Reyes, 2007). Thus, a more efficient use of the UWB spectral masks with considerable improvement of the BER parameter can be obtained when the BPSK format is used. For example, the work reported by Pan and Yao (2010-B) shows that the BER performance measured in a BPSK IR-UWBoF system is better than the BER performance provided by an IR-UWBoF system that implement the OOK modulation format. It can be seen that the use of BPSK could save energy and reduce the whole cost of the system since that optical amplifiers could be omitted. As well, note that most of the IR-UWBoF implementations shown in Table 3 only implement the pulse shape based spectral shaping (PS-SS) technique for fulfilling with the spectral masks. The works reported by Rodes et al., (2010-A) and (2010-B) generate the fifth derivative of a Gaussian pulse by using an electrical 9.6 GHz arbitrary waveform generator (E-AWG). As demonstrated by Sheng, Orlik, Haimovich, Cimini, and Jinyun Zhang (2003), the energy spectral density (ESD) of this waveform and high-order derivatives fulfill entirely with the FCC spectral masks. Therefore, the IR-UWBoF system presented by (Lopez, et al., 2010) also generates a UWB pulse similar to fifth-order derivative, however in this case, by using an optical method based on the relaxation oscillations of an optically

injected DFB laser (RO-OI-DFB) presented in Figure 36, (Xianbin Yu et al., 2009). It is important to note that the combination of the PS-SS method with BPSK signals would allow increasing the signal's transmit power without violating the spectral masks, and in this way, to extend the range in the wireless links. On the other hand, some other works implement a novel optical spectral shaping technique based on chaotic dynamics of an optical feedback laser diode in order to generate a SLF-PSD with OOK modulated IR-UWB signals. Despite this method is simple, the SLF-PSD does not fit under the spectral masks, in particular over the GPS frequency band. Therefore, additional electrical components as high-pass filters (HPF) should be used. It is worth noting that almost all IR-UWBoF systems reported in the literature do not use forward error correction (FEC) schemes to protect the transmitted signals against the impairments caused by the fiber-wireless channel. The authors of these works expose that FEC mechanisms are not necessary because of the bit error rate (BER) measured in their systems does not exceed the called FEC limit, which is about $2x10^{-3}$. However, such as mentioned in Subsection 2.2.3, there exist some applications in next generation of Home Area Networks (HANs), (Guillory, 2012) and also in the next generation of telemedicine systems, (Chowdhury et al., 2011) that to provide acceptable levels of Quality of Service (QoS) require at least a BER about $1x10^{-6}$ as mentioned by Fong, Fong, and Li (2010) and Deepak Kumar Mohapatra (2013). *Therefore, we expect that the inclusion of error correction mechanisms also will become a standard for IR-UWBoF systems in the near future*.

As an additional comment, the state of the art of IR-UWBoF systems considers the integration of these systems with next generation wavelength division multiplexing (WDM) passive optical networks (PON). Nowadays the concept known as IR-UWB over WDM-PON has started to be widely researched with the aim to provide wired services and IR-UWB signal distribution over the same infrastructure. Recently, the authors in (Pan and Yao, 2010-C, Pan and Yao, 2011-B) have demonstrated that an electrically generated UWB signal can share a single wavelength with a baseband signal in a WDM-PON system. Furthermore, Prince, et al. (2009) have also demonstrated seamless integration of a UWB service in a WDM-PON system that supports a variety of wired and wireless services. Some photonics UWB pulse generation methods have also been implemented in WDM-PON architectures, (Pan and Yao, 2011-A). For example photonic microwave

bandpass filter, (Pan and Yao, 2011-A), method based on relaxation oscillations of a directly modulated laser (DML), (Pham et al., 2011, Xianbin Yu, et al., 2013), and tunable chirped FBG with optical spectrum shaping followed by frequency-to-time conversion have been used to generate optimally power efficient IR-UWB waveforms, (Abtahi and Rush, 2011).This latter concept is an interesting proposal because of waveforms that comply with FCC spectral masks and compensates optical fiber dispersion and/or frequency responses of low cost UWB antennas can be designed in order to maximize the permissible transmit power under the spectral masks. Despite of these benefits, this technique can be deteriorated by environmental temperature variations and the cost of implementation can be high. It is important to mention that there exist other implementation of IR-UWB over fiber systems operating at millimeter waves such as (Chang et al., 2008, Xu et al., 2009, Beltran et al., 2011-A, Beltran et al., 2011-B, Chow et al., 2010). However, as mentioned before, the implementation of these systems is still complex and expensive. Therefore, the design of both HDR and LDR IR-UWB over fiber systems that simultaneously comply with spectral masks and the BER required by next generation applications is a topic of major interest in this area.
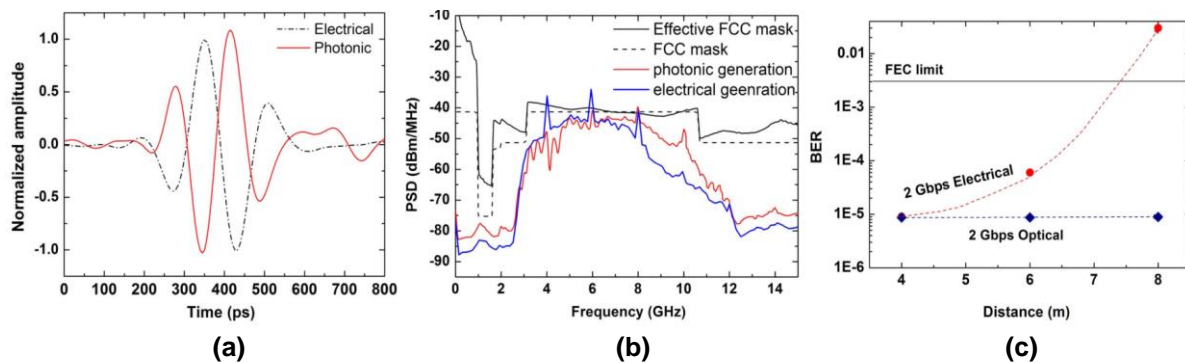
Figure 43. Comparison of electrical and photonic UWB pulse generation methods and their transmission over fiber-wireless channels. (a) Measured pulses generated by both methods (electrical and photonic). (b) Measured PSD of both pulses modulated by OOK format. (c) Experimental BER results of electrical and photonic generation systems. All results were measured after 20-km NZDSF, (Xianbin Yu; Gibbon, Rodes, Tien-Thang Pham; Monroy, 2013).

Table 3: Overview of IR-UWB over fiber systems

Data Rate (Gbps)	Fiber type (km)	Wireless reach (cm)	Pulse Generation Technique	Pulse shape	Modulation format	Channel Codification	Spectral shaping technique	BER Modulation (ROP)	Reference
0.5	SMF(5.6)	65	PS-FTT	NCP	OOK	NO	PS-SS	3×10^{-6}	(Abtahi, 2008-A)
0.625	SMF(20)	10	2-tap and 3-tap PMDLF	Monocycle and Doublet	OOK/BPM	NO	NO	$< 1 \times 10^{-3}$ OOK (-10.5 dBm) BPM (-12.8 dBm)	(Pan and Yao, 2010-B)
1.0	SMF(20)	5	E-AWG + PM-IM	NCP	OOK,BPM	NO	PS-SS	$< 1 \times 10^{-3}$ OOK (-4.3 dBm) BPM (-5.0 dBm)	(Li et al., 2012)
1.0	SMF(23)	40	RO-OI-DFB	NCP	OOK	NO	PS-SS	$< 1 \times 10^{-3}$ OOK (-15.5 dBm)	(Pham et al., 2011)
1.025	SMF(10)	20	PS-FTT	Modified Doublet	OOK	NO	PS-SS and SC-DCF with BPTSA	1×10^{-4}	(Hanawa et al., 2009)
1.25	SMF(25)	45	NLE in HNLF (NPR of a EPB)	Doublet	OOK	NO	NO	2×10^{-3}	(You Min Chang et al., 2010)
1.25	NZDSF (20)	35	NLE in HNLF (NPR + OPA)	Doublet	OOK	NO	NO	2×10^{-3}	(Chang et al., 2011)
1.44	SMF(20)	60	OFLD	NCP	OOK	NO	CL-SS	1×10^{-6}	(Zhang et al., 2013)
1.70	SMF(24)	5	2-tap PMDLF	Monocycle	OOK	NO	NO	$<1 \times 10^{-3}$ OOK ROP(-10.5 dBm)	(Pan and Yao, 2009)
2.0	SMF(25)	400	E-AWG + DIM	5th derivative	BPM	NO	PS-SS	4.9×10^{-4}	(Rodes, et al., 2010-B)
2.0	NZDSF (20)	800	E-AWG + DIM	5th derivative	OOK	NO	PS-SS	2×10^{-3}	(Rodes, et al., 2010-A)
2.0	NZDSF (20)	800	RO-OI-DFB	Similar to 5th derivative	OOK	NO	PS-SS	1×10^{-5}	(Lopez et al., 2010)
2.5	SMF(59.2)	0	PM-IM	Monocycle	OOK	LPDC	NO	1×10^{-8}	(Sakib et al., 2011)
3.125	SMF(25) + IDF(25)	310	RO-OI-DFB	NCP	OOK	NO	PS-SS	7.02×10^{-6}	(Gibbon et al., 2010)

NZDSF: Non-zero dispersion shifted fiber; **DCF**: Dispersion compensation fiber; **IDF**: inverse dispersion fiber; **HNLF**: highly nonlinear fiber; **ROP**: Received optical power; **OOK**: On-Off Keying; **BPM**: Binary phase modulation; **NCP**: Non-conventional pulse; **PM-IM**: Phase-modulation-to-intensity modulation conversion; **PMDLF**: Photonic microwave delay line filter; **PS-FTT**: Pulse shaper-frequency-to-time conversion; **RO-OI-DFB**: Relaxation oscillations of an optically injected DFB laser; **NLE**: Nonlinear effect; **OFLD**: chaotic dynamics of an optical feedback laser diode; **NPR**: nonlinear polarization rotation effect; **OPA**: optical parametric amplification effect; **EPB**: Elliptically polarized beam; **DIM**: Direct Intensity Modulation; **EIM**: External Intensity Modulation; **PS-SS**: Pulse shape based spectral shaping; **CL-SS**: Chaotic laser based spectral shaping; **LPDC**: Low parity density codes; **E-AWG**: Electrical arbitrary waveform generator; **E-IFN**: Electrical Impulse Forming Network; **SC-DCF**: Slope compensation-DCF; **BPTSA**: Bandpass tapered slot antenna.

2.7 Spectral characteristics of IR-UWBoF systems

As previously mentioned, the compliance with the spectral masks issued by radio spectrum regulatory bodies is one of the main constraints when designing compliant IR-UWB systems. In this context, the proposed optical configurations to generate high-order derivatives UWB pulses discussed in Subsection 2.6.1 and the IR-UWBoF systems reported in Table 3, in particular those using some kind of spectral shaping technique, would represent a good choice to deploy compliant IR-UWB over Fiber systems. However, as it can be seen in Figures 3, 35, 36, 38, 41, 42, 44, 45, and 46, these photonic UWB pulse generation methods and IR-UWBoF systems also exhibit some strong spectral lines at low-frequencies region violating the FCC indoor spectral mask. As already mentioned, the problem with the spectral lines presence is that the maximum achievable transmit power has to be reduced in order to comply with the spectral masks. It is evident that an IR-UWB system with a spectral line free (SLF) PSD will be able to transmit with more power over the wireless link than an IR-UWB system whose PSD shows spectral lines. Furthermore, as it is well-known, theoretically, when using BPSK (which is equivalent to BPM, Bi-phase modulation) and the input data stream consists of binary data i.i.d. with uniform distribution, the PSD should not show any spectral lines, (Villarreal-Reyes, 2007). Nevertheless, as can be seen in Figures 3, 42, 44, 45, and 46 the IR-UWBoF systems can generate spectral lines, even when they are using BPSK schemes with pseudorandom binary sequences (PBRS) of very long period. In addition, strong spectral lines in the PSD of BPSK signals naturally appear when the binary data stream is not perfectly random, which is the most commonly observed case because of not all the data sources or compression algorithms found in practical systems generate uniformly distributed i.i.d. binary data streams. Thus, to fully exploit the maximum transmit power allowed by the spectral masks, it is desirable to design IR-UWBoF schemes whose PSD is SLF, this even when the data stream is not random.
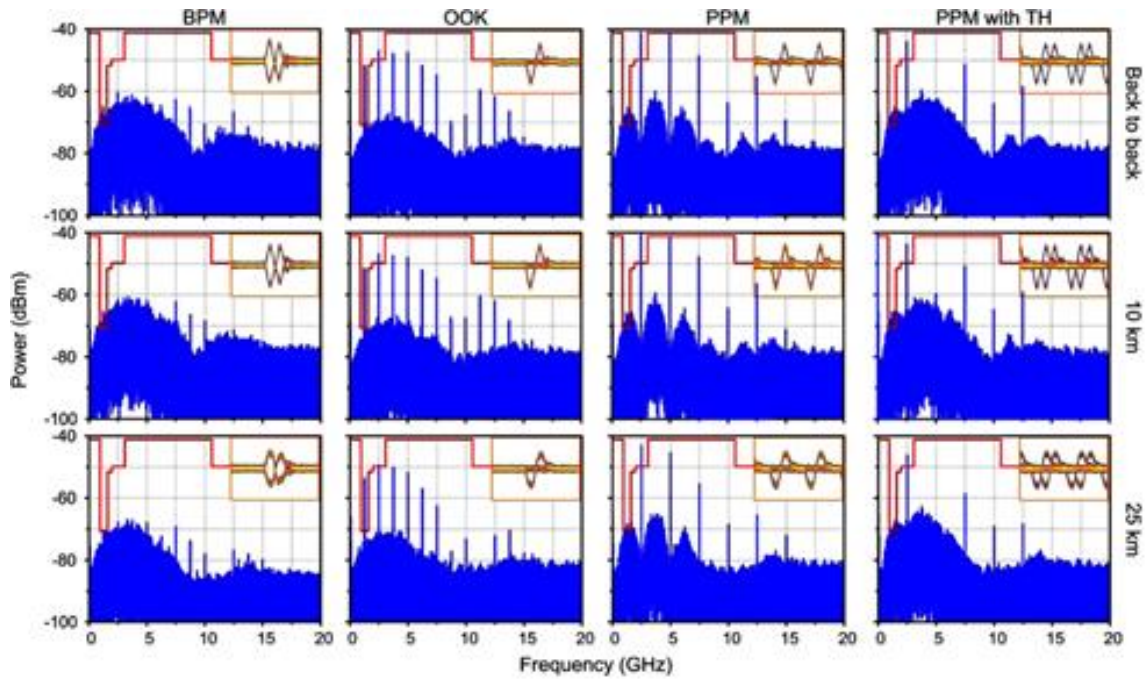
Figure 44. Eye diagrams and the electrical spectra of the UWB signals generated by the PolM-based photonic microwave bandpass filter with back-to-back, 10-km and 25-km of SMF transmissions. The UWB signals are generated using the PolM-based photonic microwave filter. The resolution bandwidth of the spectrum was configured at 1 MHz and the span of the eye diagrams was 1 ns (Pan and Yao, 2011-A).
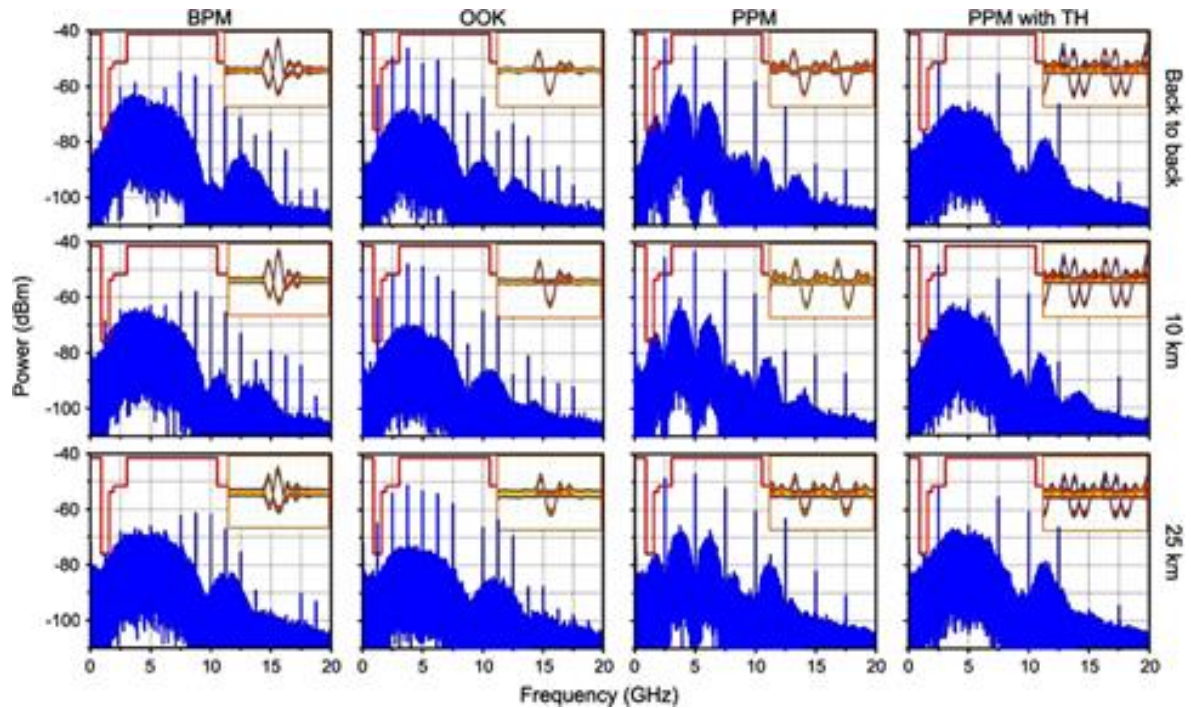
Figure 45. Eye diagrams and the electrical spectrum of the UWB signals generated by the PM-based photonic microwave bandpass filter before and after 10-km and 25-km SMF transmission. The resolution bandwidth of the spectra is 1 MHz and the span of the eye diagrams is 1 ns, (Pan and Yao, 2011-A).
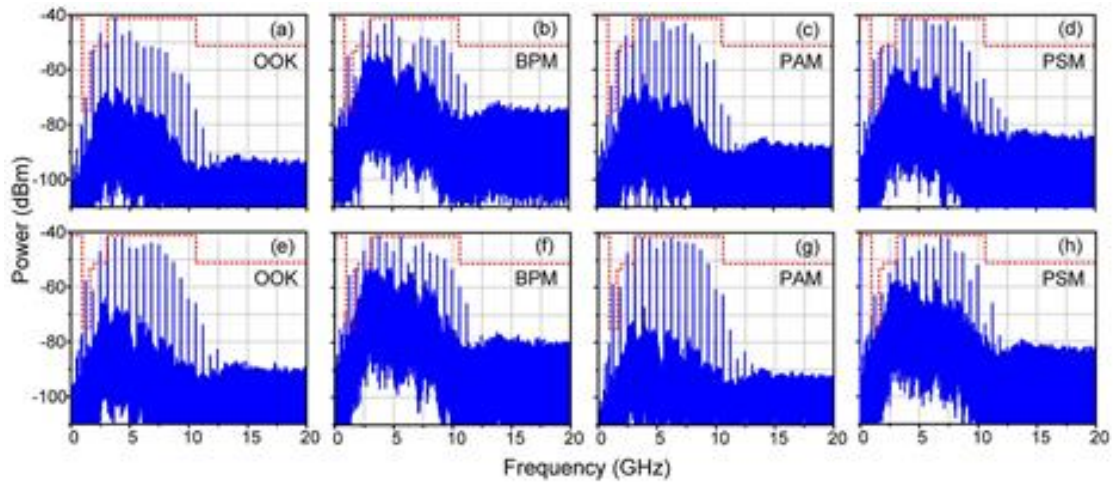
Figure 46. Electrical spectrum of the UWB signals with OOK, BPM, PAM, and PSM schemes (a)–(d) with wireless transmission; (f)–(j) with 20-km SMF and wireless transmission, (Pan and Yao, 2010-A).
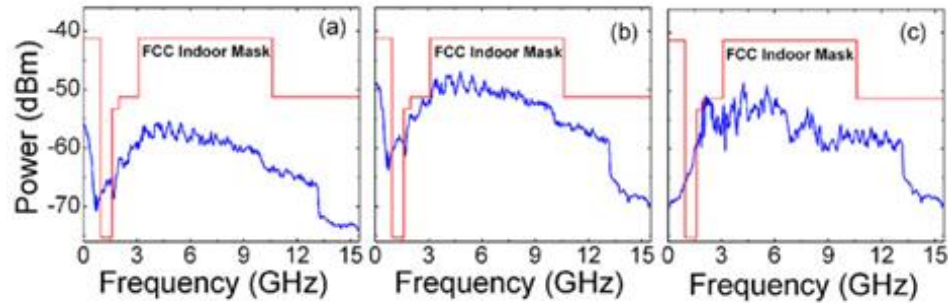
Figure 47. Power spectrum transmitted over 20-km fiber before amplified by EDFA (a), after amplified by EDFA (b), and after received by UWB antenna (c), (Zhang et al., 2013).
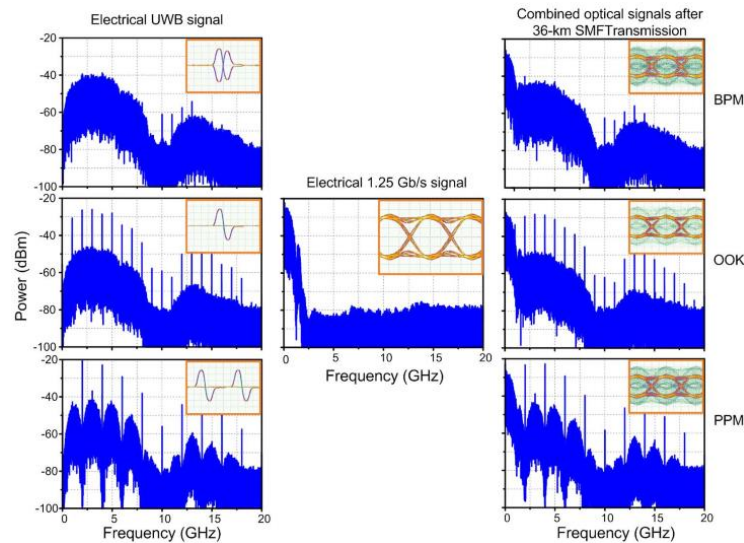
Figure 48. Eye diagrams of the 1-Gb/s electrical UWB signals with OOK, BPM, and PPM, the electrical 1.25-Gb/s wired signal, and the combined optical signals, (Pan and Yao, 2010-C).

Recently, an IR-UWBoF system able to generate a spectral line free PSD was reported by Zhang et al, (2013). The system is based on the chaotic dynamics of the optical feedback laser diode (OFLD) to implement generation of the photonic chaotic-UWB signal with OOK format. Despite the great advantage offered by this technique, the generated SLF PSD does not fit under the FCC spectral masks (see Figure 47). On the other hand, the IR-UWBoF systems using optical transmission methods such as direct and external intensity modulation with direct detection (IM/DD) technique are very attractive due to low-cost and low-power consumption deployments can be achieved. Furthermore, as can be seen in Figure 48, the PSD of a BPSK IR-UWB signal, which is formed by a pseudorandom sequence with very long period, does not present any spectral line after 36-km SMF transmission. However, as already mentioned, not all the data sources or compression algorithms found in practical systems generate perfectly random binary data streams which certainly would generate spectral lines in the PSD. Therefore, simple IR-UWBoF systems able to provide both SLF-PSD and bit error rate (BER) improvement over non-coded IR-UWBoF systems are required. *The design and implementation of IR-UWB over fiber system for LDR and HDR applications that meet with the characteristics above mentioned will be analyzed and experimentally evaluated in next chapters.*

Chapter 3. Proposal of IR-UWBoF systems with spectral line suppression capabilities

3.1 Introduction

In this chapter the design (system model) and simulation-based implementation of low-complex impulse radio (IR) ultra-wideband (UWB) over fiber (IR-UWBoF) systems with spectral line suppression capabilities are provided. These IR-UWBoF systems deals with both methods, direct and external, intensity modulation with direct detection (IM/DD) to transmit FCC-compliant IR-UWB signals through several kilometers of single mode optical fiber (SMF). The spectral shaping capabilities of proposed systems are qualitative evaluated by means of an all-configurable IR-UWBoF-IM/DD testbed implemented in the *VPITransmissionMarker^{TM}* simulation software from VPIphotonics Company. The results obtained provide preliminary information about the impact of the chromatic dispersion in the proposed systems.

3.2 System Model

An important topic that requires major consideration in the design of FCC-compliant IR-UWB systems is the selection of the waveform. As it was analyzed by Villarreal-Reyes (2007) and Arslan et al., (2006), the energy density spectrum (EDS) of the UWB pulse dictates the overall form acquired by the PSD of the IR-UWB signal. Furthermore, the waveform can determine the complexity of the pulse generation circuitry, the impact of co-existence with other spectrum users and the whole performance of the IR-UWB system, (Di Benedetto et al., 2006). Several waveforms have been proposed for IR-UWB systems. As discussed in previous chapter, the basic waveforms used in most of the original papers introducing IR-UWB systems and IR-UWBoF systems were the first and second order derivatives of the Gaussian pulse (monocycle and Gaussian doublet respectively), (Win and Scholtz, 1998, Win and Scholtz, 2000). This is due to better bit error rates (BERs) and robust multipath resilience that can be obtained as compared to different impulse signals, (Scholtz, 1993). However, the spectrum of these simple Gaussian shapes do not fit under the proposed FCC's limits. Therefore, high-order derivatives such as the fifth-order derivative of a Gaussian pulse was proposed to fit under the FCC spectral mask for indoor environments, (Sheng et al., 2003, Rodes et al., 2010-A). Therefore, the fifth-order

derivative will be considered in this work, unless otherwise stated. This waveform can be defined as (Sheng et al., 2003)

$$w_{G,5}(t) = A\left[-\frac{t^5}{\sqrt{2\pi}\sigma^{11}} + \frac{10t^3}{\sqrt{2\pi}\sigma^9} - \frac{15t}{\sqrt{2\pi}\sigma^7}\right] \times \exp\left(-\frac{t^2}{2\sigma^2}\right) \tag{14}$$

where σ can be used to control the pulse duration (see Figure 49). The amplitude spectrum of Equation (14) is

$$\left|W_{G,5}(f)\right| = A(2\pi f)^5 \times \exp\left(-\frac{[2\pi f\sigma]^2}{2}\right) \tag{15}$$
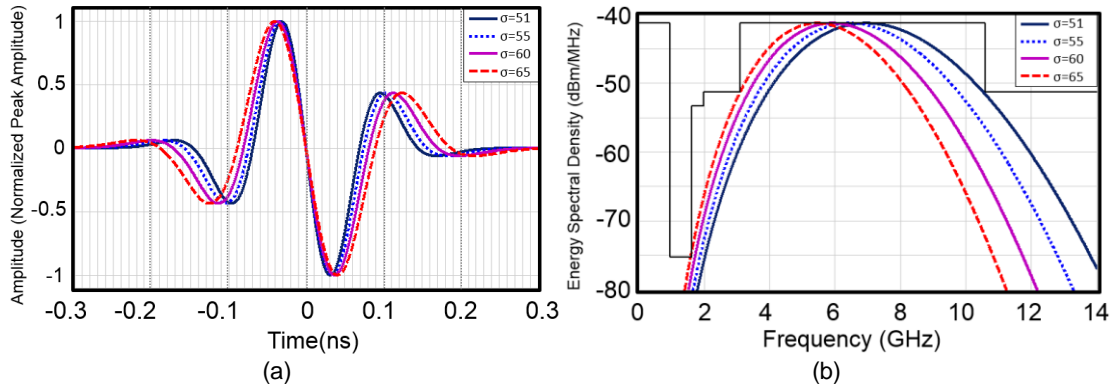
Figure 49. (a) Waveforms of the fifth-order derivative of a Gaussian pulse with σ=51 ps (dark plot), σ=55 ps (dotted blue plot) σ=60 ps (light plot) and σ=66 ps (dotted red plot). (b) Energy spectral density (ESD) of the waveforms described in (a).

It can be seen in Figure 49 as different values of σ (from 51 ps to 65 ps) change the pulse duration (t_{wT}) of the fifth-order derivative and its maximum peak emission frequency (f_M) of the energy spectral density (ESD) in time and frequency domain. Furthermore, the bandwidth (BW) measured at -10 dB of the ESD is also decreased. For example, a value of σ=51 ps substituted in equations 14 and 15 gives as result: t_{wT}≈500 ps, f_M=7.01 GHz and BW=6.612 GHz. On the other hand, substituting a value of σ=65 ps gives as result t_{wT}≈600ps, f_M=5.475 GHz and a BW=5.187 GHz. Note in Figure 49(b) that obtained values of t_{wT} have outlined the upper and lower limits for generating the fifth-order derivative pulse. Therefore, these values will be considered in the proposed system.

As noted in previous chapters, the IR-UWBoF systems can be formed of an IR-UWB transmitter similar to that shown in Figure 19 and some of the radio over fiber (RoF) architectures described in subsection 2.2.2 and subsection 2.6.1.

The system models proposed in this thesis work are shown in Figure 50 and Figure 51. These models only take into account downlink communications from a Central Node (IR-UWB transmitter and electrical-to-optical conversion process) to the RAU (optical-to-electrical conversion process) considering an optical transmission of several kilometers of single mode fiber (SMF). In order to offer a clear explanation of the proposed system models, these are subdivided in IR-UWB transmitter and RoF architecture.
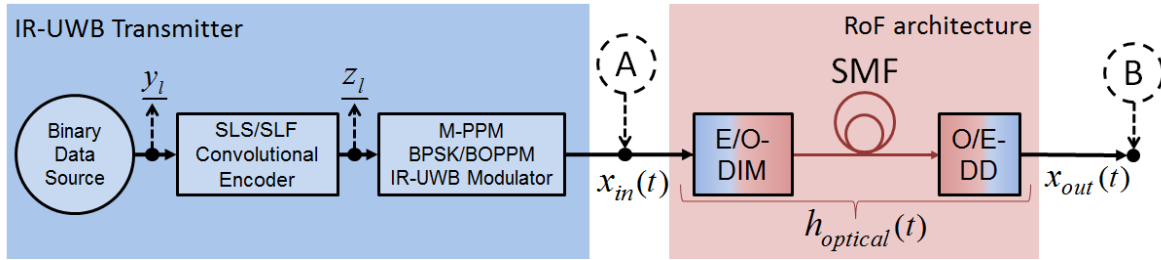
Figure 50. IR-UWBoF-DIM/DD system model.
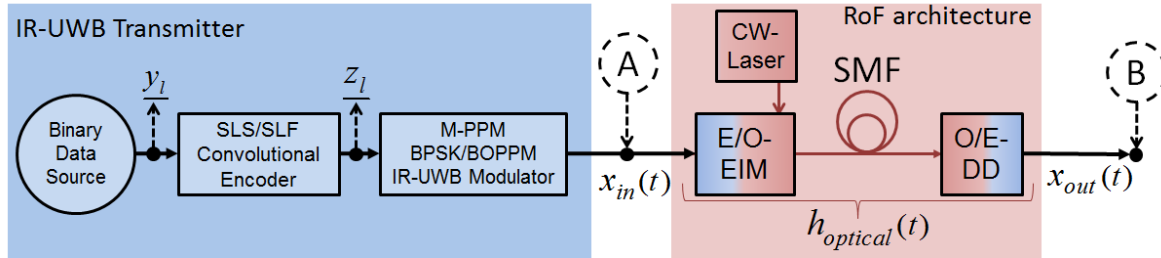
Figure 51. IR-UWBoF-EIM/DD system model.

Explaining the IR-UWB transmitter, the binary data source (BDS) is modelled by the first-order binary Markov source (BMS) such that depicted in Figure 52.
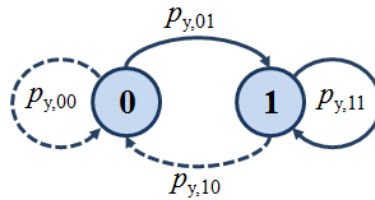
Figure 52. First order binary Markov source (BMS) model.

Typically the BMS model is used to generate balanced ($p_0=p_1=1/2$) and non-balanced (e.g. $p_0 \neq 1/2$ and $p_1 = 1-p_0$) independent identically distributed (i.i.d.) binary data streams. This characteristics is important because it is possible to model different kinds of data source present in practical implementations. Note that when $p_0=1/2$, the binary data stream, y_l, is considered as perfectly random (that is, the data stream is an i.i.d sequence of binary random variables with uniform distribution). However, as pointed out in (Pan and Yao, 2010-A), this condition is very hard to keep in practical IR-UWBoF systems.

The one step transition probabilities from this BMS can be represented as (Villarreal-Reyes, 2007)

$$p_{y,ii'} = \Pr\{y_l = i' | y_{l-1} = i\} \tag{16}$$

and

$$p_{y,00} = 1 - p_{y,01}; \qquad p_{y,11} = 1 - p_{y,10}; \tag{17}$$

where y_l and y_{l-1} is the current and the previous symbol produced by the BMS, respectively. The $p_{y,ii'}$ indicates the probability of being in state i and after one transition reach state i'. In addition, this BMS model can be defined by both the one step transition probability matrix

$$\mathbf{P} = \begin{bmatrix} p_{y,00} & p_{y,01} \\ p_{y,10} & p_{y,11} \end{bmatrix} \tag{18}$$

and the initial probability mass function $p_{y,i}^{(0)}$. Furthermore, the corresponding steady state (stationary) probabilities for this Markov chain (MC) can be found to be

$$\underline{\pi}_y = [\pi_{y,0} \ \pi_{y,1}] = [\frac{p_{y,10}}{p_{y,01} + p_{y,10}} \ \frac{p_{y,01}}{p_{y,01} + p_{y,10}}] \tag{19}$$

where $\pi_{y,0}$ and $\pi_{y,1}$ are the steady state probabilities (SSP) of generating a "0" and a "1" respectively. It is important to mention that for simplicity, our system model assumes that the MC has reached steady state and $p_{y,0}^{(0)} = \pi_{y,0}$ with $p_{y,1}^{(0)} = \pi_{y,1}$. Note that the source model

covering the i.i.d memoryless case, which will be used in this thesis work ($0<p_0<1$ and $p_1=1-p_0$), is obtained by setting $p_{y,01}=p_{y,11}=p_1$, with $p_{y,00}=p_{y,10}=p_0$, $\pi_{y,0} = p_{y,10}$ and $\pi_{y,1} = p_{y,01}$.

Once defined the BDS, the data stream, y_l, is fed to either of the convolutional encoders proposed in this thesis. A rate $1/4$ spectral line suppressive (SLS) convolutional encoder (CE) and a rate $1/2$ spectral line free (SLF)-CE are used to eliminate spectral lines in the PSD of M-PPM and BPSK/Q-BOPPM modulated signals, respectively. The main characteristics of these CEs were discussed in Section 2.5. Moreover, a deeply spectral analysis can be consulted in (Villarreal-Reyes, 2007). Figure 53 shows the generic diagram of both CEs where v is the encoder memory, κ is the number of outputs of the CE and, $(a_k^{(1)},...,a_k^{(\kappa)}, \in \{0,1\})$ and $(b_k^{(1)} \in \{0,1\})$ are the feedforward and the feedback connections respectively. For simplicity, these connections can be represented by means of polynomials or with the customary octal notation, e.g., $1+D^3+D^4 \rightarrow (10011)_2 \rightarrow (23)_8$, where "D" is the delay operator.
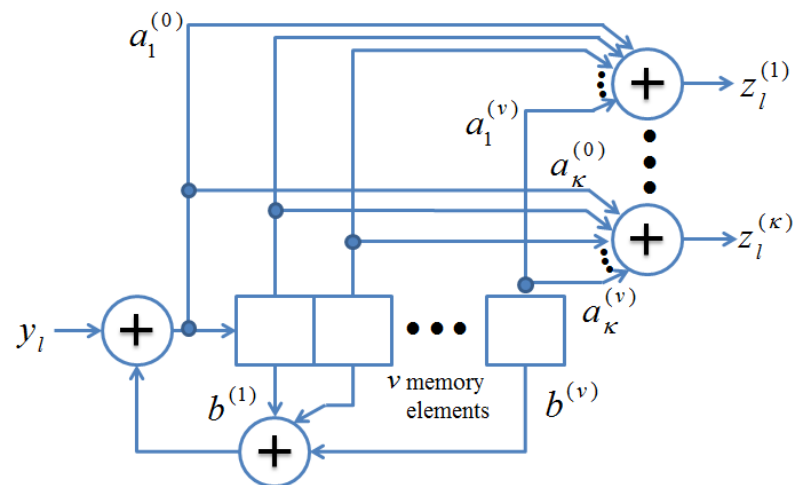
Figure 53. Generic rate $1/\kappa$ convolutional encoder.

The output symbols of the rate $1/4$ SLS-CE and the rate $1/2$ SLF-CE are connected towards an M-PPM IR-UWB modulator and a BPSK/Q-BOPPM modulator, respectively. On one hand, the four outputs, $z_l^{(1)}$ $z_l^{(2)}$ $z_l^{(3)}$ $z_l^{(4)}$, of the SLS-CE were used to determine the pulse position in one of M=16 time slots, thus a 16-PPM modulated IR-UWB signal is generated. The mathematical model for the signal, $x_{in}(t)$, at the output of the 16-PPM modulator can be derived from Equation (13):

$$x_{in}(t) = \sum_{l=-\infty}^{\infty} w(t - lT_r - [8z_l^{(4)} + 4z_l^{(3)} + 2z_l^{(2)} + z_l^{(1)}]T_\beta) \tag{20}$$

where $w(t)$ represents the UWB pulse shape used, T_r is the mean repetition time between pulses, T_β is the PPM modulation index, and $z_l^{(k)}$ are the outputs of the SLS-CE ($k=1,2,3,4$). The use of a SLS-CE is proposed in this thesis work because of the statistics of its outputs are such that, when used to drive a 16-PPM modulator, the PSD shows spectral lines at multiples of $1/T_\beta$ even when the binary data stream has a p.m.f. with $p_0 \neq 1/2$. It is important to mention that the advantage of using PPM scheme is the feasibility of implementing non-coherent electrical UWB receivers, which are preferred for designing low data rate (LDR) WPANs because of its simplicity, (Zhang et al., 2009-A). On the other hand, the output symbols of the SLF-CE, $z_l^{(1)} z_l^{(2)}$, are used to drive a BPSK or Q-BOPPM IR-UWB modulator such that the BPSK signal derived from Equation (12) can be mathematically described as:

$$x_{in}(t) = \sum_{l=-\infty}^{\infty} \{(2z_l^{(1)} - 1)w(t - (2l-1)T_r + (2z_l^{(2)} - 1)w(t - (2l)T_r\} \tag{21}$$

while the Q-BOPPM signal can be defined by

$$x_{in}(t) = \sum_{l=-\infty}^{\infty} \{(2z_l^{(1)} - 1)w(t - lT_r - z_l^{(2)}T_\beta) \tag{22}$$

which was derived from Equation (12) as well. In this case, the statistics of the outputs, $z_l^{(1)} z_l^{(2)}$, are such that when used to drive a BPSK or Q-BOPPM IR-UWB modulator the PSD will not show any spectral lines, even when the binary data stream, y_l, has a p.m.f. with $p_0 \neq 1/2$. The generation of a SLF PSD will allow to increase the signals transmit power and consequently improving the BER of the system. Note that when using BPSK two UWB pulses are required to transmit the equivalent to one information bit. In contrast, when using Q-BOPPM just one UWB pulse is required to transmit one information bit. In addition, it is important to mention that coherent receivers used to demodulate BPSK and Q-BOPPM signals result to be more complex than non-coherent. Nevertheless, high-data rates UWB-WPANs can be deployed.

Once the modulated IR-UWB signals have been generated, they are feed to the RoF architectures. For example, the 16-PPM IR-UWB transmitter could be integrated with the RoF architecture that use the direct intensity modulation (DIM) with direct detection (DD) technique in order to implement a low cost and low complexity IR-UWBoF system designed for Wireless Sensor Applications. As mentioned in subsection 2.2.1, DIM is the simplest intensity modulation method used to convert electrical UWB signals to optical signals, (Cox et al., 2006, Hui and O'Sullivan, 2009). On the other hand, the BPSK/Q-BOPPM IR-UWB transmitter could be integrated with both RoF architectures shown in Figure 50 and Figure 51 in order to provide high data rate (HDR) communications. However, it is important to consider that the EIM/DD architecture can provide important advantages over the direct-modulation method. Some of these are high stability, wide frequency modulation bandwidths and zero frequency chirp in high-speed optical communications systems. The optical signal obtained in both IM methods is then transmitted through a single-mode fiber (SMF). At the receiver module, both electrical modulated IR-UWB signals are recovered from the transmitted optical signal, resulting in the output signal $x_{out}(t)$ (point B in Figure 50 and Figure 51):

$$x_{out}(t) = x_{in}(t) * h_{optical}(t) \tag{23}$$

where $x_{in}(t)$ is the input signal given by Equations (20) to (22) and $h_{optical}(t)$ takes into account the mathematical expressions provided in subsection 2.2.1.1.

3.3 Design and implementation of IR-UWBoF-IM/DD testbeds in *VPITransmissionMaker^TM* simulation software

As previously mentioned, in order to improve the BER of the system the transmit power of a SLF-PSD of IR-UWB signals could be increased whereas it is compliant with the UWB regulations. In this sense, the purpose of this subsection is to show preliminary results about the spectral line suppression capabilities of the proposed IR-UWBoF-IM/DD systems when a spectral line free (SLF)-convolutional encoder (CE) is used. In order to obtain this preliminary results, simulation testbeds were designed and implemented in the *VPITransmissionMarker^TM* simulation software provided by VPIphotonics Company.

It is important to mention that this simulation software has been widely recognized by the international photonics community during the last years, and proof of that are several publications, presentations at conferences, contributions to optical text books, white papers, among others works reported in (VPIPhotonics, 2016-A). Mainly, this simulation software has been used to accelerate the design of new photonic systems and subsystems for short-range, access, metro and long haul optical transmission systems (VPIPhotonics,2016-B). Furthermore, the flexibility offered by this simulation software allows technology upgrade and component substitution strategies to be developed for existing optical communications systems. This latter advantage allows to save time and implementation cost because of preliminary results can be obtained in a fast and accurate way.

In brief, the *VPItransmissionMaker^{TM}* simulation software has a graphical user interface (GUI) where several predesigned modules of optical and electrical devices can be selected to design and implement hybrid (electrical and photonic) communication systems. In each module, a mathematical model with configuration parameters determining the behavior of electrical or optical devices are programmed. Furthermore, in some of these modules, it is possible to incorporate measurements of the transfer function of electrical devices in order to provide simulation results very close to experimental results. In regard to the signal analysis, this simulation software has the *VPIphotonicsAnalyzer* tool to display and analyze electrical and optical signals in time and frequency domain. For example, waveforms, PSD of these waveforms, and eye diagrams or constellation diagrams used to estimate the bit error rate (BER) of communication systems can be observed by means of this tool. In addition, functionalities of *VPItransmissionMaker^{TM}* software can be expanded by using the co-simulation focus with Python, MATLAB®, C++, or COM interface. By using this focus it is possible to create any device or process, which do not form part of all predesigned modules, and, importantly, such user-defined devices can be fully integrated into the simulation framework. The hierarchical design approach followed in this simulator allows creating compound devices (subcircuits) which can be used in the same way as native and co-simulated devices. For example, the design and generation of UWB waveforms can be first generated in MATLAB® and then these can be integrated to the simulation framework by using the co-

simulation modules. Figure 54 shows the simulation software presenting the PSD of a UWB pulse train. It is important to mention that the data provided by the simulator are obtained in numeric format, which offer the possibility of performing an off-line analysis by using numerical analysis software such as MATLAB®, Mathematica, Maple, etc.
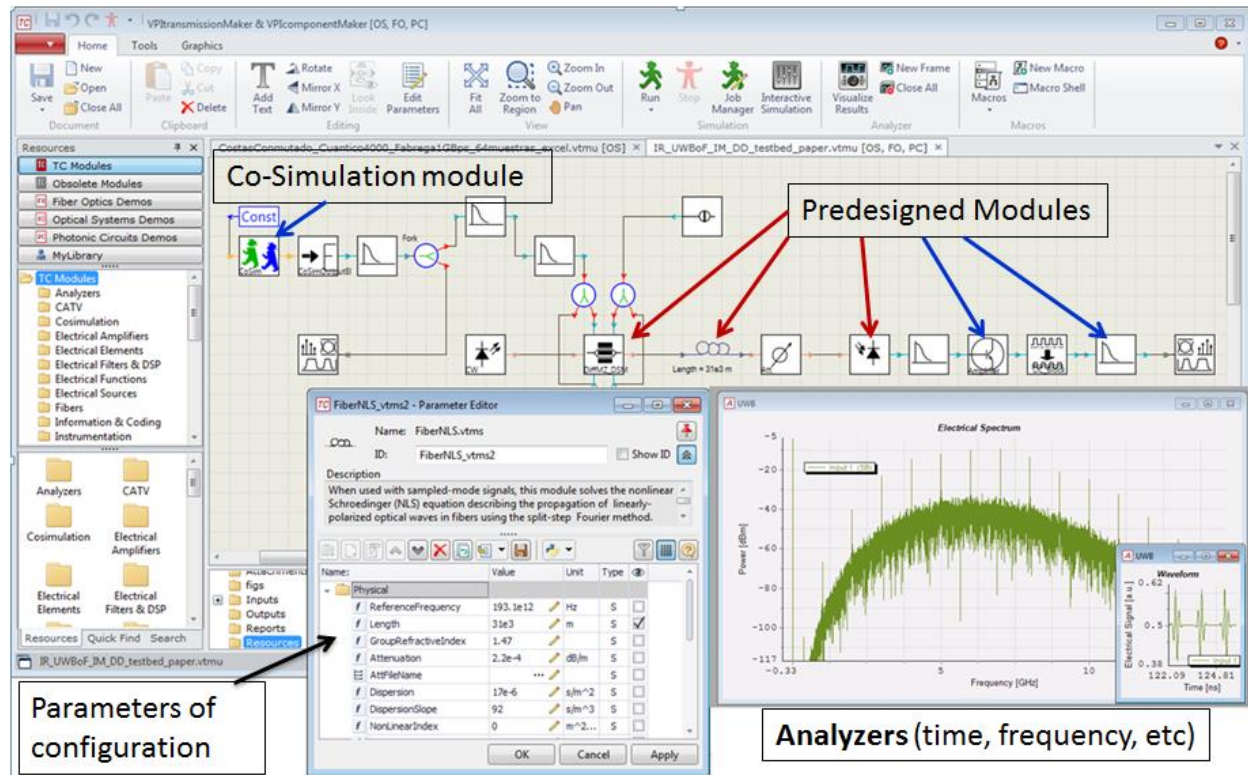
Figure 54. *VPItransmissionMaker^TM* **simulation software.**

Figure 55 and Figure 56 show the SLF-IR-UWBoF-DIM/DD and SLF-IR-UWBoF-EIM/DD testbeds implemented in the *VPITransmissionMarker^TM* simulation software. In both figures, it can be seen that the IR-UWB transmitter was implemented by using two modules: the *CoSimInterface* module, which was used to obtain the numeric data of non-coded and coded IR-UWB signals generated in MATLAB®, and the *CosimOutputEl* module, which allowed to convert these numeric data into electrical signals. It is important to mention that the IR-UWB signals generated by this transmitter were based on particular cases of Equations defined in Section 2.3 and Section 3.2.
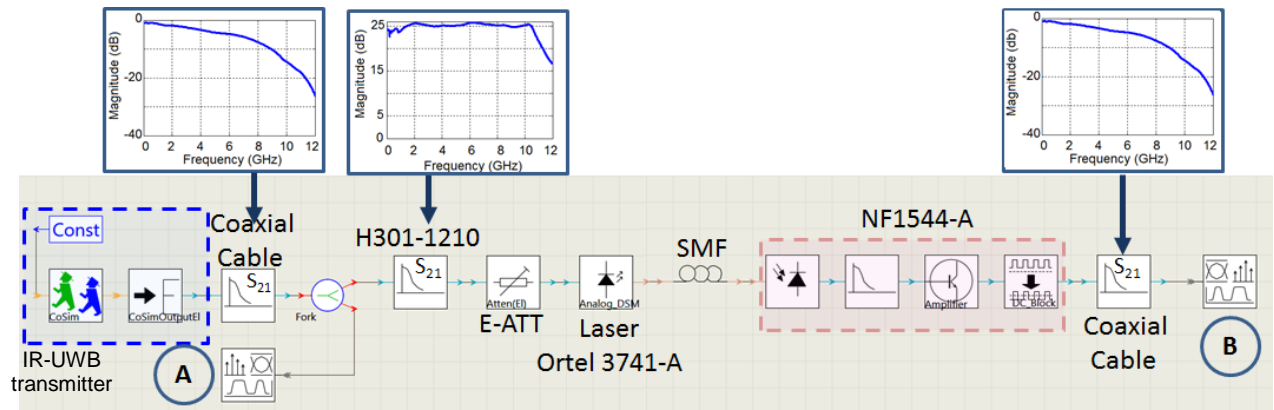
Figure 55 . IR-UWBoF-DIM/DD system implemented on _VPItransmissionMaker_^TM.
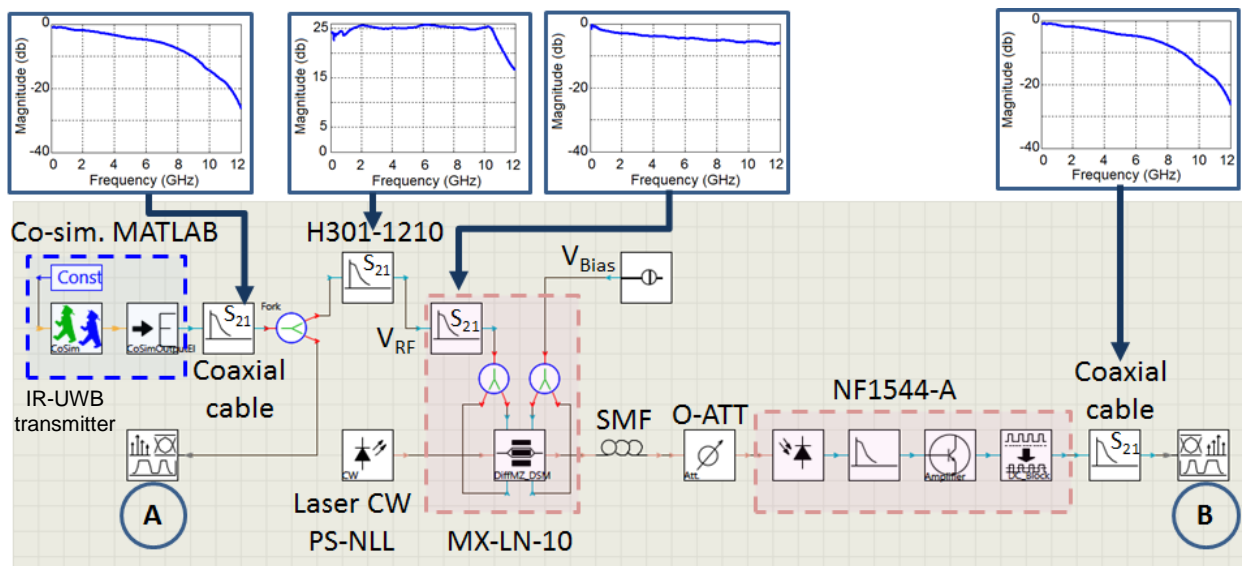
Figure 56. IR-UWBoF-EIM/DD system implemented on _VPItransmissionMaker_^TM.

The IR-UWB signal coming from the simulated transmitter is connected to the RoF architecture (DIM/DD or EIM/DD) through coaxial cables and optical modulator drivers such as the H301-1210 from JDS Uniphase and DR-AN-10-MO from Photline. In the testbed, these electrical devices were simulated with their transfer functions (frequency response), which were measured with a 13 GHz vector network analyzer (VNA). The numeric files obtained from the VNA were added to the simulated testbed by means of the _FilterEl_ module. All these measurements can be identified in both figures with the label "S_{21}".

On the other hand, both radio over fiber (RoF) architectures, DIM/DD and EIM/DD, were implemented by using predesigned optical and electrical modules. The configuration parameters of these modules were adjusted according to typical values provided in datasheets and/or by numeric data obtained from experimental measurements. A detailed description of these two testbeds is given in next paragraphs. In addition, the schematics of the RoF architectures here shown can be reviewed in subsection 2.2.1.1.

Firstly, the *LaserAnalogDSM* module was used to simulate the direct intensity modulation (DIM) method. This module is a simple laser model intended to simulate the small-signal characteristics of lasers, such as lasers driven with low modulation depth analog waveforms. Important parameters to describe the laser including: RIN (at a specified power), power output, linewidth, laser bias, threshold current. All these parameters were set according to the distributed feedback (DFB) laser 3741-A from ORTEL Emcore. It is important to mention that other parameters such as slope efficiency, alpha factor, and adiabatic chirp factor were heuristically configured. Therefore, simulation results obtained using this module could be slightly different to experimental results.

Secondly, the external intensity modulation (EIM) method was simulated with the modules: *LaserCW*, *FilterEl, ModulatorDiffMZ_DSM* and *DC_Source*. The *LaserCW* module was used to model important parameters of a continuous wave (CW) distributed feedback (DFB) laser such as *EmissionFrequency*, *AvergePower*, *Linewidth, Azimuth,* among others. Thus, these module parameters were established according to typical values reported in the datasheets of commercial low linewidth wavelength division multiplexing (WDM) tunable laser sources such as the pure spectrum narrow linewidth laser (PS-NLL) manufactured by Teraxion or the OCSCS TLS-AG from Yenista Optics. In regard to the design and implementation of a commercial Mach-Zehnder modulator (MZM) in this simulated testbed, the *FilterEl* module was used to simulate the RF electrode transfer function of the one-driver 10-Gb/s MZM with zero chirp performance MX-LN-10 from Photline. The zero-chirp one-driver MZM functioning of this MZM was simulated with the *ModulatorDiffMZ_DSM* module, which was configured as a *balanced single drive*. In addition, the module parameters *VpiCD*, *VpiRF*, and *Extinction Ratio* were modified with measured values obtained from MX-LM-10. As mentioned subsection 2.2.1.1, the quadrature points (QP) are the best operating points to convert electrical analog signals

to optical signals when a MZM is employed. Therefore, the module *DC_Source* was used to produce the constant-amplitude electrical signal for biasing the modulator at the QP. Thirdly, to simulate a length of standard single mode fiber (SMF) in the testbed, the *FiberNLS* module was employed. This module solves the nonlinear Schrödinger (NLS) equation describing the propagation of linearly-polarized optical waves in fibers using the split-step Fourier method. Even though this module can model the optical fiber non-linear effects, these were omitted by configuring to zero the *NonLinear Index* module parameter. This omission can be carried out because in the analysis performed a WDM spectrum is not considered. As well, the optical power density inside the fiber is very few to produce these nonlinear effects. Therefore, only some parameters such as *Length*, *Attenuation* and *Dispersion* were modified according to typical values of SMF-28 and measured values.

Finally, the photoreceiver was implemented in the simulation software by using the modules: *photodiode, FilterEl, AmpSysEl* and *DC_Block*. The *photodiode* module was configured to operate as PIN photodiode. Furthermore, module parameters such as *Responsivity*, *ThermalNoise*, *Temperature*, *Voltage, LoadResistence,* and *DarkCurrent* were established according to values provided in the datasheet of a commercial NF1544-A photoreceiver manufactured by New Focus. The *FilterEl* module was used as a 12 GHz Gaussian low-pass filter to limit the photoreceiver bandwidth according to the real one. The *AmpSysEl* was used to amplify the electrical signal coming out the photodiode and the *DC_Block* module was used to remove the DC component of this electrical signal.

As mentioned, the analysis in time and frequency domain of electrical signals was made by using the *VPIphotonicsAnalyzer* tool which was launched by the *SignalAnalyzer* module after a simulation process was finished. This module was connected at the IR-UWB transmitter's output and at the photodetector's output. On the other hand, the *VPIphotonicsAnalyzer* tool was configured according to the specifications provided by FCC (2002) considering an r.m.s. spectrum analyzer with a 1 MHz Gaussian resolution bandwidth (RBW).

3.4 Preliminary results

This section introduces PSD obtained from the proposed simulation BPSK/Q-BOPPM IR-UWBoF testbeds using a rate $1/2$ SLF convolutional encoder. Additionally, PSD simulations for traditional non-coded IR-UWBoF systems using binary PPM (BPPM) and BPSK are reported for comparison purposes.
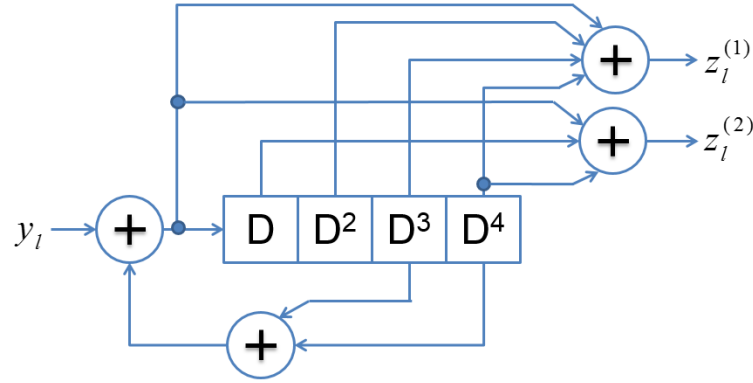
Figure 57. Rate $1/2$ Spectral Line Free Convolutional Encoder (SLF-CE) with feedforward and feedback polynomials $(27,31)_8$ and $(23)_8$, respectively.

The signal parameters used to evaluate the proposed IR-UWBoF testbed are as follows: T_r=1 ns, T_β=0.5 ns, and $w(t)$ = fifth-order derivative of a Gaussian pulse with pulse duration T_w=0.5 ns. For each PSD simulation, a data stream, y_l, consisting of $10,000$ bits was generated. In addition, two different distributions for the data stream were considered, one with a p.m.f. equal to p_0=1/5 and p_1=4/5, and another with p_0=2/5 and p_1=3/5. The SLF-CE implemented has memory v=4 with feedforward polynomials represented by $(27,31)_8$ and feedback polynomial by $(23)_8$. The diagram of this SLF-CE is shown in Figure 57.

For the coded BPM and Q-BOPPM IR-UWBoF systems, the encoder outputs, $z_l^{(1)}$ $z_l^{(2)}$, are used to drive the UWB modulator as described by Equations (21) and (22). For the case of the non-coded IR-UWB systems, the data stream, y_l, is used to drive the BPPM and BPSK UWB modulators which can be described by Equation (9).

The PSDs for the non-coded BPPM/BPSK and the proposed SLF convolutionally coded BPSK/Q-BOPPM IR-UWBoF-DIM/DD testbed are presented in Figure 58 and Figure 59 with p_0=1/5 and p_0=2/5, respectively. The FCC spectral mask for indoor UWB transmissions

is plotted in both figures as reference. The PSDs shown in both figures were obtained with a *SignalAnalyzer* module connected at the IR-UWB transmitter's output (TPA) and at the DIM/DD architecture output (TPB) considering different lengths of SMF (from 0-km to 30-km). To make relevant PSD comparisons between the different PSD of the non-coded and convolutionally coded IR-UWB systems considered, the pulse amplitude generated by the simulated IR-UWB transmitter was set to the same power level for all simulations. Furthermore, it is important to mention that the PSDs shown in both figures also take into account the noise level of a 40 GHz electrical spectrum analyzer (ESA) FSV40 manufactured by Rohde and Schwarz (R&S). On the other hand, the PSDs for the non-coded BPPM/BPSK and the proposed SLF convolutionally coded BPSK/Q-BOPPM IR-UWBoF-EIM/DD testbed are presented in Figure 60 and Figure 61 with $p_0=1/5$ and $p_0=2/5$, respectively. Similar to previous set of figures (58 and 59), the pulse amplitude generated by the simulated IR-UWB transmitter was established to the same power level for all simulations.
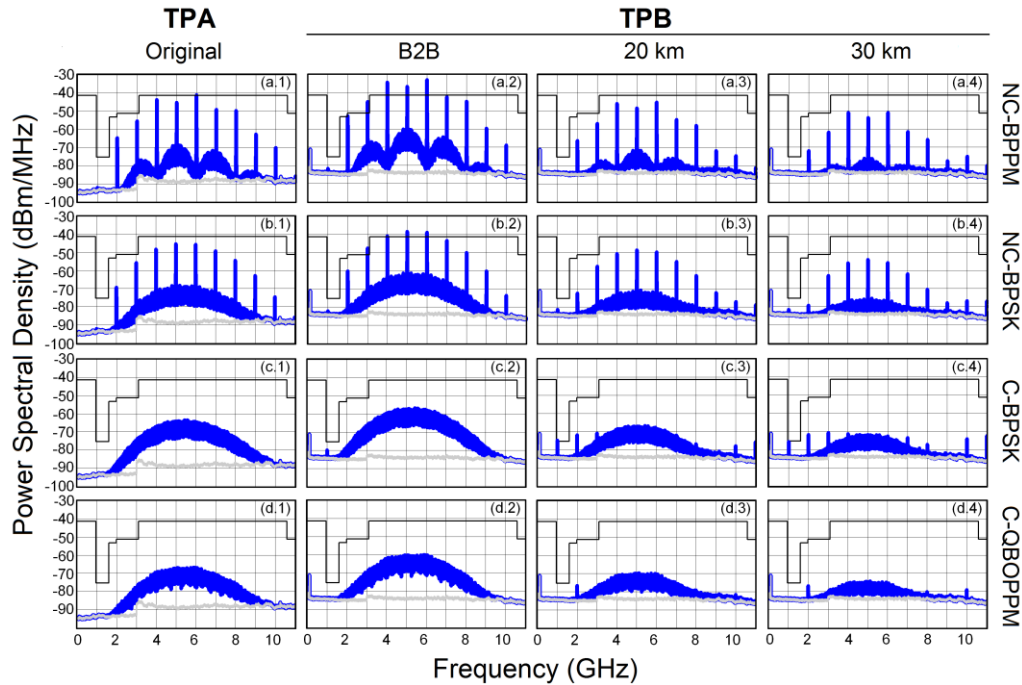
Figure 58. Simulated PSDs at the input and output of the IR-UWBoF-DIM/DD testbed (see Figure 50) using the rate $1/2$ SLF-CE shown in Figure 56 for B2B, 20-km and 30-km of fiber length for $p_0=1/5$.
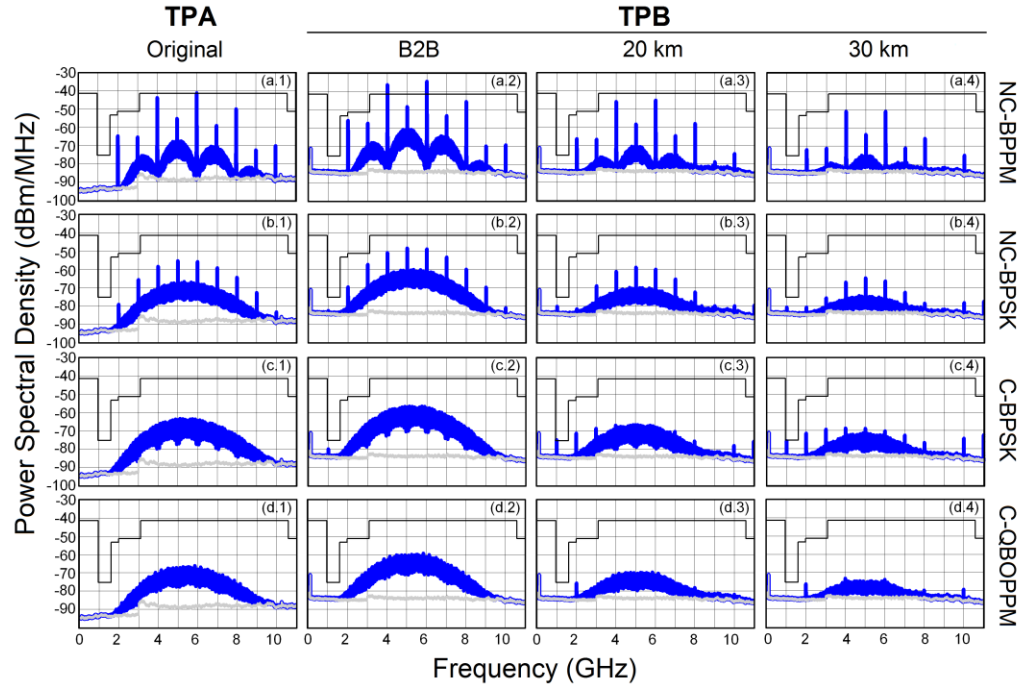
Figure 59. Simulated PSDs at the input and output of the IR-UWBoF-DIM/DD testbed (see Figure 50) using the rate 1/2 SLF-CE shown in Figure 57 for B2B, 20-km and 30-km of fiber length for p_0=2/5.
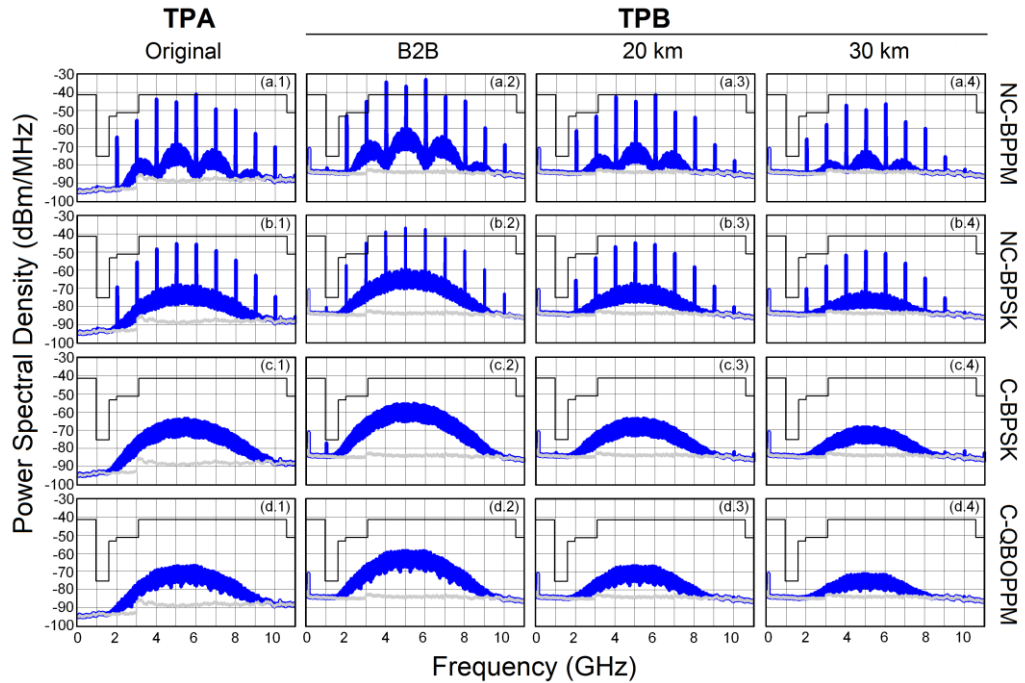
Figure 60. Simulated PSDs at the input and output of the IR-UWBoF-EIM/DD testbed (see Figure 51) using the rate 1/2 SLF-CE shown in Figure 57 for B2B, 20-km and 30-km of fiber length for p_0=1/5.
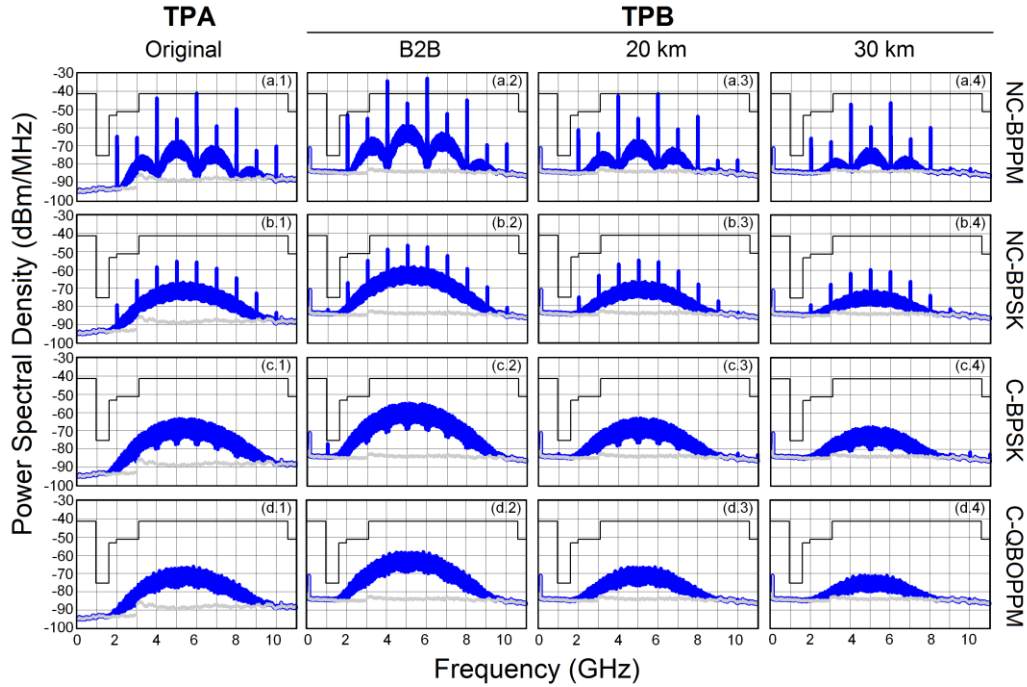
Figure 61. Simulated PSDs at the input and output of the IR-UWBoF-EIM/DD testbed (see Figure 51) using the rate $1/2$ **SLF-CE shown in Figure 57 for B2B,** 20**-km and** 30**-km of fiber length for** p_0**=2/5.**

Analyzing the PSDs of non-coded IR-UWBoF testbeds (DIM/DD and EIM/DD), it can be seen that spectral lines appear spaced each 1 GHz. This was expected, as it is well-known that for unbalanced (i.e., $p_0 \neq 1/2$) data streams, y_l, the binary PPM (BPPM) and BPSK IR-UWB signals exhibit strong spectral lines in the PSD (see Villarreal-Reyes, 2007). As discussed in Section 2.4, in order to fit under the FCC spectral mask, commonly the transmit power of these non-coded signals are decreased. This reduction would impact negatively the BER of both systems. In contrast, note that the PSDs of both proposed SLF convolutionally coded testbeds (C-BPSK and C-QBOPPM) do not present any spectral lines in B2B configuration. Nevertheless, strong spectral lines in the PSD of SLF convolutionally coded IR-UWBoF-DIM/DD testbeds (BPSK and Q-BOPPM) can be seen in Figure 58 (c and d) and Figure 59 (c and d) when 20-km and 30-km of SMF are considered. These spectral lines are result of the inherent frequency chirp effect produced by modulating directly the laser's injection current and the chromatic dispersion effect of the SMF. Figure 62 shows the evolution of the fifth-order derivative transmitted through of the DIM/DD simulated testbed. In this figure, it can be seen as the pulses at the end of a 20-km and 30-km of SMF transmission are not complementary as in B2B configuration. As mentioned by Pan and Yao, (2010-A), pulses which are not complementary produce

spectral lines in the PSD. On the other hand, the PSDs of convolutionally coded IR-UWBoF-EIM/DD testbeds do not show any spectral line (see Figure 60 and Figure 61). It can be also observed that spectral line suppression of the SLF-CE is conserved for all tested fiber lengths. Figure 63 shows the evolution of the fifth-order derivative transmitted through of the EIM/DD simulated testbed considering 20-km and 30-km of SMF. It can be seen that negative and positive pulses are practically complementary. Furthermore, the transmit power of these signals can be also significantly incremented without violating the FCC regulation. Therefore, when adjusting the transmit power of this IR-UWBoF-EIM/DD testbed to the maximum level allowed by the spectral mask, a significant improvement in the wireless transmission range and/or BER performance would be achieved compared to the analyzed non-coded IR-UWBoF testbeds and those convolutionally coded IR-UWBoF-DIM/DD testbeds.
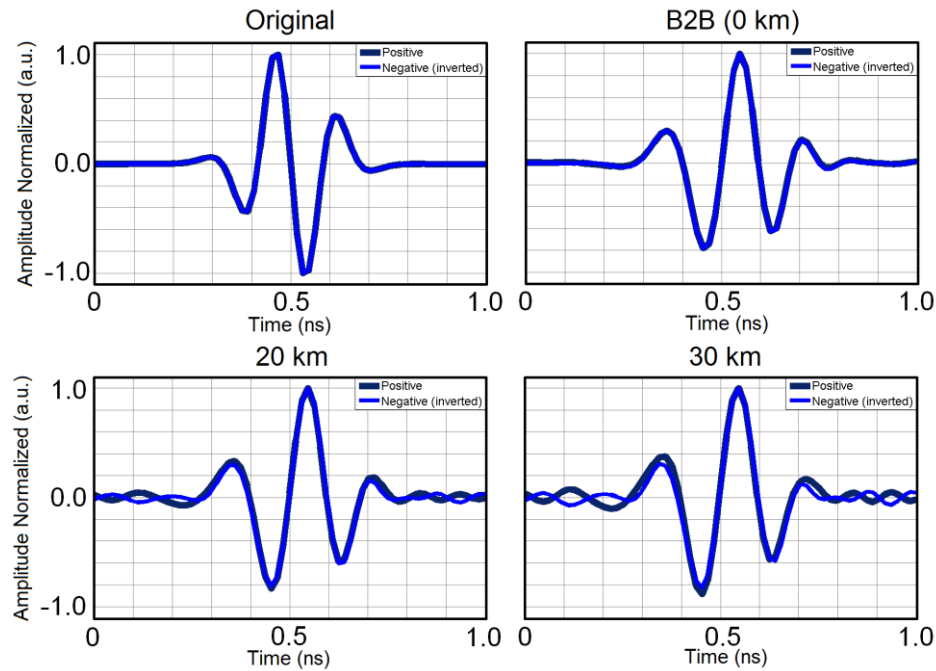
Figure 62. Simulated waveforms at the input (point A) and output (point B) of the IR-UWBoF-DIM/DD testbed (see Figure 50).
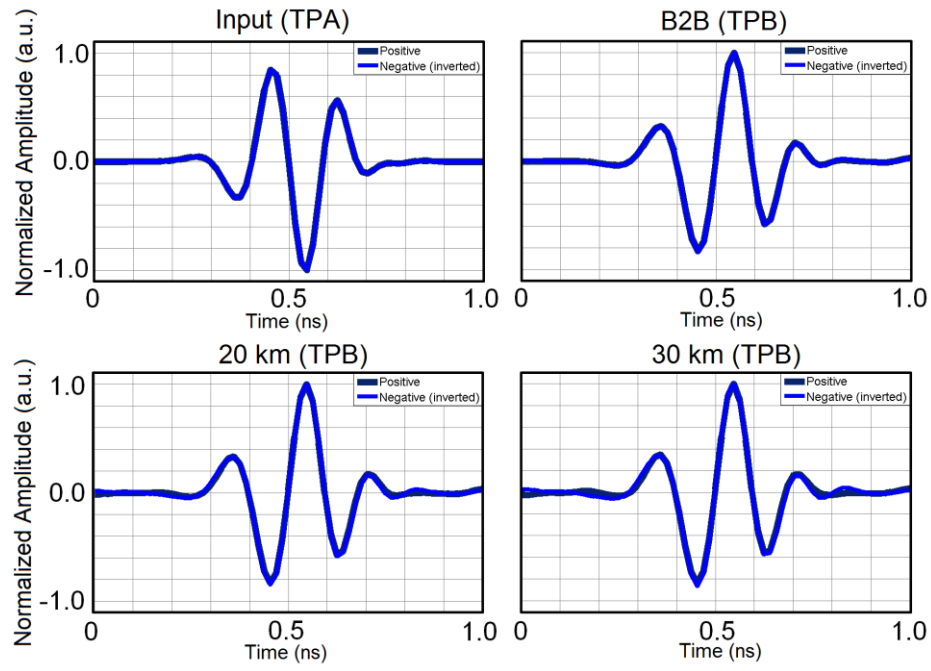
Figure 63. Simulated waveforms at the input (point A) and output (point B) of the IR-UWBoF-EIM/DD testbed (see Figure 51).

Chapter 4. Experimental studies of IR-UWBoF systems with spectral line suppression capabilities

4.1 Introduction

The purpose of this chapter is to show experimental results of the spectral shaping capabilities of convolutionally coded M-PPM/BPSK/Q-BOPPM IR-UWBoF-IM/DD systems proposed in Section 3.2. First, spectral line suppression assessments of a low complexity M-PPM IR-UWBoF system designed for low data rate (LDR) WPAN applications are provided. The optical configuration of this system is based on the direct intensity modulation with direct detection (DIM/DD) technique considering lengths of 20-km and 30-km of single mode fiber (SMF). Afterwards, the high-data rate (HDR) IR-UWBoF-EIM/DD system designed on *VPITransmissionMarker^{TM}* simulation software is experimentally implemented and evaluated. A validation process of this simulation testbed is carried out by calculating the spectral distortion factor (SDF) between simulated and experimental PSDs. Finally, the spectral line suppression capabilities of two HDR IR-UWBoF systems that use both IM/DD optical configurations, direct and external, are evaluated considering a fiber-wireless channel. The impact of the chromatic dispersion effect in all practical implementations described is also discussed.

4.2 Practical implementation of a low data rate (LDR) M-PPM IR-UWBoF-DIM/DD system

As discussed in Section 2.3, UWB technology has inherent properties such as low power consumption, tolerance against multipath fading, and very good time domain resolution which makes it a key enabler for LDR-wireless sensor networks (WSN) deployments, (Zhang et al., 2009-A). Furthermore, it is expected that several of these LDR-WSNs will be interconnected by RoF architectures in order to transport information generated by hundreds or thousands of sensors deployed in several application areas within "smart cities". In this context, the low complexity M-PPM IR-UWBoF systems that use the DIM/DD technique with non-coherent UWB receivers will provide a low cost and low power solution to cover all these novel application areas.

The system model of a convolutionally coded M-PPM IR-UWBoF-DIM/DD system was described in Section 3.2. As non-coherent receivers are preferred in low complexity LDR-WSN deployments, a rate $1/4$ spectral line suppressive convolutional encoder (SLS-CE) specially designed for TH-PPM / M-PPM systems was selected for this practical implementation. The diagram of this SLS-CE is shown in Figure 64, where it can be seen that the feedforward and feedback connections are $(30, 4, 22, 21)_8$ and $(23)_8$ respectively.
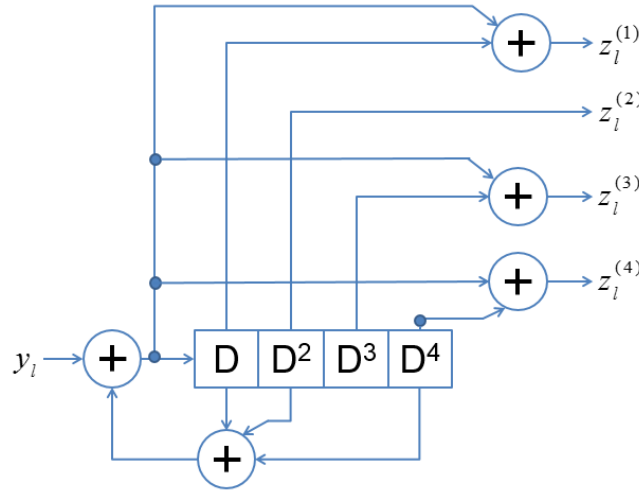
Figure 64. Rate 1/4 Spectral Line Suppressive Convolutional Encoder (SLS-CE) with feedforward and feedback polynomials ($30, 4, 22, 21)_8$ **and (**$23)_8$**, respectively.**

As it was deeply analyzed by Villarreal-Reyes (2007), the statistics of the SLS-CE's outputs are such that when used to drive a 16-PPM modulator, the PSD only shows spectral lines at multiples of $1/T_\beta$ even when the data stream provided by the binary data source has a p.m.f. with $p_0 \neq 1/2$. In order to show this, a value of $p_0 = 1/4$ is used to evaluate the spectral line suppression capabilities of the proposed 16-PPM IR-UWBoF-DIM/DD system. The diagram of this practical implementation is shown in Figure 65.
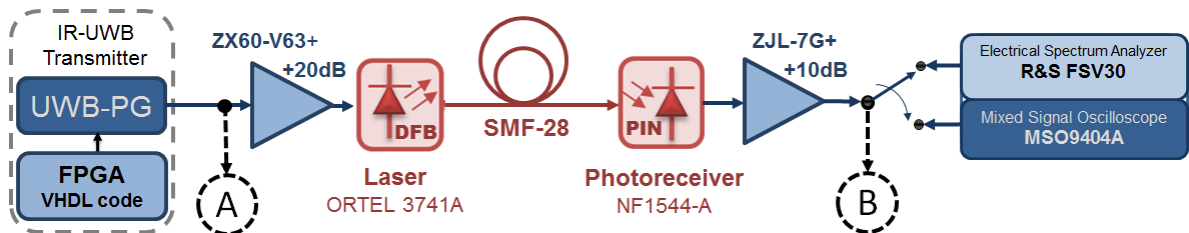
Figure 65. Connecting diagram of the experimental 16-PPM IR-UWBoF-DIM/DD setup.
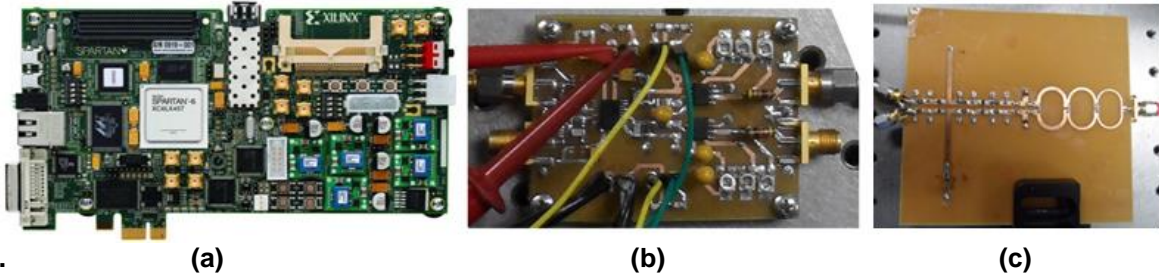
(a) **(b)** **(c)**
Figure 66. (a) SP605 Xilinx-Spartan FPGA board. (b) Preamplifier stage (c) BPKS pulse generator (PG). The electronic circuit boards shown in (b) and (c) form part of the UWB-PG depicted in Figure 65.

The IR-UWB transmitter was implemented by using a Field Programmable Gate Array (FPGA) board where the binary data source (BDS), the rate $1/4$ SLS-CE and the 16-PPM modulator were programmed in VHDL code. This board was then connected to a UWB Pulse Generator (UWB-PG) similar to that proposed by Zhifeng Lin, Wei Lei, and Kaihang Li (2010). The UWB-PG was designed using microstrip lines, Schottky and Step Recovery diodes. Figure 66 shows the components used to implement the IR-UWB transmitter.

The output of the UWB-PG (test point A in Figure 65) was connected a 6 GHz electrical amplifier with 20 dB gain. This provided the amount of electrical power used to modulate a CW DFB laser with 10MHz linewidth and emitting light at 1550nm. The optical fiber link consisted of 30 km of SMF-28. The IR-UWB signals were electrically recovered by means of a 12 GHz photodetector (PD) connected at the fiber output. The PD output was connected to a 7 GHz electrical amplifier with 10 dB gain to compensate some losses caused by the optical section. A 30 GHz Electrical Spectrum Analyzer (ESA) was connected at the system output (test point B on Figure 65) in order to digitize and store the IR-UWB signals PSD. A resolution bandwidth of 1 MHz was used to capture the PSDs. In addition a Mixed Signal Oscilloscope MSO9404A also was connected to obtain the UWB pulses in time domain.

The UWB signal parameters used to demonstrate that the proposed system does not add spectral lines to the SLS-CE 16-PPM PSD are as follows: $T_r = 240$ ns, $T_\beta = 15$ ns and $w(t)$ has a Gaussian pulse with duration $T_w \approx 850$ ns as shown in Figure 67. A binary data stream, y_l, with pmf $p_0 = 1/4$ and $p_1 = 3/4$ was fed to SLS-CE input. As one data bit is

transmitted per pulse, an equivalent data rate of 4.16 Mbps is achieved. This data rate is adequate for WSN applications.
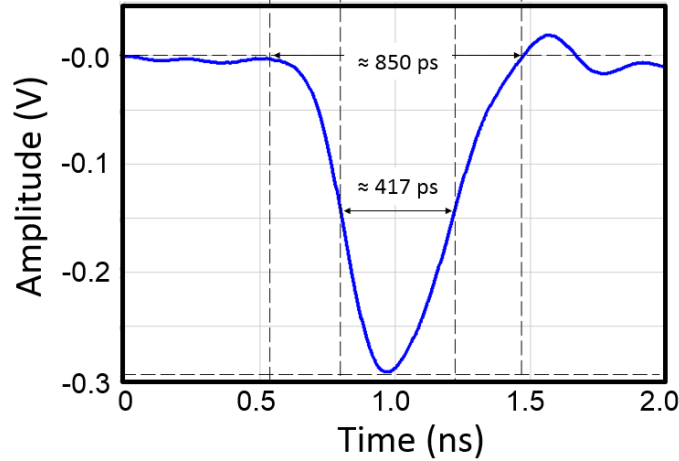
Figure 67. Gaussian pulse generated by the UWB Pulse Generator depicted in Figure 65.

The measured PSDs for the proposed SLF convolutionally coded 16-PPM IR-UWBoF system are shown in Figure 68. The PSD measurements were performed in test point (TP)A and TPB as indicated in Figure 65. Back-to-back (B2B) and 30 km of SMF-28 configurations were considered in the optical link. It can be seen in Figure 68(a) that the original PSD only shows spectral lines at multiples of 66.67 MHz ($1/T_\beta$) as expected. This confirms the spectral line suppression capabilities of the SLS-CE for unbalanced data streams. Furthermore, it can also be observed in Figure 68(b) and Figure 68(c) that the spectral line suppression capabilities of this SLS-CE are preserved for all fiber lengths tested. Thus, it can be concluded that the proposed low complexity 16-PPM IR-UWBoF system does not add spectral lines to the UWB PSD. In contrast to preliminary results shown in Section 3.4, in particular those plotted in Figure 58(c.3-c.4) and Figure 59(c.3-c.4), where strong spectral lines appear in the PSD of SLF IR-UWB-DIM/DD systems after 20-km and 30-km of SMF. In fact, only power losses caused by fiber attenuation and E/O-O/E conversion processes were observed.

Due to the pulse generator (UWB-PG) provides a Gaussian pulse (see Figure 67) with a PSD ranging from DC to approximately 2 GHz, an up-converter stage has to be connected to the output (TPB) of the system shown in Figure 65. This would allow shifting the energy

spectrum of the IR-UWB signal within UWB frequency range (from 3.1 to 10.6 GHz) such as is used in (Colli-Vignarelli, Feldman, Robert, and Dehollaini, 2011-B).
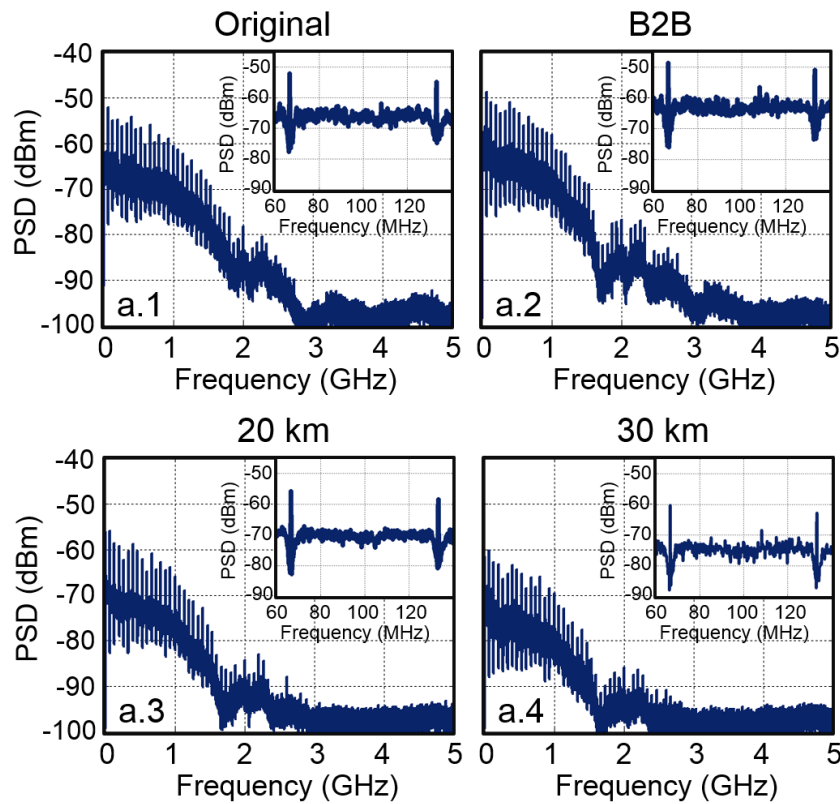
Figure 68. Experimental PSD measurements of the 16-PPM IR-UWBoF system. TPA: (a) Original; TPB: (b) B2B and (c) 30 km of SMF-28.

4.3 Practical implementation of high data rate (HDR) BPSK/Q-BOPPM IR-UWBoF-IM/DD systems

This subsection is divided in two parts. On one hand, the HDR-IR-UWBoF-EIM/DD system designed on *VPITransmissionMarker^{TM}* simulation software is now experimentally implemented and evaluated in Optical Communications laboratory at CICESE Research Center. Furthermore, the power spectral densities (PSDs) obtained from the simulation IR-UWBoF-EIM/DD testbed are validated with PSDs measured in the practical implementation here described. This validation process is carried out by calculating the spectral distortion factor (SDF), (Jazayerifar et al., 2008, Valente and Cartaxo, 2010), between the simulated and experimental PSDs. On the other hand, both HDR IR-UWBoF systems, DIM/DD and EIM/DD, with wireless transmission are also experimentally

implemented by using different electrical and photonics components (e.g. optical modulator driver, electro-optic modulator, photodetector, coaxial cables). The spectral line suppression capabilities of both systems are also evaluated from B2B to 30 km of SMF considering a wireless transmission of 20-30 cm. These last systems were implemented in SAMOVAR CNRS laboratory at Telecom SudParis.

4.3.1 Experimental evaluations of the HDR1 IR-UWBoF-EIM/DD system analyzed in Chapter 3

The connection diagram of the experimental HDR IR-UWBoF-EIM/DD system evaluated in this subsection (which will be identified as HDR1 system in subsequent sections), and its practical implementation in Optical Communications laboratory at CICESE Research Center are shown in Figure 69 and Figure 70, respectively.
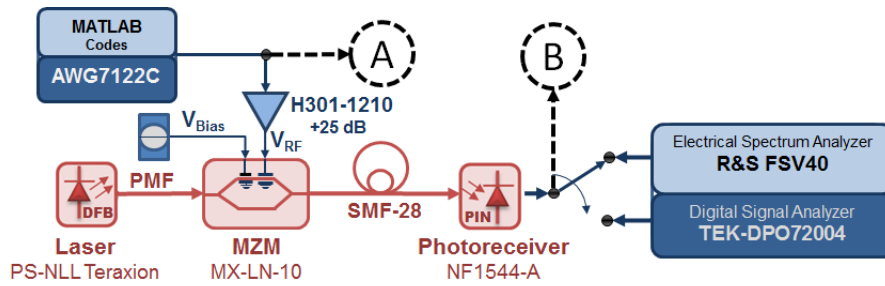
Figure 69. Connecting diagram of the experimental HDR1 SLF IR-UWBoF-EIM/DD setup.

In order to carry out the spectral line suppression evaluation of the practical system, first, non-coded BPPM/BPSK IR-UWB signals and convolutionally coded BPSK/Q-BOPPM IR-UWB signals are generated in MATLAB®considering the same signal parameters provided in Section 3.4. For convenience these signal parameters are summarized in Table 4. Once obtained the numeric data of the generated IR-UWB signals, they are loaded into an electrical arbitrary waveform generator (E-AWG) with a 9.6-GHz bandwidth and a 24 GSa/s sample rate. It is important to mention that both parameters, bandwidth and sampling rate, from the E-AWG and the coaxial cable used in the implementation can limit considerably the time width and therefore the PSD of the IR-UWB signals. In this sense, a characterization of the pulses created by the E-AWG, which were measured using coaxial cables with 10 GHz bandwidth, was made before transmitting the IR-UWB signals toward to the RoF IM/DD architecture.
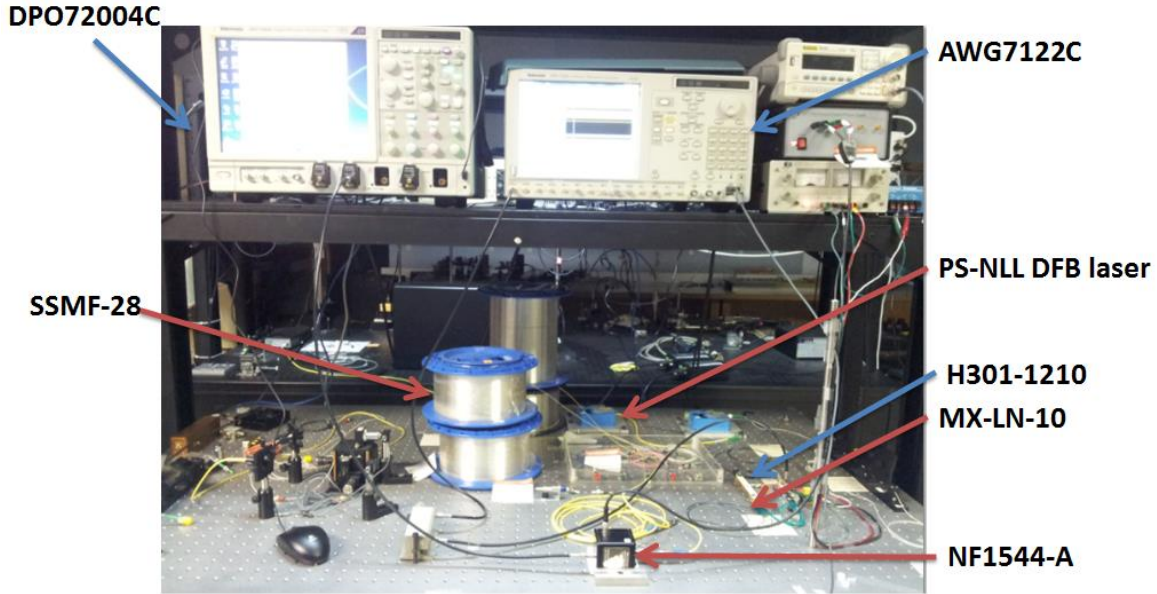
Figure 70. Experimental HDR1 SLF IR-UWBoF-EIM/DD setup implemented in Optical Communications laboratory at CICESE Research Center.

Some results obtained of this characterization are shown in Figure 71. For example, Figure 71(a) shows the simulated waveforms of the fifth-order derivative of a Gaussian pulse with $T_w \approx 500$ ps ($\sigma=51$ ps), $T_w \approx 600$ ps ($\sigma=65$ ps), and the experimental waveform created by the E-AWG when $T_w \approx 500$ ps. It can be seen that the experimental pulse is more like to the simulated pulse with $\sigma=65$ ps than when $\sigma=51$ ps is used. As mentioned, this is due to the limited bandwidth/sampling rate of the E-AWG, and frequency response of coaxial cables used in the implementation. In addition, the energy spectral density (ESD) of experimental pulse and the PSD of periodic pulse train (simulated and experimentally measured) with $T_r=10$ ns are shown in Figure 71(b).

In addition, Figure 72 shows the power spectral densities (PSDs) of the non-coded and coded IR-UWB signals inputted to the RoF-EIM/DD architecture. As we expected, it can be observed that the rate $1/2$ SLF convolutional code is able to eliminate spectral lines of Q-BOPPM IR-UWB signals even when an unbalanced data stream drives the SLF-CE.

Table 4: Signal parameters used in the IR-UWB transmitter of the experimental HDR1 SLF IR-UWB-EIM/DD system implemented in Optical Communications laboratory at CICESE Research Center.

Binary data stream [y_l]:	Frames of 10,000 bits with two p.m.f.: p_0=1/5 and p_1=4/5; p_0=2/5 and p_1=3/5
PPM modulation index [T_β]:	0.5 ns
Mean repetition time between pulses [T_r]:	1.0 ns
Waveform [$w(t)$]:	Fifth-order derivative of a Gaussian pulse
Pulse width [T_{wT}]	500 ps (simulated) ≈ 600 ps (experimental)
Spectral line free convolutional encoder [SLF-CE] used for coded signals:	Feedforward $(27, 31)_8$ and feedback $(23)_8$ polynomials with memory v=4. (see Figure 57)
TH and DS multiplication codes:	Not used

(a)   (b)
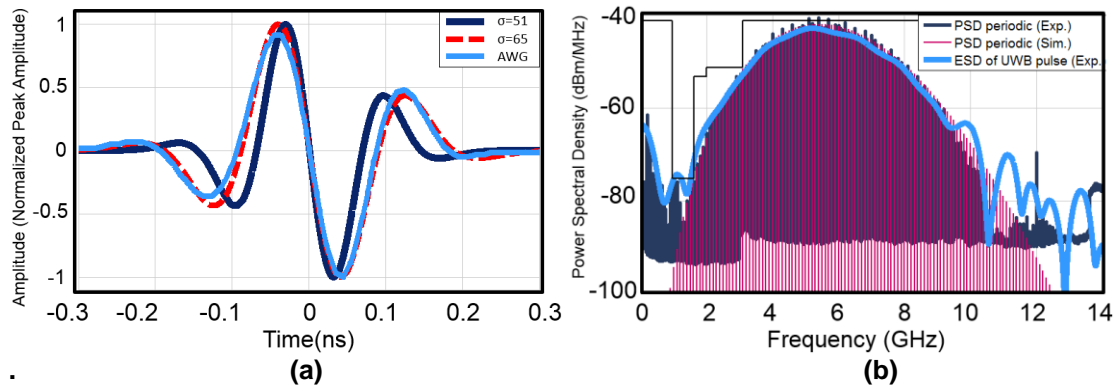
Figure 71. (a) Waveforms of the fifth-order derivative of a Gaussian pulse with σ=51 ps (dark plot), σ=65 ps (dotted red plot) and the UWB pulse experimentally generated by the AWG7122C (light blue plot). (b) Energy spectral density (ESD) of the experimental UWB pulse (light blue plot), simulated PSD (red plot) and experimental PSD (dark blue plot) of a periodic pulse train with T_r=10 ns.
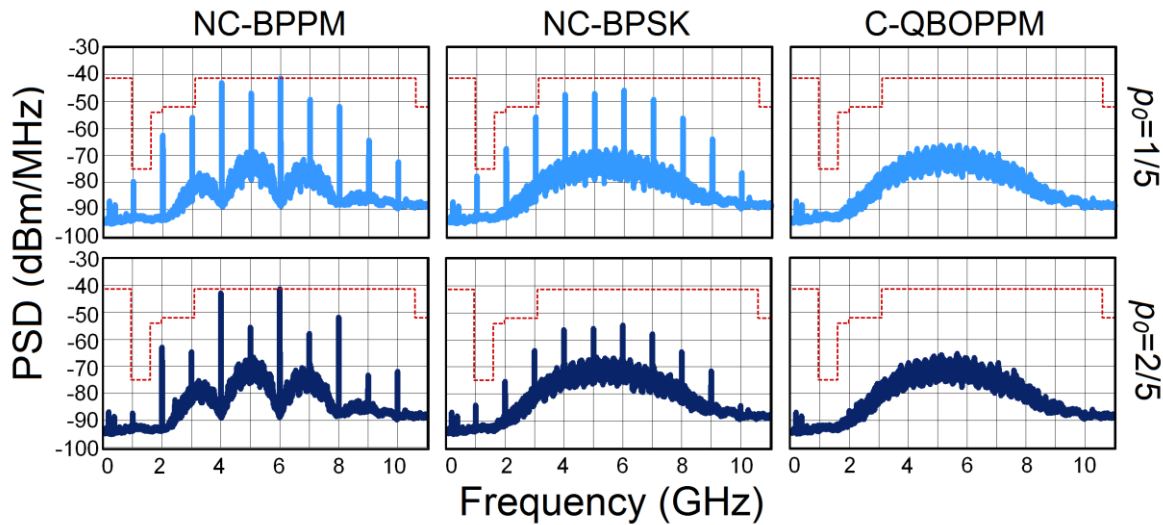
Figure 72. Experimental PSD of non-coded BPPM/BPSK IR-UWB signals and the rate $1/2$ spectral line free convolutionally coded Q-BOPPM IR-UWB signal generated with the AWG7122C. The signal parameters used to generate these PSDs are summarized in Table 4. The transmit power of the three signals was set at the same power level, taking as reference the PSD of the NC-BPPM signal.

At the output of the E-AWG (test point A in Figure 69) is connected an electrical 10 GHz modulator driver. It permits to provide the appropriate voltage and to match the impedance between the E-AWG and the electro-optic modulator. The electrical generated IR-UWB signals modulate the output beam of a 1550-nm CW DFB laser using an external Mach Zehnder Modulator (MZM) with 12 GHz electro-optic bandwidth. The optical fiber link consists of spools of standard single mode fiber (SMF-28) with fiber lengths of 5, 10, and 15 km. At the output of the fiber, the IR-UWB signals are electrically recovered by means of a 12 GHz bandwidth photoreceiver. A 1000 V/A gain transimpedance amplifier is integrated into the receiver. At the receiver output (test point B in Figure 69) is connected a 20 GHz real-time digital oscilloscope with 50 GSa/s and a 40 GHz electrical spectrum analyzer (ESA), whose resolution bandwidth (RBW) was set to 1 MHz. Both instruments have been used to digitize and store the IR-UWB signals in time and frequency domain.

Figure 73 shows the measured PSDs for the non-coded PPM/BPSK and the proposed convolutionally coded BPSK/Q-BOPPM IR-UWBoF systems. The FCC spectral mask for indoor UWB scenarios is plotted in these figures as reference. The measurements were performed after 0 km (back-to-back, B2B), 20-km, and 30-km of SMF transmission. All PSD measurements were obtained at test point B (TPB) of the system (see Figure 69). To make relevant PSD comparisons between different IR-UWB-IM/DD systems considered in this research, the pulse amplitude generated by the E-AWG was set to the same power level for all schemes. The light-blue plots correspond to UWB signals generated when the data stream, y_l, has a p.m.f. p_0=1/5 and p_1=4/5. On the other hand, the dark-blue plots correspond to UWB signals with p.m.f. p_0=2/5 and p_1=3/5. Figure 73(a) and Figure 73(b) show PSDs with strong spectral lines spaced at 1 GHz intervals, such as those PSDs for non-coded IR-UWBoF-EIM/DD systems shown in Section 3.4. As mentioned, this was expected because unbalanced data streams, y_l, will show strong spectral lines in the PSD. In contrast, note in Figures 73(c) and 73(d) that the PSDs of the experimental SLF convolutionally coded IR-UWBoF-EIM/DD systems do not present any spectral lines. Furthermore, it can be also observed that the spectral line suppression of the SLF-CCs is conserved for all tested fiber lengths. These measurements confirm the preliminary results provided in subsection 3.4, the optical link does not produce any additional spectral lines in the proposed SLF BPSK/Q-BOPPM IR-UWBoF-EIM/DD system. Last on Figure 73, it is observed power losses for 20-km and 30-km of SMF.

These are mainly attributed to fiber attenuation and the optical connectors used to assemble the fiber link.
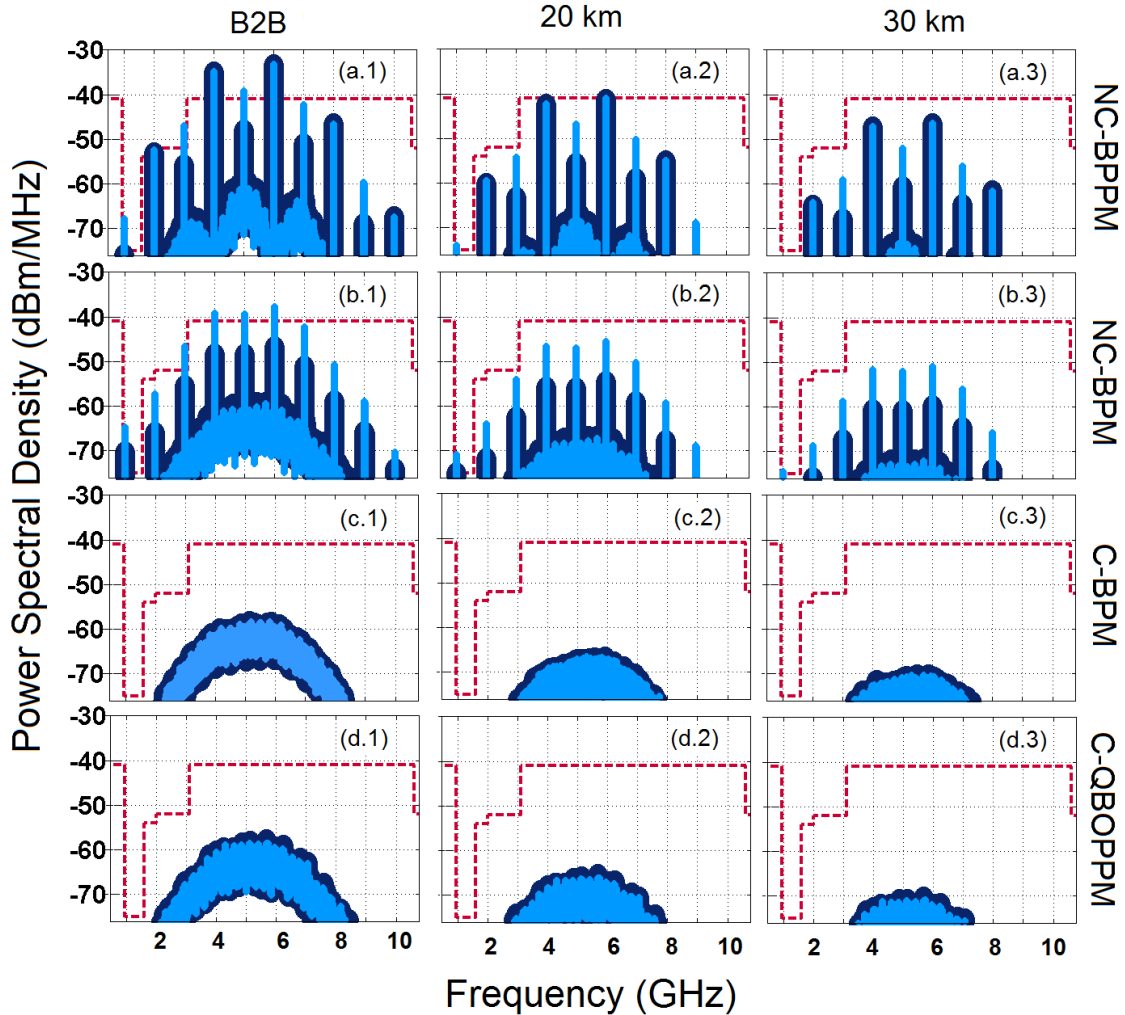
Figure 73. Experimental PSD plots measured at the output of the HDR1 SLF IR-UWBoF setup (point B in Figure 69) for B2B, 20-km and 30-km SMF. The measured PSD plots correspond to following IR-UWBoF systems: (a) non-coded binary PPM; (b) non-coded BPM(BPSK); (c) SLF convolutionally coded BPM; and (d) SLF convolutionally coded Q-BOPPM.

Figure 74 shows IR-UWB pulse patterns before and after the fiber transmission. In Figure 74(a), an ideal Q-BOPPM IR-UWB signal is presented. The Q-BOPPM IR-UWB signal generated by the E-AWG is shown in Figure 74(b). It can be seen that this signal has small oscillations around the zero level compared to the ideal MATLAB® signal. These oscillations can be attributed to the E-AWG bandwidth and bit resolution. Figure 74(c) shows the measured pulse pattern after electrical-to-optical and optical-to-electrical conversion processes, where some signal degradations introduced mainly by the optical

driver modulator can be observed. In Figures 74(d) and 74(e), the pulse pattern after 20-km and 30-km of fiber transmission are shown. Note in these plots some signal degradation due to power losses and chromatic dispersion. To improve the pulse shape after fiber transmission, optical amplifiers and chromatic dispersion compensation modules could be used. However, this will increase the complexity and cost of the whole IR-UWBoF-EIM/DD system. Furthermore, note that despite the impairments observed after fiber transmission, the PSDs of the proposed SLF convolutionally coded IR-UWBoF-EIM/DD system do not show any spectral lines. Therefore, when adjusting the transmit power of this system to the maximum level allowed by the spectral mask, a significant improvement in the wireless transmission range and/ or BER performance will be achieved compared to the systems discussed in Section 2.6.
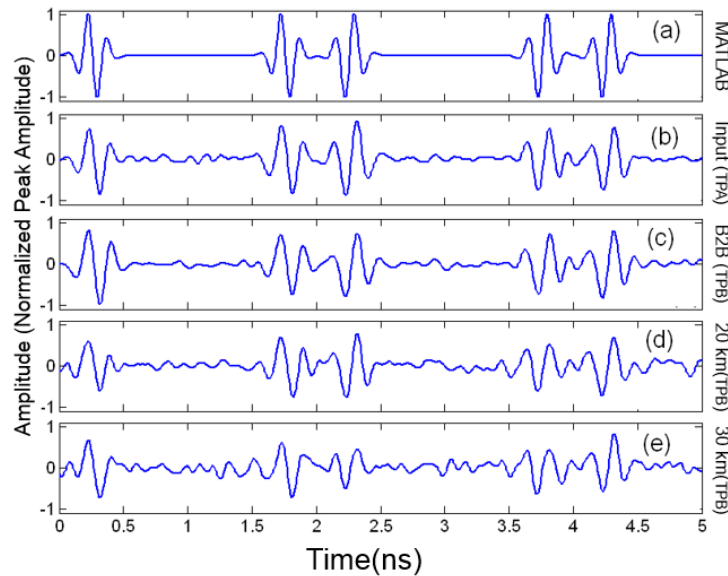
Figure 74. Degradation of SLF convolutionally coded Q-BOPPM IR UWB signals after the fiber transmission: (a) MATLAB® signal; (b) as measured at point A in Figure 69; (c) as measured in B2B configuration at point B in Figure 69; (d) as measured after 20-km SMF transmission; and (e) as measured after 30-km SMF transmission.

On the other hand, the IR-UWBoF-EIM/DD simulation testbed proposed in this thesis work was experimentally validated by using the figure of merit "Spectral Distortion Factor" (SDF) introduced in (Jazayerifar et al., 2008, Valente and Cartaxo, 2010). For our case, this SDF can be mathematically represented as

$$SDF = 1 - \frac{\langle S_e(f) \rangle \langle S_s(f) \rangle}{\sqrt{\langle S_e(f) \rangle \langle S_e(f) \rangle \langle S_s(f) \rangle \langle S_s(f) \rangle}} \qquad (24)$$

where $S_e(f)$ represent the experimentally measured PSD and $S_s(f)$ is the PSD obtained from the simulation testbed. Basically this figure of merit provides a numerical value corresponding to the correlation between both PSDs. These values are contained within [0, 1], where values near to zero indicate a high-degree of similarity between PSDs. The comparison between simulated and experimental power spectral densities (PSDs) are shown from Figure 75 to 77. Light color plots represent PSDs obtained from the IR-UWB testbed implemented in the *VPITransmissionMarker^{TM}* simulation software, whereas dark color plots depict PSDs experimentally measured from the practical implementation shown in Figure 70. Furthermore, the noise floor of the ESA FSV40 was plotted in gray color plot as a reference. It can be seen in all these figures that there exist a great similarity between both PSDs simulated and experimental. These similarities were quantitatively verified with Equation 24, giving values below than 0.1 for all PSDs evaluated. According to results obtained, it is possible to say that the IR-UWBoF simulation testbed implemented in the VPITranmissionMakerTM can be used as an experimental system to analyze and to evaluate IR-UWB transmissions through optical fiber links in a fast and accurate manner.
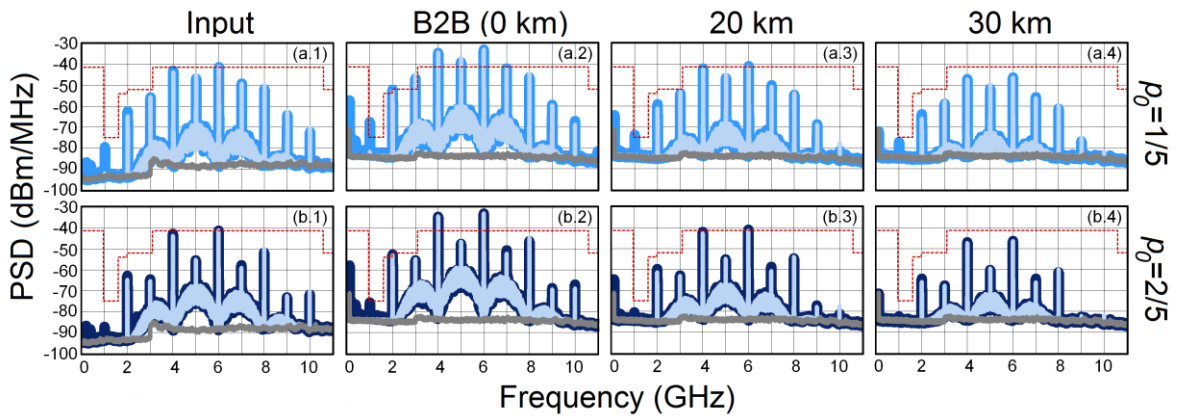
Figure 75. Comparison of simulated and measured power spectral densities (PSDs) of a non-coded BPPM IR-UWBoF-EIM/DD system. Simulated PSDs are represented with light color plots and measured PSDs with dark color plots.
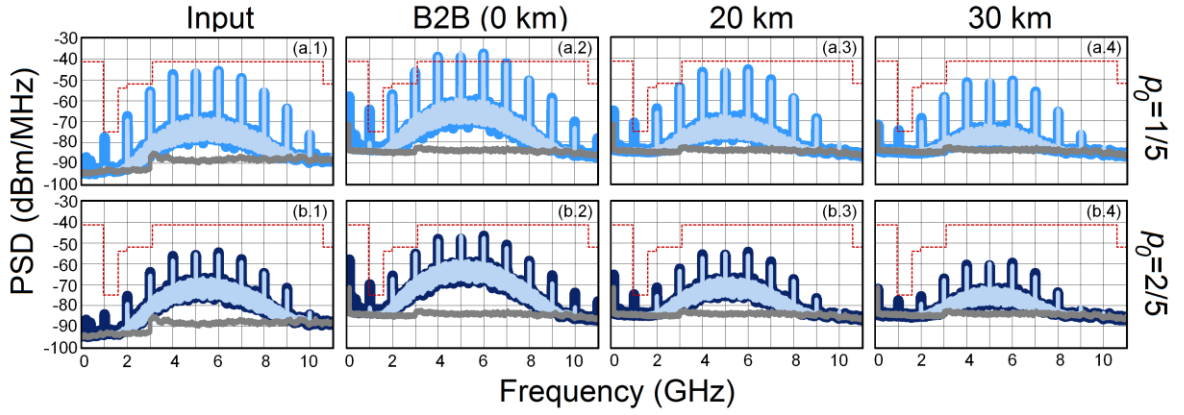
Figure 76. Comparison of simulated and measured power spectral densities (PSDs) of a non-coded BPSK IR-UWBoF-EIM/DD system. Simulated PSDs are represented with light color plots and measured PSDs with dark color plots.
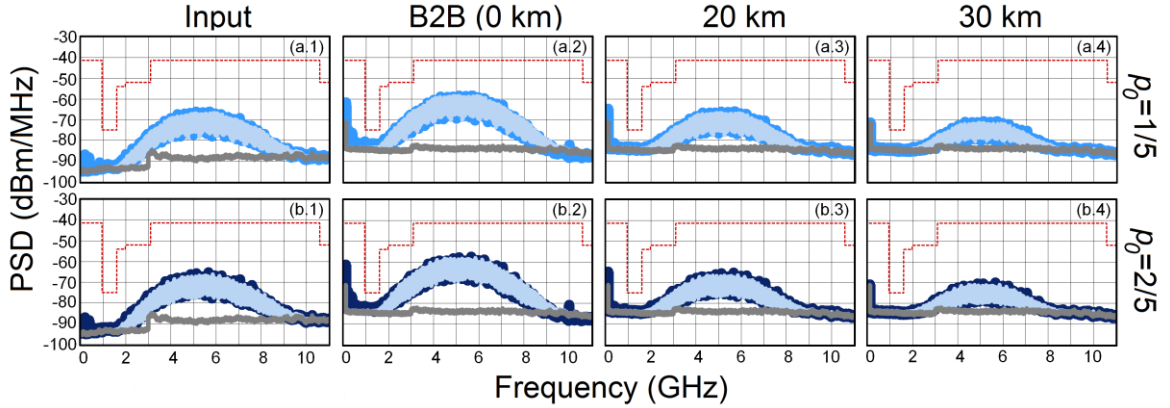
Figure 77. Comparison of simulated and measured power spectral densities (PSDs) of a convolutionally coded Quaternary BOPPM IR-UWBoF-EIM/DD system. Simulated PSDs are represented with light color plots and measured PSDs with dark color plots.

4.3.2 Experimental evaluation of a HDR IR-UWBoF DIM/DD system considering a fiber-wireless channel

The connecting diagram of the proposed SLF IR-UWBoF-DIM/DD experimental system is illustrated in Figure 78 and the setup implemented in SAMOVAR CNRS laboratory at Telecom SudParis is shown in Figure 79.
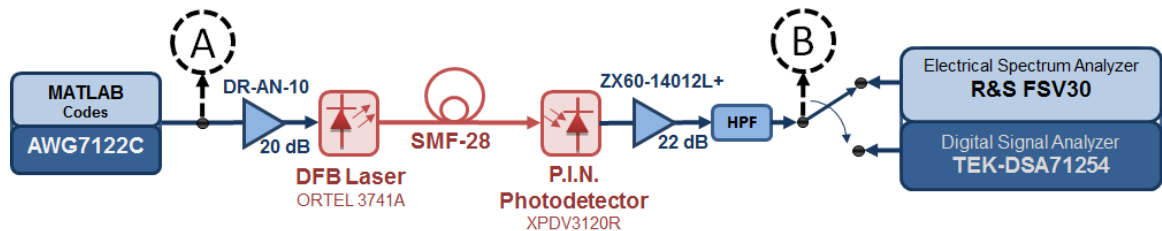
Figure 78. Connecting diagram of the experimental HDR SLF IR-UWBoF-DIM/DD setup.

In a similar way to the HDR1 system described in previous subsection, the IR-UWB transmitter is formed by an arbitrary waveform generator (E-AWG) with 9.6-GHz bandwidth, which was used for generating experimentally IR-UWB signals previously obtained with MATLAB® (Equation (9), (21) and (22) determine these IR-UWB signals). The simulated and experimentally generated waveforms, as well as their energy spectrum densities (ESDs) are shown in Figure 80. It is important to mention that 20 GHz coaxial cables were used in the experimental setup. Therefore, a PSD with a bandwidth greater than PSDs depicted in Figure 72 and Figure 73 can be observed.
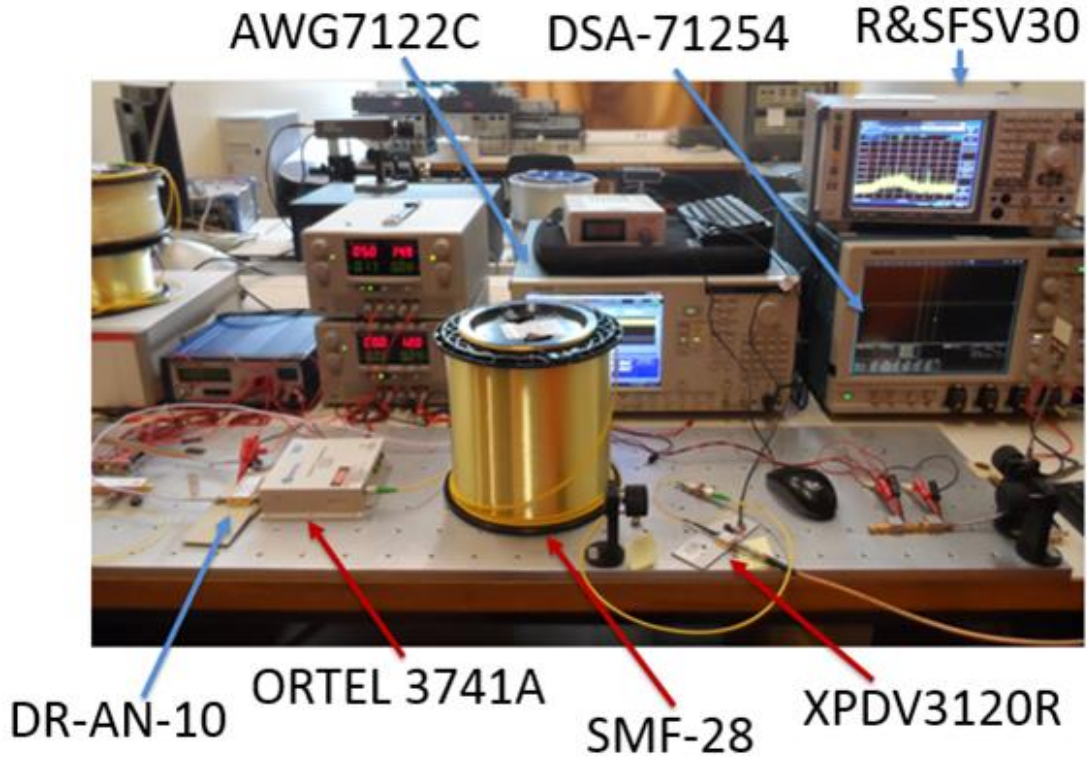
Figure 79. Experimental HDR SLF IR-UWBoF-DIM/DD setup implemented in SAMOVAR CNRS laboratory at Telecom SudParis.

Table 5: Signal parameters used in the IR-UWB transmitter of SLF IR-UWB-IM/DD systems experimentally implemented in SAMOVAR CNRS laboratory at Telecom SudParis.

Binary data stream [y_l]:	Frames of 1024 bits with two p.m.f.: p_0=1/5 and p_1=4/5; p_0=2/5 and p_1=3/5
PPM modulation index [T_β]:	0.5 ns
Mean repetition time between pulses [T_r]:	1.0 ns
Waveform [$w(t)$]:	Fifth-order derivative of a Gaussian pulse
Pulse width [T_{wT}]	500 ps (simulated) ≈ 580 ps (experimental)
Spectral line free convolutional encoder [SLF-CE] used for the coded signals:	Feedforward $(27, 31)_8$ and feedback $(23)_8$ polynomials with memory v=4. (see Figure 57)
TH and DS multiplication codes:	Not used
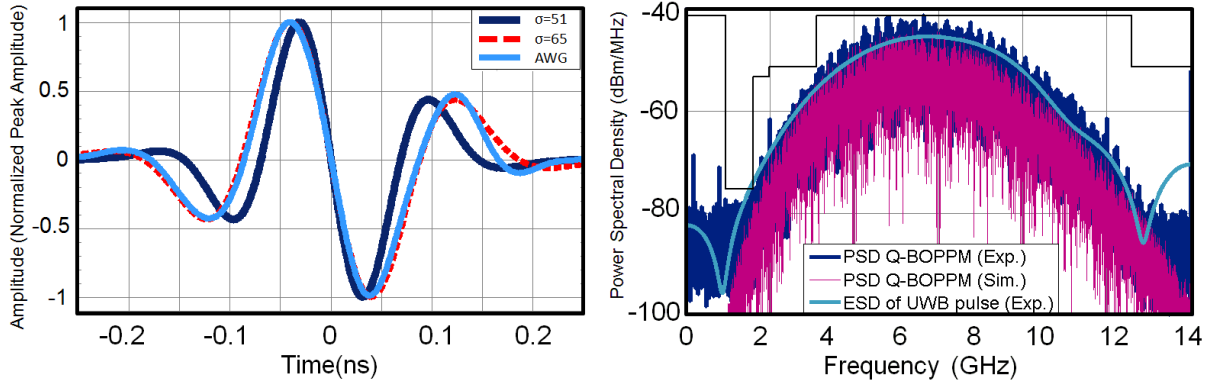
Figure 80. (a) Waveforms of the fifth-order derivative of a Gaussian pulse with $\sigma=51$ ps (dark plot), $\sigma=65$ ps (dotted red plot) and the UWB pulse experimentally generated by the AWG7122C (light blue plot). (b) Energy spectral density (ESD) of the experimental UWB pulse (light blue plot), simulated (red plot) and experimental (dark blue plot) PSD of a Q-BOPPM IR-UWB signal with $T_r=1$ns.
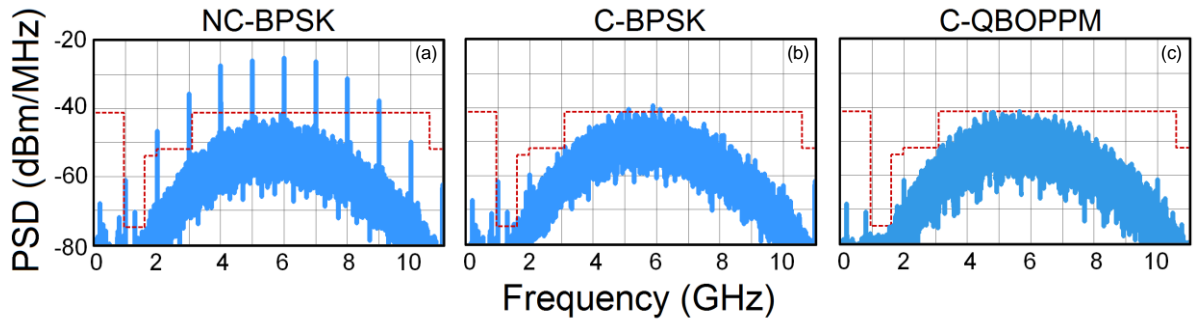
Figure 81. Experimental PSD of the non-coded BPSK IR-UWB signal and rate $1/2$ spectral line free convolutionally coded BPSK/Q-BOPPM IR-UWB signals generated with the AWG7122C. The signal parameters used to generate these PSDs are summarized in Table 5. The transmit power of the three signals was set at the same power level, taking as reference the PSD of the convolutionally coded Q-BOPPM signal.

On the other hand, Figure 81 shows three power spectral densities of IR-UWB signals: a) non-coded BPSK, b) SLF convolutionally-coded BPSK and c) SLF convolutionally-coded Q-BOPPM. All three signals consider an unbalanced data source (i.e. a data stream with p.m.f. $p_0=1/5$). Similar to results shown in Figure 72, the rate 1/2 SLF convolutional code (CC) is able to eliminate a great number of spectral lines (almost all) of BPSK/Q-BOPPM IR-UWB signals even when an unbalanced binary data source is connected to the input encoder. Nevertheless, Figure 81(a-c) shows PSDs with strong spectral lines below of 2.4 GHz and above of 9.9 GHz. It is assumed that these additional spectral lines appear as consequence of ringing and non-complementary UWB pulses generated by the E-AWG. Furthermore, it can be seen in Figure 81(c) that the rate 1/2 SLF-CC can eliminate more spectral lines by using Q-BOPPM signals than by using BPSK signals (see Figure 81b).

Apparently, this could be due to Q-BOPPM modulation format provide more randomness than the BPSK modulation scheme with N_w=2, where two consecutive pulses are transmitted by symbol. Unlike of rate 1/2 SLF-CC Q-BOPPM signals where one pulse is transmitted by symbol.

As it can be seen in Figure 78, this IR-UWB transmitter was connected to a 12 GHz optical modulator driver. This device was used to amplify electrical signals generated by the E-AWG and to enable appropriate impedance matching between the E-AWG and the RF input of a 1550 nm distributed feedback (DFB) laser. These amplified IR-UWB signals were able to modulate directly the laser's injection current to obtain optical IR-UWB signals, which were transmitted over an optical link formed by spools of 10-km, 20-km of standard single-mode fiber (SMF-28). At the output of the SMF, the IR-UWB signals were electrically recovered by means of a 75 GHz photodetector. In order to compensate some losses originated by the electrical-to-optical and optical-to-electrical conversion processes, two 14 GHz electrical amplifiers in cascade configuration were connected at photodetector output and after this section a high pass filter was added with the purpose to eliminate additional spectral lines generated by AWG at low frequencies. Additionally, a 12 GHz real-time digital signal analyzer (DSA) with 50 GSa/s and a 30 GHz electrical spectrum analyzer (ESA) have been connected at the output of the system (Test Point B in Figure 78). Both instruments have been used to digitize and store non-coded and convolutionally coded IR-UWB signals in time and frequency domain. Table 6 summarize the main technical characteristics of the equipment and devices used in this testbed.

The PSDs of the IR-UWB signals at the output of the system with B2B, 20-km and 30-km of SMF are shown in Figure 82. To make relevant PSD comparisons between different IR-UWB-IM/DD systems considered in this research, the pulse amplitude generated by the E-AWG was set to the same power level for all schemes. The light blue plots represent binary data streams with a p.m.f. p_0=1/5 and the dark blue plots those binary data streams with a p.m.f. p_0=2/5. It can be observed in all PSDs of Figure 82 that there exists additional spectral lines at frequencies above of 9.9 GHz and in the case of C-BPSK (Figure 82-b) there is a strong spectral line at 2 GHz. This spectral line could be due to ringing and/or non-complementary UWB pulses generated by the E-AWG (see the spectral line at 2 GHz in the PSD of Figure 81-b and Figure 81-c). On the other hand, the evolution of these

additional spectral lines along the fiber link shows the frequency chirp effect produced by the direct intensity modulation method which is augmented by the chromatic dispersion effect of SMF fiber. It can be seen in Figure 82 (a/b/c.2) and Figure 82 (a/b/c.3) as the power magnitude of these spectral lines increases as SMF length increases as well. Furthermore, it is possible to see as this combined effect (frequency chirp and chromatic dispersion) degradates the PSD shape in all schemes reported after 20-km of SMF transmission. In addition, as it was expected, we may observe that SLF convolutionally coded Q-BOPPM IR-UWB signals provides a spectral line free PSD over the SMF lengths tested (this sentence is true if we do not take into account the strong spectral line at 10 GHz, which it is generated by the E-AWG).

Previous results differ to those results reported in Section 3.4, in regard to the number of additional spectral lines that appear in the PSD after 20-km and 30-km of SFM transmission. Despite of this difference, the impact of the frequency chirp and chromatic dispersion were fully identified in this experimental setup.

Table 6. Measuring instruments and electrical/optical devices used in the SLF IR-UWBoF DIM/DD system implemented in SAMOVAR CNRS laboratory at Telecom SudParis.

| M. Instruments	Characteristics	Electrical devices	Characteristics
Arbitrary Waveform Generator (AWG7122C)	BW= 9.6 GHz Sample Rate= 24G Sa/s	Optical Modulator Driver (DR-AN-10-MO)	BW=12 GHz Gain: 20 dB
Digital Signal Analyzer (TEK-DSA71254)	BW= 12 GHz Sample Rate= 50 GSa/s	Amplifier (ZX60-14012L+)	BW=14 GHz
Spectrum Analyzer (R&S FSV30)	BW= 30 GHz Res. BW= 1 MHz Video BW= 3 MHz	High Pass Filter (VHF-2700A+)	BW=2.7-8.5 GHz
Optical Devices	**Characteristics**	**Optical Devices**	**Characteristics**
Laser DFB (ORTEL 3741A)	Opt. Power = 10 dBm Linewidth= 10 MHz BW_{RFmod}=0.1-10 GHz	Single Mode Fiber (SMF-28)	Reels of 10 km and 20 km
P.I.N photodetector (XPDV3120R)	BW=75 GHz	Optical Attenuator	5 dB
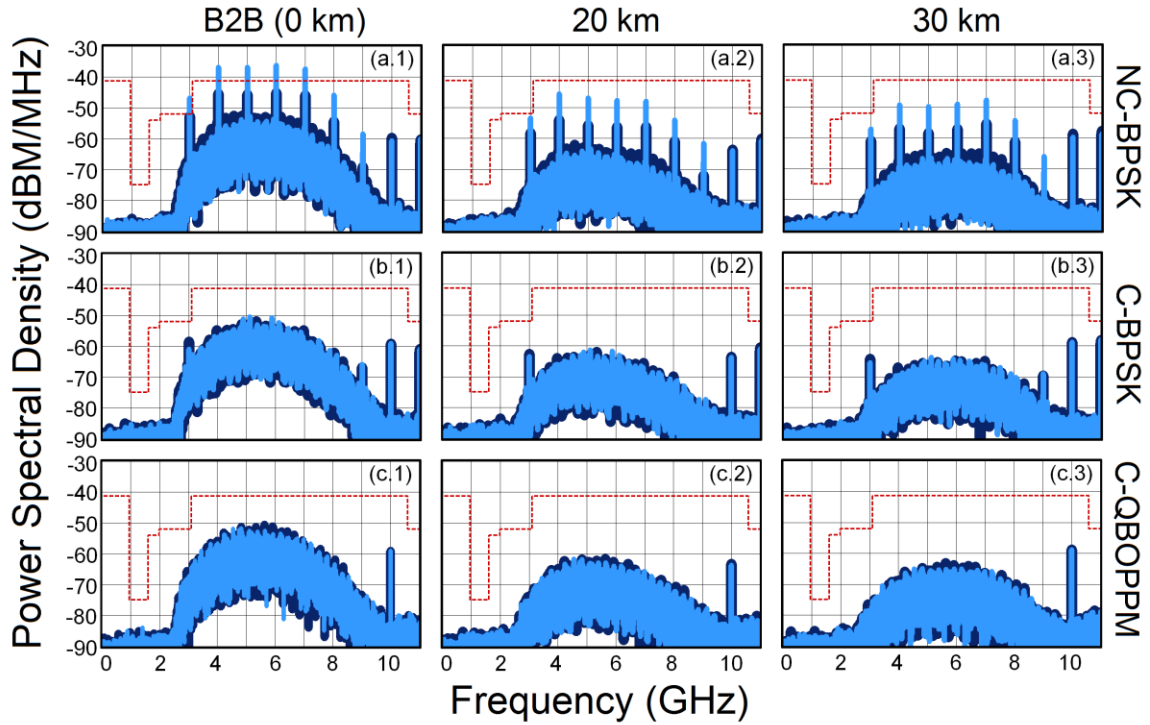
Figure 82. Experimental PSDs of the non-coded BPSK IR-UWB signal and SLF convolutionally coded BPSK/Q-BOPPM IR-UWB signals transmitted over 20-**km and** 30-**km of SMF-28 using DIM/DD RoF system. The signal parameters used for generating non-coded and convolutionally coded signals are summarized in Table 5.**

Finally, the spectral line suppression capabilities of the proposed SLF IR-UWBoF-DIM/DD system were evaluated over a fiber-wireless channel. Figure 83 depicts the connection diagram of the proposed system. As it can be seen in this figure, UWB signals were radiated into the free space by an Omni-directional antenna (KBOR AntRad-4). The wireless transmission distance was set at 0.3 m. This distance can be increased if high-gain electrical amplifiers are used (Xianbin Yu et al., 2013). The radiated UWB signals were received by a similar Omni-directional antenna, which is connected directly to an electrical spectrum analyzer (ESA) in order to obtain the PSD. Technical characteristics of this equipment are described in Table 6.

Figure 83. Connecting diagram of the experimental SLF IR-UWBoF DIM/DD system with wireless transmission.
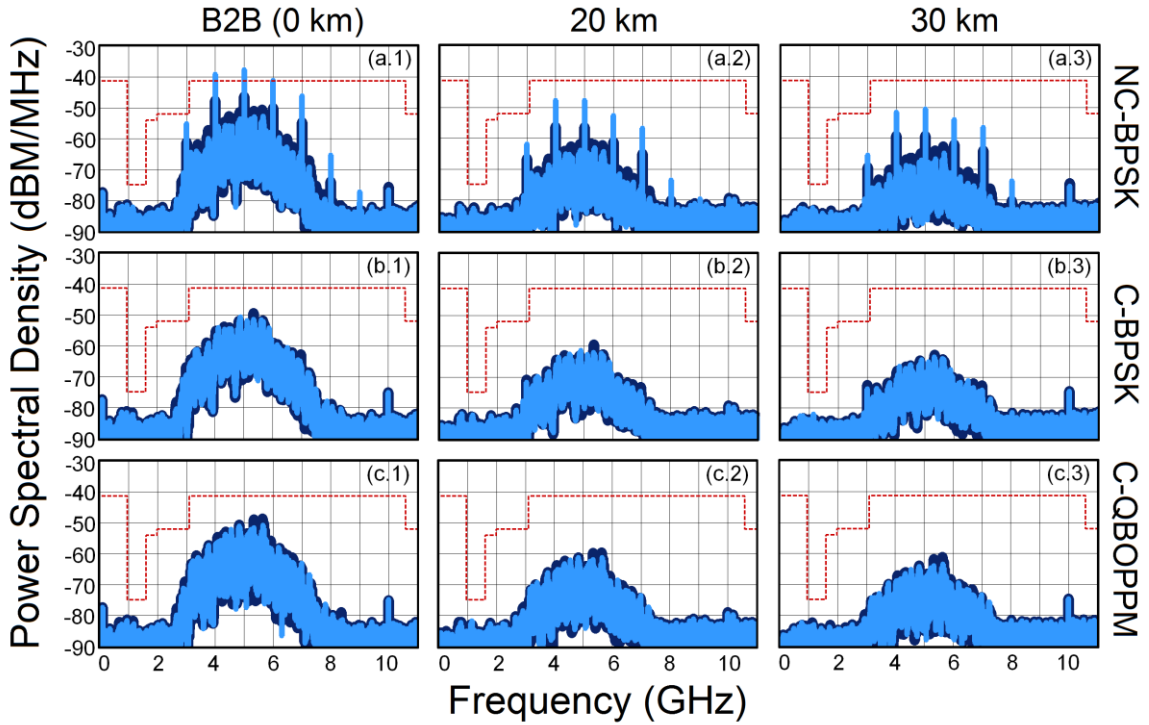
Figure 84. Experimental PSDs of the non-coded BPSK IR-UWB signal and SLF convolutionally coded BPSK/Q-BOPPM IR-UWB signals transmitted over 20-**km and** 30-**km of SMF-28 using DIM/DD RoF system with** 30 **cm of wireless transmission. The signal parameters used for generating non-coded and convolutionally coded signals are summarized in Table 5.**

Figure 84 shows the measured PSDs after the wireless transmission. A noticeable bandwidth reduction can be observed with respect to PSDs at the output of the RoF-DIM/DD architecture (see Figure 82). As expected, the frequency response and bandwidth limitations of these low cost antennas have modified the PSD shape. However, additional spectral lines below of 2.4 GHz and above 9 GHz are not present.

4.3.3 Experimental evaluations of a HDR2 IR-UWBoF EIM/DD system considering a fiber-wireless channel

The connecting diagram of the high data rate (HDR2) SLF IR-UWBoF-EIM/DD system that use external intensity modulation is depicted in Figure 85 and the practical setup implemented in SAMOVAR CNRS laboratory at Telecom SudParis is shown in Figure 86.
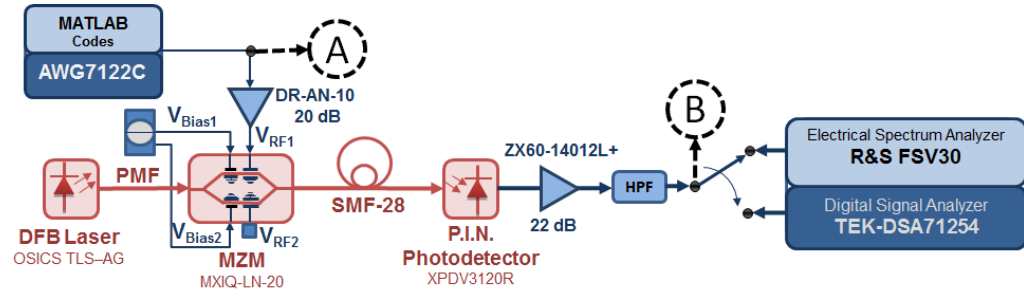
Figure 85. Connecting diagram of the HDR2 SLF IR-UWBoF EIM/DD system.
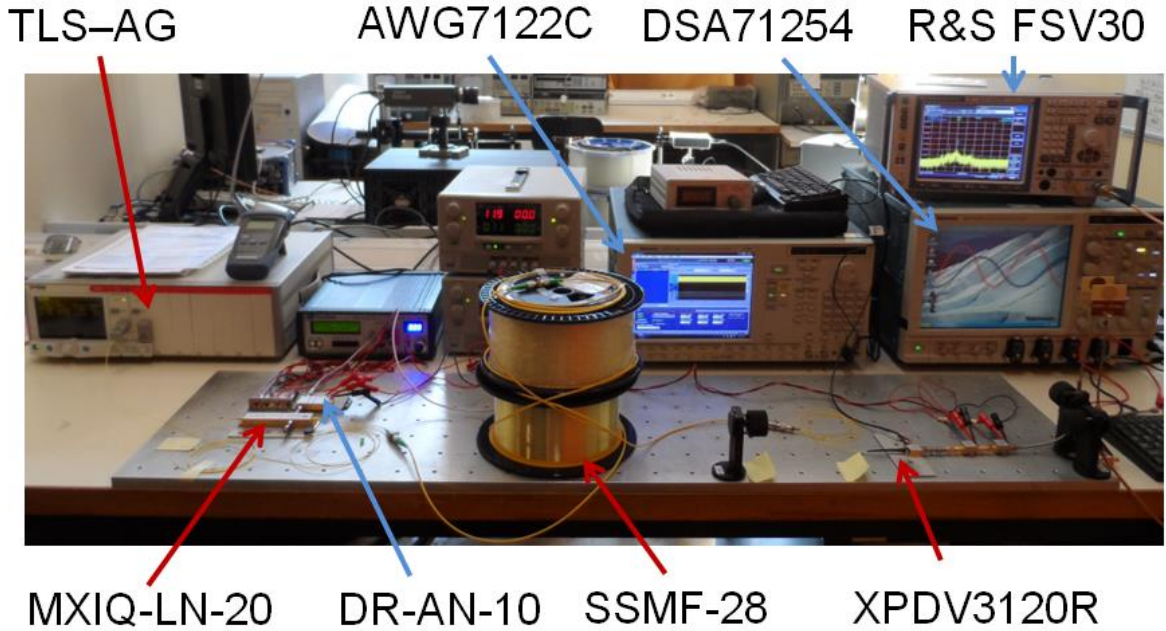
Figure 86. Experimental implementation of the HDR2 SLF IR-UWBoF EIM/DD system.

The system is formed by the IR-UWB transmitter described in previous subsection, and a 12 GHz RoF EIM/DD architecture. At the output of the IR-UWB transmitter (Test Point A in Figure 85) is connected a 12 GHz optical modulator driver. This device was used to amplify electrical signals generated by the E-AWG and to enable appropriate impedance matching between the E-AWG and the RF input of a 20 GHz dual parallel Mach-Zehnder Modulator (MZM). This dual-drive MZM has two arms which can be used to implement complex optical modulations, however, in our experimental evaluations only one RF input was used to modulate externally the light emitted by a 1550 nm DFB laser. The other MZM's RF port was terminated to 50 ohms. The optical fiber link of the RoF architecture was formed by spools of SMF-28 with fiber lengths of 10-km and 20-km. At the output of the fiber, the IR-UWB signals were electrically recovered by means of a 75 GHz

photodetector. In order to compensate some losses originated by the electrical-to-optical and optical-to-electrical conversion processes, two 14 GHz electrical amplifiers in cascade configuration were connected at photodetector output and after this section a high-pass filter was added with the purpose to eliminate additional spectral lines generated by E-AWG at low frequencies. In addition, a 12 GHz real-time digital signal analyzer (DSA) with 50 GSa/s and a 30 GHz electrical spectrum analyzer (ESA) have been connected at the Test Point B pointed out in Figure 85. Both instruments have been used to digitize and store non-coded and coded IR-UWB signals in time and spectral domain. In addition, it is important to mention that a bench top automatic bias controller (MBC-IQ-BT from Photline) was used to operate in the "QUAD point" of the transfer function of this dual-parallel MZM, ensuring a stable functioning over time and environmental conditions.

Table 7. Measuring Instruments and electrical/optical components used in the HDR2 SLF IR-UWBoF EIM/DD system implemented in the SAMOVAR CNRS laboratory at Telecom SudParis.

| M. Instruments	Characteristics	Optical Devices	Characteristics
Arbitrary Waveform Generator (AWG7122C)	BW= 9.6 GHz Sample Rate= 24G Sa/s	Laser DFB (ORTEL 3741A)	Optical Power= 14.5 dBm LW= 100 KHz
Digital Signal Analyzer (TEK-DSA71254)	BW= 12 GHz Sample Rate= 50 GSa/s	Single Mode Optical Fiber (SSMF-28)	Reels of 10 km and 20 km
Spectrum Analyzer (R&S FSV40)	BW= 30 GHz Resolution BW= 1 MHz Video BW= 3 MHz	Dual Parallel Mach Zehnder Modulator (MXIQ-LN-20)	$V_{\pi DC1}=6.8V$; $V_{\pi DC2}=6.9V$; $V_{\pi DC3}=16.5V$; $V_{\pi RF1}=5.6V$; $V_{\pi RF1}=5.5V$; $BW_{RF1}=12$ GHz $BW_{RF2}=12$ GHz
		P.I.N photodetector (XPDV3120R)	BW=75 GHz
Electrical Devices	**Characteristics**	**Electrical Devices**	**Characteristics**
Amplifier (ZX60-14012L+)	BW=14 GHz	High Pass Filter (VHF-2700A+)	BW=2.7-8.5 GHz
Optical Modulator Driver (DR-AN-10-MO)	BW=12 GHz	MBC-IQ-BT	VCD1=2.92; VCD2=1.7; VCD3=0
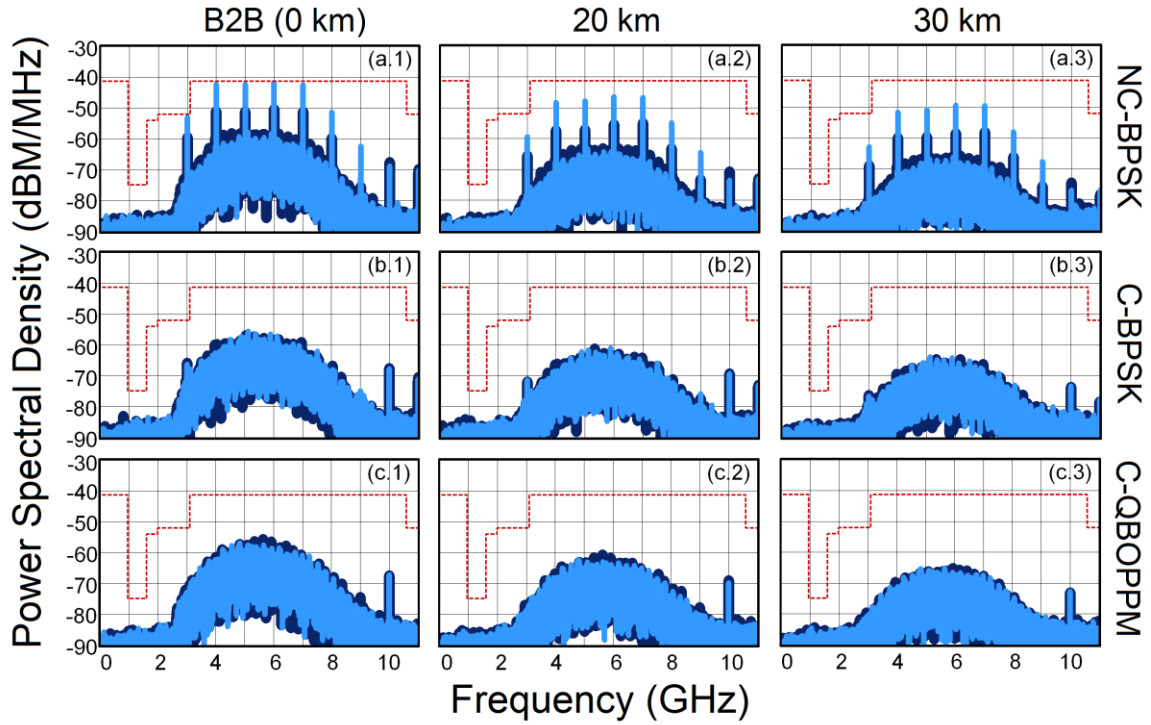
Figure 87. Experimental PSDs of the non-coded BPSK IR-UWB signal and SLF convolutionally coded BPSK/Q-BOPPM IR-UWB signals transmitted over 20-km and 30-km of SMF28 using EIM/DD RoF system. The signal parameters used for generating non-coded and convolutionally coded signals are summarized in Table 5.

The same non-coded and rate $1/2$ SLF convolutionally coded IR-UWB signals discussed in previous subsections were initially generated in MATLAB® and then loaded into the AWG7122C. The PSDs obtained after 20-km and 30-km of SMF transmission are shown in Figure 87. The light blue plots represent the binary data streams with a p.m.f. $p_0=1/5$ and the blue dark plots those with a p.m.f. $p_0=2/5$. It can be observed in all PSDs of Figure 87 that there exists additional spectral lines at high frequencies (> 9 GHz). Similar to previous testbed (see Figure 82), it can be assumed that the spectral lines are emerging due to the ringing and non-complementary UWB pulses generated by the E-AWG. It is important to highlight that in this PSDs the power magnitude of these additional spectral lines decrease whereas the fiber length is increased. In addition, the PSD shape is not modified noticeable after 20-km of SMF transmission. This is due to the electrical-to-optical conversion process is operating in linear region and there not exist frequency chirping in this optical configuration.
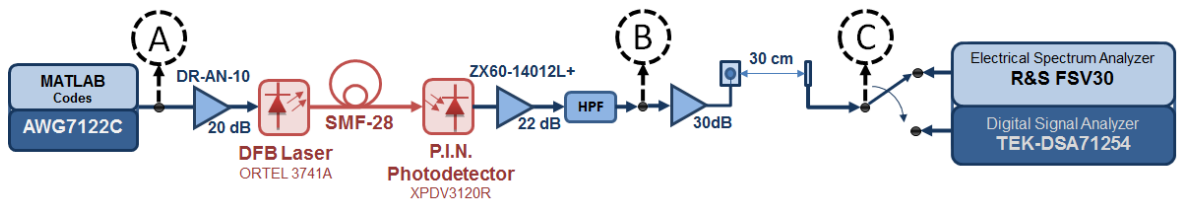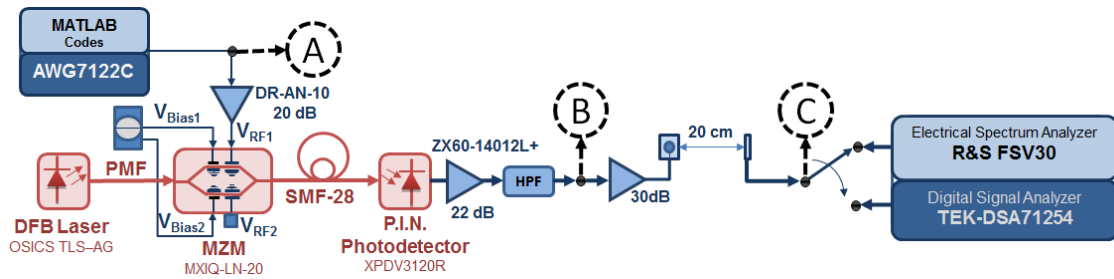
Figure 88. Connecting diagram of the experimental HDR2 SLF IR-UWBoF EIM/DD system with wireless transmission.
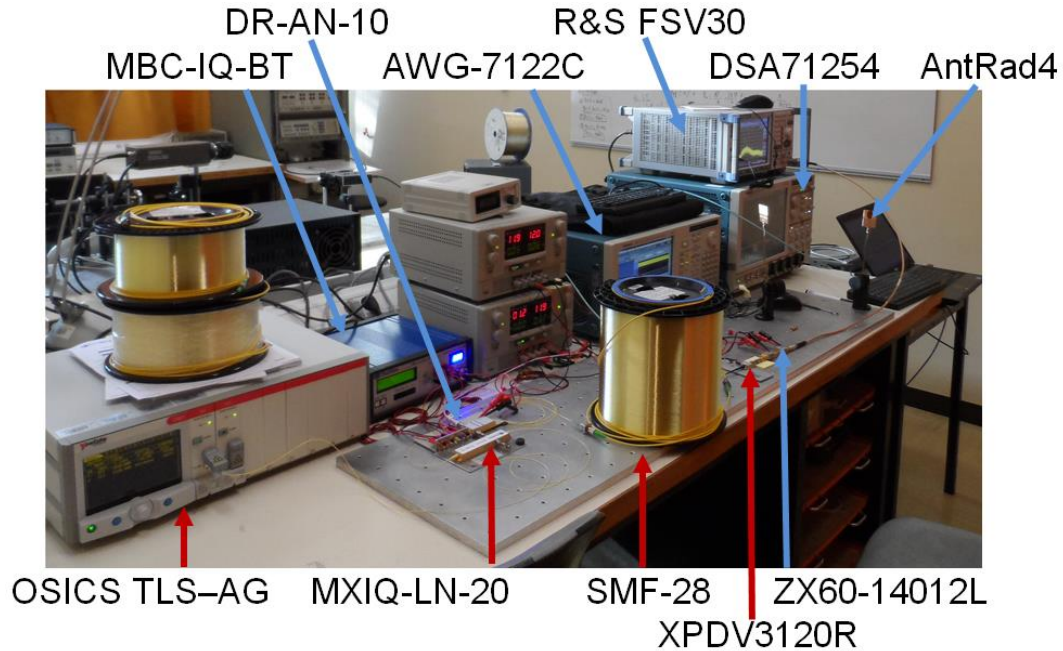
Figure 89. Experimental implementation of the HDR2 SLF IR-UWBoF EIM/DD system with wireless transmission.

On the other hand, the spectral line suppression capabilities of this HDR2 system were evaluated over a fiber-wireless channel. Figure 88 shows the connection diagram of the SLF HDR2 IR-UWBoF-EIM/DD with wireless transmission and Figure 89 shows the experimental setup implemented in SAMOVAR CNRS laboratory.

A line-of-sigh (LOS) wireless channel with antenna separation of 20-cm was used to carry out our assessments. The same Omni-directional antennas described in previous subsection were used in this setup. The power spectral densities (PSDs) obtained from this system are shown in Figure 90. As it can see in this figure there exist a noticeable reduction of the transmitted bandwidth. However, it is important to note that additional spectral lines are not present in the PSDs of all schemes after the wireless transmission.
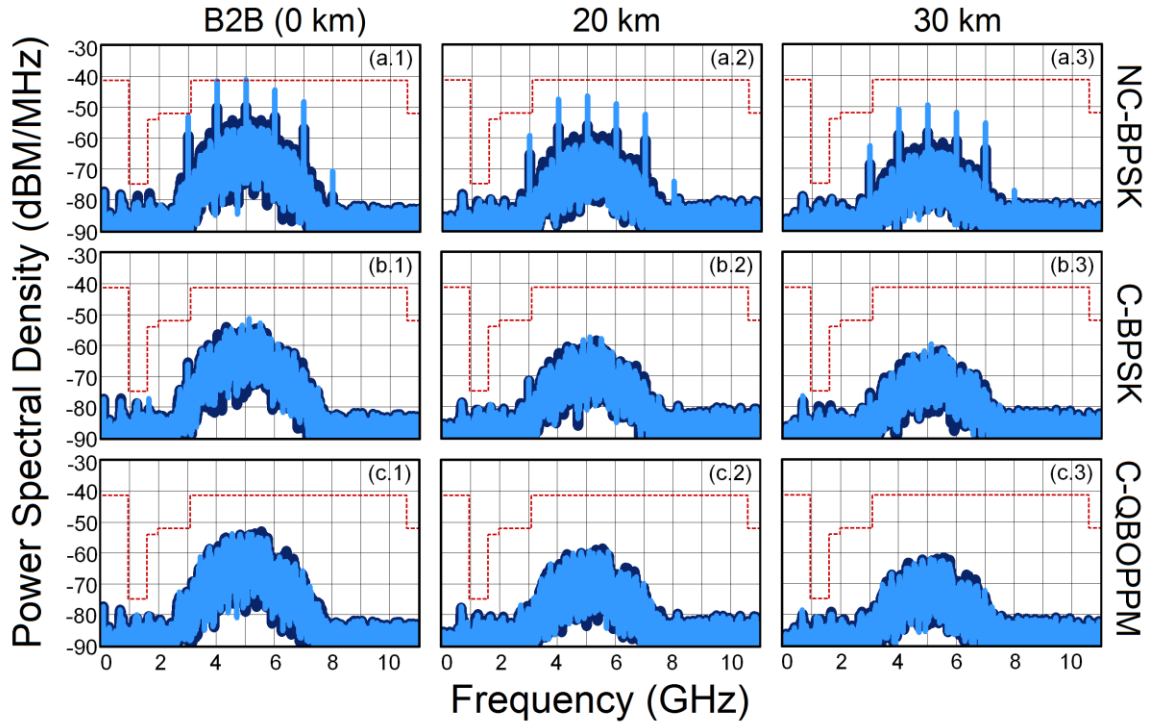
Figure 90. Experimental PSDs of the non-coded BPSK IR-UWB signal and SLF convolutionally coded BPSK/Q-BOPPM IR-UWB signals transmitted over 20-km and 30-km of SMF-28 using EIM/DD RoF system with 20 cm of wireless transmission.

4.4 Summary and discussion

In Section 4.2 a low-cost and low-complexity spectral line suppressive convolutionally encoded 16-PPM IR-UWBoF-DIM/DD system designed for WSNs applications was proposed. This system uses a spectral line suppressive (SLS) convolutional code (CC) to achieve spectral line suppression in the power spectral density (PSD). Experimental results have shown that the system does not distort or add spectral lines to the IR-UWB signal PSD transmitted over 30 km of a single-mode fiber, thus demonstrating its feasibility to interconnect WSN deployments.

In subsection 4.3.1 the experimental implementation of the spectral line free (SLF) BPSK/Q-BOPPM IR-UWBoF-EIM/DD simulation testbed proposed in Chapter 3 was analyzed. In addition, the spectral line suppression capabilities of the proposed system were reported. As it can be seen in this subsection, this system has been able to generate SLF-PSDs for all tested fiber lengths, even when the binary data stream at the input of the system was unbalanced ($p0 \neq 1/2$). Furthermore, the IR-UWBoF-EIM/DD simulation

testbed designed and implemented in the *VPITransmissionMarker^TM* simulation software was experimentally validated by using the figure of merit "spectral distortion factor" (SDF). Results of this validation process were satisfactory. It was found a great similarity between the PSDs obtained from the simulation testbed with those PSDs measured from the experimental setup. Therefore, this simulation testbed now could be used as an experimental system where spectral characteristics of non-coded and coded IR-UWB signals would be analyzed and evaluated in a fast and accurate way.

In subsection 4.3.2 and 4.3.3, experimental implementations of two high data rate (HDR) spectral line free (SLF) IR-UWBoF systems that use both IM/DD-RoF architectures, direct and external, were described. In addition, the spectral line suppression capabilities of these experimental systems considering fiber-wireless links were reported. Experimental results obtained after 20-km and 30-km of SMF transmission, have shown the capability of both systems to suppress spectral lines within UWB frequency band (from 3.1 GHz to 10.6 GHz). Despite of these important results, it is worth to mention that strong spectral lines were observed at frequencies above of 9 GHz in all measured PSDs. It is assumed that these spectral lines emerged mainly due to UWB pulses generated by the E-AWG were not complementary, (Pan and Yao, 2010-A). In regard to the impact of the chromatic dispersion effect observed in both RoF architectures (DIM and EIM), on one hand, the power spectral densities (PSDs) of IR-UWBoF DIM/DD systems shown a slight degradation after 20-km SMF transmission. On the other hand, the PSDs of of IR-UWBoF EIM/DD systems do not show any noticeable degradation for all length of SMF. We assume that this degradation was resulted of the frequency chirp effect produced by the direct intensity modulation (DIM) method which is augmented by the chromatic dispersion effect of SMF fiber. As it can be seen in Figure 82 this combined effect tends to be more evident as the fiber length is increased. Regarding to the wireless transmission, the assessments performed confirm that the spectral shaping capabilities of both systems are kept for fiber-wireless channels considered.

Chapter 5. Contributions, conclusions and areas of future research

5.1 Contributions

The main contributions of this thesis work are two Impulse-Radio Ultra-wideband over Fiber (IR-UWBoF) systems with spectral line suppression capabilities. High-Data Rate (HDR) and Low-Data Rate WPAN applications can be covered with each one of the proposed systems. The proposed HDR-IR-UWBoF system uses a rate $1/2$ spectral line free (SLF) convolutional encoder (CE) able to suppress all spectral lines in the PSD of BPSK/Q-BOPPM IR-UWB signals even when the binary stream at the encoder input is generated by an unbalanced binary data source ($p_0 \neq 1/2$). This system uses the external IM/DD technique in order to provide stability in high data rate communications without generating additional spectral lines in the electrical-to-optical and optical-to electrical conversion processes. Furthermore, as it was experimentally demonstrated, the fiber-wireless link formed by 30 km of SMF and 20 cm of line of sight (LOS) wireless transmission do not generate additional spectral lines in the PSD. On the other hand, the proposed LDR IR-UWBoF system uses a rate $1/4$ spectral line suppressive (SLS)-CE designed for suppressing several spectral lines in the PSD of M-PPM IR-UWB signals that follows non-uniform distributions. This system uses a very simple IR-UWB transmitter, which is connected to a RoF architecture that utilizes the direct IM/DD technique. The combination of both elements allow to implement a low cost and low complexity IR-UWBoF system that can be used for wireless sensor networks applications in next smart city scenarios. In addition, an experimentally validated IR-UWBoF-EIM/DD simulation testbed was provided. This testbed was designed and implemented in the *VPITransmissionMarker^{TM}* simulation software from VPIphotonics Company.

5.2 Conclusions

In this thesis a low-cost and low-complexity spectral line suppressive convolutionally encoded 16-Pulse Position Modulation (PPM) Impulse Radio Ultra-wideband over fiber (IR-UWBoF) system designed for wireless sensor networks (WSNs) applications has been proposed. The spectral line suppression capability of the proposed system has been experimentally demonstrated for non-perfectly random input data streams. It has been

shown that these capabilities are kept over fiber links up to 30 km using a low-cost and low-complex direct intensity modulation with direct detection (DIM/DD)-Radio over Fiber (RoF) architecture, thus showing its feasibility to interconnect WSNs deployments. Furthermore, a simple high data rate (HDR) IR-UWBoF system that considers the use of spectral line free convolutional codes (SLF-CCs) to suppress the spectral lines in the power spectral density (PSD) has been proposed. The spectral line suppression capabilities of the proposed HDR SLF convolutionally coded IR-UWBoF system has been experimentally demonstrated for unbalanced ($p_0{\neq}1/2$) i.i.d. input binary data streams. It has been shown that these capabilities are kept over fiber links up to 30 km with 20 cm of wireless transmission using the external intensity modulation with direct-detection (EIM/DD) RoF architecture. These spectral line suppression capabilities enable to increase power transmission compared with traditional IR-UWBoF implementations, thus, improving the transmission range and/or the BER. Finally, in this thesis a HDR IR-UWBoF-EIM/DD testbed designed and implemented in the *VPITransmissionMaker^{TM}* simulation software was provided. The validation process of this simulation testbed was performed by means of the spectral distortion factor (SDF) between the PSD of IR-UWB signals generated by this simulation testbed and the experimental PSD of signals obtained from the system described in subsection 4.3.1. The results of this validation process show that the simulated testbed can be used as an experimental system to analyze and to evaluate IR-UWB transmissions through optical fiber links in a fast and accurate manner.

5.3 Areas of future research

Some interesting areas of future research identified are:

- Perform bit error rate (BER) evaluations of the proposed SLF/SLS IR-UWBoF-IM/DD systems considering wireless transmission in multipath channels and multi-user scenarios.

- Theoretical and experimental analysis of channel coding with spectral shaping capabilities for IR-UWB over Free Space Optics systems (IR-UWBoFSO).

- Turbo-codification with spectral line suppression capabilities specially designed for IR-UWBoF systems.

- Proposal of an all-optical technique that allow to eliminate spectral lines in the PSD of IR-UWB transmissions in order to fit under the FCC spectral masks.

List of references

Abraha, S. T. (2012). Impulse radio ultra wideband over fiber techniques for broadband in-building network application. Diss. Ph. D. thesis. Eindhoven: Tech. Univ. Eindhoven.

Abraha, S., Okonkwo, C., Gamage, P., Tangdiongga, E., and Koonen, T. (2012). Routing of power efficient ir-uwb wireless and wired services for in-building network applications. Journal of Lightwave Technology, *30*(11), 1651-1663. doi:10.1109/JLT.2012.2189554.

Abraha, S., Okonkwo, C., Tangdiongga, E., and Koonen, A. (2011). Power-efficient impulse radio ultrawideband pulse generator based on the linear sum of modified doublet pulses. *36*, 2363-2365 . doi:10.1364/OL.36.002363.

Abtahi, M., and Rusch, L. (2011). RoF Delivery over PONs of Optically Shaped UWB Signals for Gigabit/s Wireless Distribution in the Home. IEEE Journal on Selected Areas in Communications, *29*(6), 1304-1310. doi:10.1109/JSAC.2011.110617.

Abtahi, M., Dastmalchi, M., LaRochelle, S., and Rusch, L. (2009). Generation of Arbitrary UWB Waveforms by Spectral Pulse Shaping and Thermally-Controlled Apodized FBGs. *J*ournal of Lightwave Technology, *27*(23), 5276-5283. doi:10.1109/JLT.2009.2031128.

Abtahi, M., Mirshafiei, M., LaRochelle, S., and Rusch, L. (2008-A). All-Optical 500-Mb/s UWB Transceiver: An Experimental Demonstration. Journal of Lightwave Technology, *26*(15), 2795-2802. doi:10.1109/JLT.2008.925621.

Abtahi, M., Magne, J., Mirshafiei, M., Rusch, L., and LaRochelle, S. (2008-B). Generation of Power-Efficient FCC-Compliant UWB Waveforms Using FBGs: Analysis and Experiment. Journal of Lightwave Technology, *26*(5), 628-635. doi: 10.1109/JLT.2007.916586.

Aedudodla, S., Vijayakumaran, S., and Wong, T. (2006). Ultra-wideband signal acquisition with hybrid DS-TH spreading. IEEE Transactions on Wireless Communications, *5*(9), 2504-2515. doi:10.1109/TWC.2006.1687774.

Aiello, G., and Rogerson, G. (2003). Ultra-wideband wireless systems. IEEE Microwave Magazine, *4*(2), 36-47. doi:10.1109/MMW.2003.1201597.

Alexander, S. (1997). Optical Communication Receiver Design. Bellingham, Washington: SPIE Opt. Eng. Press.

Arslan, H., Chen, Z., and Di Benedetto, M. (2006). Ultra Wideband Wireless Communication. Wiley Interscience.

Baykas, T., Sum, C.-S., Lan, Z., Wang, J., Rahman, M., Harada, H., and Kato, S. (2011). IEEE 802.15.3c: the first IEEE wireless standard for data rates over 1 Gb/s. IEEE Communications Magazine, *49*(7), 114-121. doi:10.1109/MCOM.2011.5936164.

Bellorado, J., Ghassenzadeh, S., Kavcic, A., Tarokh, B., and Tarokh, V. (2004). Time-hopping sequence design for narrowband interference suppression. Vehicular Technology Conference, 2004. VTC2004-Fall. 2004 IEEE 60t, *6*, 3925-3929. doi:10.1109/VETECF.2004.1404813.

Beltran, M., Jensen, J., Llorente, R., and Monroy, I. (2011-A). Experimental Analysis of 60-GHz VCSEL and ECL Photonic Generation and Transmission of Impulse-Radio Ultra-Wideband Signals. IEEE Photonics Technology Letters, *23*(15), 1055-1057. doi:10.1109/LPT.2011.2153841.

Beltran, M., Jensen, J., Yu, X., Llorente, R., Rodes, R., Ortsiefer, M., and Monroy, I. (2011-B, June). Performance of a 60-GHz DCM-OFDM and BPSK-Impulse Ultra-Wideband System with Radio-Over-Fiber and Wireless Transmission Employing a Directly-Modulated VCSEL. IEEE Journal on Selected Areas in Communications, *29*(6), 1295-1303. doi:10.1109/JSAC.2011.110616

Bolea, M., Mora, J., Ortega, B., and Capmany, J. (2009). Optical UWB pulse generator using an N tap microwave photonic filter and phase inversion adaptable to different pulse modulation formats. Optics Express, *17*, 5023-5032. doi:10.1364/OE.17.005023

Bolea, M., Mora, J., Ortega, B., and Capmany, J. (2010). Flexible Monocycle UWB Generation for Reconfigurable Access Networks. IEEE Photonics Technology Letters, *22*(12), 878-880. doi:10.1109/LPT.2010.2047011.

Boubaker, N., and Letaief, K. (2003). Ultra wideband DSSS for multiple access communications using antipodal signaling. IEEE International Conference on Communications, 2003. ICC '03. 3, 2197-2201. IEEE. doi:10.1109/ICC.2003.1204047.

Casimer DeCusatics. (2008). Handbooks of Fiber Optic Data Communication(A Practical Guide to Optical Networking), (3rd ed.). California: Academic Press.

CEPT/ECC. (2006-A). ECC Decision of 24 March 2006 on the harmonised conditions for devices using Ultra-Wideband (UWB) technology in bands below 10.6 GHz, CEPT/ECC.

CEPT/ECC. (2006-B). ECC Decision of 1 December 2006 on the harmonised conditions for devices using Ultra-Wideband (UWB) technology with Low Duty Cycle (LDC) in the frequency band 3.4 - 4.8 GHz, CEPT/ECC.

Chang, Q., Tian, Y., Ye, T., Gao, J., and Su, Y. (2008). A 24-GHz Ultra-Wideband Over Fiber System Using Photonic Generation and Frequency Up-Conversion. IEEE Photonics Technology Letters, *20*(19), 1651-1653. doi:10.1109/LPT.2008.2002746.

Chang, Y. M., Lee, J., Lee, H.-S., Yan, L., and Lee, J. H. (2011). Generation and Distribution of 1.25 Gb/s Ultrawideband Doublet Pulses Based on the Combination of Nonlinear Polarization Rotation and Parametric Amplification. Journal of Lightwave Technology, *29*(6), 931-938. doi:10.1109/JLT.2011.2109698.

Chengliang Yang, Li Xia, Songnian Fu, and Deming Liu. (2014-A). A UWB pulse generation based on a phase modulator and programmable filter. Optics Communications, *318*, 166–170. doi:10.1016/j.optcom.2013.12.080.

Chengliang Yang, Li Xia, Songnian Fu, and Deming Liu. (2014-B). Reconfigurable UWB Pulse Generation Based on Multi-Taps and a Programmable Filter. IEEE Photonics Technology Letters, *26*(14), 1395-1398. doi:10.1109/LPT.2014.2325893.

Chiddix, J., Laor, H., Pangrac, D., Williamson, L., and Wolfe, R. (1990). AM video on fiber in CATV systems: need and implementation. IEEE Journal on Selected Areas in Communications, *8*(7), 1229-1239. doi:doi: 10.1109/49.59122.

Chow, C., Kuo, F., Shi, J., Yeh, C., Wu, Y., Wang, C., and Pan, C. (2010). 100 GHz ultra-wideband (UWB) fiber-to-the-antenna (FTTA) system for in-building and in-home networks. Optics Express, 473-478. doi:10.1364/OE.18.000473.

Chowdhury, A., Chien, H.-C., Fan, S.-H., Yu, J., Jayant, N., and Chang, G.-K. (2011). Radio over fiber technology for next-generation e-health in converged optical and wireless access network. Optical Fiber Communication Conference and Exposition (OFC/NFOEC), and the National Fiber Optic Engineers Conference, 1-3. doi:10.1364/OFC.2011.OTuF1.

Colli-Vignarelli, J., and Dehollain, C. (2011-A). A Discrete-Components Impulse-Radio Ultrawide-Band (IR-UWB) Transmitter. IEEE Transactions on Microwave Theory and Techniques, *59*(4), 1141-1146. doi:10.1109/TMTT.2011.2114194.

Colli-Vignarelli, J., Feldman, A., Robert, S., and Dehollaini, C. (2011-B). A discrete-component Impulse-Radio Ultra-Wide Band (IR-UWB) receiver with I/Q demodulation. 7th Conference on Ph.D. Research in Microelectronics and Electronics (PRIME), 245-248. doi:10.1109/PRIME.2011.5966279.

Cooper, A. (1990). Fibre/radio for the provision of cordless/mobile telephony services in the access network. Electronics Letters, *26*(24), 2054-2056. doi:10.1049/el:19901325.

Cox, C. I., Ackerman, E., Betts, G., and Prince, J. (2006). Limits on the performance of RF-over-fiber links and their impact on device design. IEEE Transactions on Microwave Theory and Techniques, *54*(2), 906-920. doi:10.1109/TMTT.2005.863818.

Dai, Y., and Yao, J. (2010). Nonuniformly Spaced Photonic Microwave Delay-Line Filters and Applications. IEEE Transactions on Microwave Theory and Techniques, *58*(11), 3279-3289. doi:10.1109/TMTT.2010.2074570.

DeCusatics, C. (2008). *Handbooks of Fiber Optic Data Communication(A Practical Guide to Optical Networking)*, 3ed. California: Academic Press.

Deepak Kumar Mohapatra. (2013). e-Health Applications. IJCA Proceedings on International Conference in Distributed Computing and Internet Technology 2013, 6-11.

Di Benedetto , M., and Giancola, G. (2004). Understanding Ultra Wide Band Radio Fundamentals. Prentice Hall.

Di Benedetto , M., Kaiser, T., Molish, A., Oppermann , I., Politano, C., and Porcino , D. (2006). *UWB* Communication Systems: A Comprehensive Overview. Hindawi Publishing Corporation.

Djordjevic, I., Ryan, W., and Vasic, B. (2010). *Coding for Optical Channels.* New York: Springer-Verlag.

Dong, J., Zhang, X., Xu, J., and Huang, D. (2007). All-optical ultrawideband monocycle generation utilizing gain saturation of a dark return-to-zero signal in a semiconductor optical amplifier. Optics Letters, *32*, 2158-2160. doi:10.1364/OL.32.002158.

Dong, J., Zhang, X., Zhang, Y., and Huang, D. (2008). Optical UWB doublet pulse generation using multiple nonlinearities of single SOA. Electronics Letters, *44*(18), 1083-1084. doi:10.1049/el:20080439.

Dong, J., Zhang, Y., Yu, Y., Huang, D., and Zhang, X. (2010). Photonic generation of power-efficient ultra-wideband waveforms using a single semiconductor optical amplifier. Communications and Photonics Conference and Exhibition (ACP), 2010 Asia, 693-694. doi:10.1109/ACP.2010.5682693.

ECMA-368. (2008). Standard ECMA-368: High rate ultra wideband PHY and MAC standard. 3rd. ECMA International.

Federal Communications Comission. (2002). First Report and Order, revision of part 15 of the Commission's rules regarding ultra-wideband transmission systems. ET Docket 98-153, FCC 02-48.

Feng, H., Xiao, S., Yi, L., & Hu, W. (2014-A). Photonic Generation of Reconfigurable Orders Ultrawideband Signals by Using Cascaded RSOAs. IEEE Photonics Technology Letters, *26*(9), 908-910. doi:10.1109/LPT.2014.2309934.

Feng, H., Fok, M., Xiao, S., Ge, J., Zhou, Q., Locke, M., and Hu, W. (2014-B). A Reconfigurable High-Order UWB Signal Generation Scheme Using RSOA-MZI Structure. IEEE Photonics Journal, 1-7. doi:0.1109/JPHOT.2014.2306832.

Fernandes, J., and Wentzloff, D. (2010). Recent advances in IR-UWB transceivers: An overview. Circuits and Systems (ISCAS), Proceedings of 2010 IEEE International Symposium on, 3284-3287. doi:10.1109/ISCAS.2010.5537916.

FierceWirelessTech. (2013). AT&T, Verizon and others ride the DAS wave. Topics: Network Infrastructure. Reference obtained from: http://www.fiercewireless.com/tech/special-reports/att-verizon-and-others-ride-das-wave.

Foerster, J. (2002). The performance of a direct-sequence spread ultrawideband system in the presence of multipath, narrowband interference, and multiuser interference. IEEE Conference on Ultra Wideband Systems and Technologies. Digest of Papers. 87-91. Baltimore, MD, USA: IEEE. doi:10.1109/UWBST.2002.1006325.

Fong, B., Fong, A., and Li, C. (2010). Telemedicine technologies: information technologies in medecine and telehealth. John Wiley and Sons.

Forouzan, A., and Abtahi, M. (2003). Application of convolutional error correcting codes in ultrawideband M-ary PPM signaling. IEEE Microwave and Wireless Components Letters, *13*(8), 308-310. doi:10.1109/LMWC.2003.815700.

Forouzan, A., Nasiri-kenari, M., and Salehi, J. (2002). Performance analysis of time-hopping spread-spectrum multiple-access systems: uncoded and coded schemes. IEEE Transactions on Wireless Communications, *1*(4), 671-681. doi:10.1109/TWC.2002.804186.

Fye, D. (1990). Design of fiber optic antenna remoting links for cellular radio applications. Vehicular Technology Conference, 622-625. Orlando, FL: IEEE. doi:10.1109/VETEC.1990.110394.

Gang Chen, and Shilong Pan. (2012). Photonic generation of ultrawideband signals based on frequency-dependent gain saturation in a reflective semiconductor optical amplifier. Optics Letters, *37*, 4251-4253. doi:10.1364/OL.37.004251.

Gaudino, R., Cardenas, D., Bellec, M., Charbonnier, B., Evanno, N., Guignard, P., and Jager, D. (2010). Perspective in next-generation home networks: Toward optical solutions? IEEE Communications Magazine, *48*(2), 39-47. doi:10.1109/MCOM.2010.5402662.

Gezici, S., Kobayashi, H., Poor, H., and Molisch, A. (2005). Performance evaluation of impulse radio UWB systems with pulse-based polarity randomization. IEEE Transactions on Signal Processing, *53*(7), 2537-2549. doi:10.1109/TSP.2005.849197.

Ghavami, M., Michael, L., and Kohno, R. (2007). Ultra Wideband Signals and Systems in Communication Engineering, (2nd. ed). John Wiley & Sons.

Gibbon, T., Yu, X., Gamatham, R., Gonzalez, N., Rodes, R., Jensen, J., and Monroy, I. (2010). 3.125 Gb/s Impulse Radio Ultra-Wideband Photonic Generation and Distribution Over a 50 km Fiber With Wireless Transmission. IEEE Microwave and Wireless Components Letters, *20*(2), 127-129. doi:10.1109/LMWC.2009.2039049.

Guillory., J. (2012). Radio over Fiber (RoF) for the future home area networks. Université Paris-Est.

Hanawa, M., Mori, K., Nakamura, K., Matsui, A., Kanda, Y., and Nonaka, K. (2009). Dispersion tolerant UWB-IR-over-fiber transmission under FCC indoor spectrum mask. Optical Fiber Communication - incudes post deadline papers, 2009. OFC 2009. Conference on, 1-3. San Diego, CA: IEEE. doi:10.1364/OFC.2009.OTuJ3.

Hancke, G. P., Silva, B. C., and Hancke, J. G. (2013). The Role of Advanced Sensing in Smart Cities. Sensors, *13*(1), 393-425. doi:10.3390/s130100393.

Hayajneh, T., Almashaqbeh, G., Ullah, S., and Vasilakos, A. (2014). A survey of wireless technologies coexistence in WBAN: analysis and open research issues. Wireless Networks, *20*, 2165-2199.

Huang, H., Xu, K., Li, J., Wu, J., Hong, X., and Lin, J. (2008). UWB Pulse Generation and Distribution Using a NOLM Based Optical Switch. Journal of Lightwave Technology, *26*(15), 2635-2640. doi:10.1109/JLT.2008.927785.

Huang, M., Lee, S., and Park, S.-C. (2009). A WLAN and Bluetooth Coexistence Mechanism for Health Monitoring System. Consumer Communications and Networking Conference, 2009. CCNC 2009. 6th IEEE, 1-5. Las Vegas, NV. doi:10.1109/CCNC.2009.4784800.

Hui , R., & O' Sullivan, M. (2009). Fiber Optic Measurement Techniques. Academic Press.

Ibrahim, J., and Buehrer, R. (2006). Two-stage acquisition for UWB in dense multipath. IEEE Journal on Selected Areas in Communications, *24*(4), 801-807. doi:10.1109/JSAC.2005.863832.

IEEE Recommended Practice for Information technology. (2003). Local and metropolitan area networks-- Specific requirements-- Part 15.2: Coexistence of Wireless Personal Area Networks with Other Wireless Devices Operating in Unlicensed Frequency Bands. IEEE Std 802.15.2-2003. doi:10.1109/IEEESTD.2003.94386.

IEEE Std. 802.15.4-2011. (2011). Part 15.4: Low-Rate Wireless Personal Area Networks (LR-WPANs). IEEE.

Jazayerifar, M., Cabon, B., and Jawad, A. (2008). Transmission of Multi-Band OFDM and Impulse Radio Ultra-Wideband Signals Over Single Mode Fiber. Journal of Lightwave Technology, *26*, 2594-2603.

Jianji Dong, Xinliang Zhang, Jing Xu, Dexiu Huang, Songnian Fu, and P. Shum. (2007). Ultrawideband monocycle generation using cross-phase modulation in a semiconductor optical amplifier. Optics Letters, *32*, 1223-1225. doi:10.1364/OL.32.001223.

Jianqiang Li, Songnian Fu, Kun Xu, Jian Wu, Jintong Lin, Ming Tang, and Shum, P. (2008). Photonic ultrawideband monocycle pulse generation using a single electro-optic modulator. Optics Letter, *33*, 288-290. doi:10.1364/OL.33.000288.

Jian-Yu Zheng, Ming-Jiang Zhang, An-Bang Wang, and Yun-Cai Wang. (2010). Photonic generation of ultrawideband pulse using semiconductor laser with optical feedback. Optics Letters, *35*, 1734-1736. doi:10.1364/OL.35.001734.

Kahlon, N., and Kaur, G. (2014). Various Dispersion Compensation Techniques for Optical System: A Survey. Open Journal of Communications and Software, *1*(1), 64-73.

Kaszubowska, A., Anandarajah, P., and Barry, L. (2002). Improved performance of a hybrid radio/fiber system using a directly modulated laser transmitter with external injection. IEEE Photonics Technology Letters, *14*(2), 233-235. doi:10.1109/68.980532.

Kim, C.-J., Leem, C.-s., Kang, S.-c., and Lee, J. (2008). Policy and Technology of Dynamic Spectrum Access in Korea. Cognitive Radio Oriented Wireless Networks and Communications, 2008. CrownCom 2008. 3rd International Conference on, 1-4. Singapore. doi:10.1109/CROWNCOM.2008.4562456.

Kohno, R., and Takizawa, K.-i. (2006). Detection and Avoidance Based on Soft-Spectrum Adaptation of UWB Interference to Existing Radio Systems. Spread Spectrum Techniques and Applications, 2006 IEEE Ninth International Symposium on 435-439. Manaus-Amazon. doi:10.1109/ISSSTA.2006.311809.

Koonen, T. (2006). Fiber to the Home/Fiber to the Premises: What, Where, and When? *Proceedings of the IEEE, 94*(5), 911-934. doi:10.1109/JPROC.2006.873435.

Kouakou, K., Clavier, L., Issa, D., and Rolland, P.-A. (2010). Pulse shaping with width randomisation for IR-UWB signal. Wireless Technology Conference (EuWIT), 2010 European, 157-16). Paris:

Kumar, A., Shin, K., Choi, Y.-J., and Niculescu, D. (2012). On time-domain coexistence of unlicensed and licensed spectrum users. Dynamic Spectrum Access Networks (DYSPAN), 2012 IEEE International Symposium on, 223-234. Bellevue, WA: IEEE. doi:10.1109/DYSPAN.2012.6478133.

Lannoo, B., Dixit, A., Colle, D., Bauwelinck, J., Dhoedt, B., Jooris, B., and Demeester, P. (2015). Radio-over-fibre for ultra-small 5G cells. Transparent Optical Networks (ICTON), 2015 17th International Conference on, 1-4. Budapest: IEEE. doi:10.1109/ICTON.2015.7193591.

Le, Q. T., Briggmann, D., and Kuppers, F. (2014). Generation of FCC-compliant ultra-wideband waveforms using directly modulated semiconductor distributed-feedback laser. Communications and Electronics (ICCE), 2014 IEEE Fifth International Conference on, 12-16. Danang: IEEE. doi:10.1109/CCE.2014.6916672.

Lethien, C., Loyez, C., and Vilcot, J. (2005). Potentials of radio over multimode fiber systems for the in-buildings coverage of mobile and wireless LAN applications. IEEE Photonics Technology Letters, *17*(12), 2793-2795. doi:10.1109/LPT.2005.859533.

Li, J., Kuo, B.-P., and Wong, K. K.-Y. (2009). Ultra-Wideband Pulse Generation Based on Cross-Gain Modulation in Fiber Optical Parametric Amplifier. IEEE Photonics Technology Letters, *21*(4), 212-214. doi:10.1109/LPT.2008.2010058.

Li, P., Chen, H., Chen, M., and Xie, S. (2011). A power-efficient photonic OOK and BPSK modulated Gigabit/s IR-UWB over fiber system. Microwave Photonics, 2011 International Topical Meeting on & Microwave Photonics Conference, 2011 Asia-Pacific, MWP/APMP, 254-257. Singapore. doi:10.1109/MWP.2011.6088718.

Li, P., Chen, H., Chen, M., and Xie, S. (2012). Gigabit/s Photonic Generation, Modulation, and Transmission for a Reconfigurable Impulse Radio UWB Over Fiber System. IEEE Photonics Journal, *4*(3), 805-816. doi:10.1109/JPHOT.2012.2198804.

Lin, C.-T., Chen, J., Peng, P.-C., Peng, C.-F., Peng, W.-R., Chiou, B.-S., and Chi, S. (2007). Hybrid Optical Access Network Integrating Fiber-to-the-Home and Radio-Over-Fiber Systems. IEEE Photonics Technology Letters, *19*(8), 610-612. doi:10.1109/LPT.2007.894326.

Lin, S., and Costello, D. (1983). Error Control Coding: Fundamentals and Applications. Prentice-Hall.

Lopez, R., Caballero, A., Yu, X., Gibbon, T., Jensen, J., and Monroy, I. (2010). A Comparison of Electrical and Photonic Pulse Generation for IR-UWB on Fiber Links. IEEE Photonics Technology Letters, *22*(5), 263-265. doi:10.1109/LPT.2009.2037826.

Majhi, S., Madhukumar, A., Nasser, Y., and Hélard, J. (2010). Power Spectral Analysis of Orthogonal Pulse-Based TH-UWB Signals. Vehicular Technology Conference (VTC 2010-Spring), 2010 IEEE 71st, 1-5. Taipei: IEEE. doi:10.1109/VETECS.2010.5493877.

McKinney, J., Lin, I., and Weiner, A. (2006). Shaping the Power Spectrum of Ultra-Wideband Radio-Frequency Signals. IEEE Transactions on Microwave Theory and Techniques, *54*(12), 4247-4255. doi:10.1109/TMTT.2006.885573.

Ming-Jiang Zhang, Tie-Gen Liu, An-Bang Wang, Jian-Yu Zheng, Li-Na Meng, Zhao-Xia Zhang, and Yun-Cai Wang. (2011). Photonic ultrawideband signal generator using an optically injected chaotic semiconductor laser. Optics Letters, *36*, 1008-1010. doi:10.1364/OL.36.001008.

Mitchell, J. E. (2009). Radio-over-Fiber (RoF) Networks. Broadband Access Networks: Technologies and Deployments, 283--300. Springer US. doi:10.1007/978-0-387-92131-0_13.

Molisch, A., Li, Y., Nakache, Y., Orlik, P., Makoto Miyake, Yunnan Wu, and Jinyun Zhang. (2005). A low-cost time-hopping impulse radio system for high data rate transmission. EURASIP Journal on Applied Signal Processing, 397-412. doi:10.1155/ASP.2005.397.

Moreno, V., Mora, J., Muriel, M., and Capmany, J. (2015). Scalable High-Order UWB Pulse Generation Employing an FBG-Based Photonic Superstructure. IEEE Photonics Technology Letters, 27(20), 2146-2149. doi:10.1109/LPT.2015.2454952.

Moreno, V., Rius, M., Mora, J., Muriel, M., and Capmany, J. (2014). Scalable UWB photonic generator based on the combination of doublet pulses. Optics Express, *22*, 15346-15351. doi:10.1364/OE.22.015346.

Nakache, Y., and Molisch, A. (2006). Spectral shaping of UWB signals for time-hopping impulse radio. IEEE Journal on Selected Areas in Communications, *24*(4), 738-744. doi:10.1109/JSAC.2005.863817.

Nasiri-Kenari, M., and Shayesteh, M. (2005). Performance analysis and comparison of different multirate TH-UWB systems: uncoded and coded schemes. IEE Proceedings in Communications, *152*, 833 - 844. doi:10.1049/ip-com:20045309.

Ng'oma, A., Yang, H., and George, J. (2011). Integrated fiber-wireless networks: What, why and how. in AFRICON, 2011, 1-6. Livingstone: IEEE. doi:10.1109/AFRCON.2011.6072190.

Omomukuyo, O., Thakur, M., and Mitchell, J. (2013). Simple 60-GHz MB-OFDM Ultrawideband RoF System Based on Remote Heterodyning. IEEE Photonics Technology Letters, *25*(3), 268-271. doi:10.1109/LPT.2012.2234735.

Pan Ou, Ye Zhang, and Chun-Xi Zhang. (2008). Optical generation of binary-phase-coded, direct-sequence ultra-wideband signals by polarization modulation and FBG-based multichannel frequency discriminator. Optics Express, *16*, 5130-5135. doi:10.1364/OE.16.005130.

Pan, S., and Yao, J. (2009). Photonic generation of chirp-free UWB signals for UWB over fiber applications. Microwave Photonics, 2009. MWP '09. International Topical Meeting on, 1-4. Valencia: IEEE.

Pan, S., and Yao, J. (2010-A). UWB-Over-Fiber Communications: Modulation and Transmission. Journal of Lightwave Technology, *28*(16), 2445-2455. doi:10.1109/JLT.2010.2043713.

Pan, S., and Yao, J. (2010-B, October). A UWB Over Fiber System Compatible With WDM-PON Architecture. IEEE Photonics Technology Letters, *22*(20), 1500-1502. doi:10.1109/LPT.2010.2064763.

Pan, S., and Yao, J. (2010-C). Simultaneous Provision of UWB and Wired Services in a WDM-PON Network Using a Centralized Light Source Photonics Journa. IEEE Photonics Journal, *2*(5), 712-718. doi:10.1109/JPHOT.2010.2060476.

Pan, S., and Yao, J. (2011-A). IR-UWB-Over-Fiber Systems Compatible with WDM-PON Networks. Journal of Lightwave Technology, *29*(20), 3025-3034. doi:10.1109/JLT.2011.2165275.

Pan, S., and Yao, J. (2011-B). Provision of IR-UWB wireless and baseband wired services over a WDM-PON. Optics Express, B209-B217. doi:10.1364/OE.19.00B209.

Patel, M., and Wang, J. (2010). Applications, challenges, and prospective in emerging body area networking technologies. IEEE Wireless Communications, *17*(1), 80-88. doi:10.1109/MWC.2010.5416354.

Pham, T.-T., Yu, X., Dittmann, L., and Monroy, I. (2011). Integration of Optically Generated Impulse Radio UWB Signals Into Baseband WDM-PON. IEEE Photonics Technology Letters, *23*(8), 474-476. doi:10.1109/LPT.2011.2109943.

Piazzo, L., and Romme, J. (2003). Spectrum control by means of the TH code in UWB systems. Vehicular Technology Conference, 2003. VTC 2003-Spring. The 57th IEEE Semiannual. 3, 1649-1653. doi:10.1109/VETECS.2003.1207102.

Pietrzyk, M., and Weber, J. (2005). Performance of UWB-IR with polarity randomization and interleaved coding-modulation on multipath fading channels. Vehicular Technology Conference, 2005. VTC 2005-Spring. 2005 IEEE 61st. 2, 1365-1369. IEEE. doi:10.1109/VETECS.2005.1543532.

Prince, K., Jensen, J., Caballero, A., Yu, X., Gibbon, T., Zibar, D., and Monroy, I. (2009). Converged Wireline and Wireless Access Over a 78-km Deployed Fiber Long-Reach WDM PON. IEEE Photonics Technology Letters, *21*(17), 1274-1276. doi:10.1109/LPT.2009.2025699.

Proakis, J. (1995). Digital Communications, (3th. ed.). McGraw Hill.

Qing Wang, and Yao, J. (2007). Switchable optical UWB monocycle and doublet generation using a reconfigurable photonic microwave delay-line filter. Optics Express*, 15*, 14667-14672. doi:10.1364/OE.15.014667.

Qing Wang, Fei Zeng, Blais, S. and Yao, J. (2006). Optical ultrawideband monocycle pulse generation based on cross-gain modulation in a semiconductor optical amplifier. Opt. Lett.*, 31*, 3083-3085 . doi:10.1364/OL.31.003083.

Quang Trung Le, Briggmann, D., and Kuppers, F. (2014). Generation of FCC-compliant ultra-wideband waveforms using directly modulated semiconductor distributed-feedback laser. 2014 IEEE Fifth International Conference on Communications and Electronics (ICCE), 12-16. doi:10.1109/CCE.2014.6916672.

Rahim, M. (2010). Interference Mitigation Techniques to Support Coexistence of Ultra-Wideband Systems. Jörg Vogt Verlag.

Ramachndran, I., and Roy, S. (2005). Acquisition of direct-sequence ultra-wideband signals. IEEE Wireless Communications and Networking Conference 2005, 752 - 757.

Rateb, A., Syed-Yusof, S., and Fisal, N. (2010). Improvement of Ultra-wideband Link Performance over Bands Requiring Interference Mitigation in Korea. ETRI Journal, *32*, 44-52.

Reggiani, L., and Maggio, G. (2006). Coherent vs. Non-Coherent Detection for Orthogonal Convolutional Modulation: A Trade-Off Analysis. Ultra-Wideband, The 2006 IEEE 2006 International Conference on, 43-48. doi:10.1109/ICU.2006.281513.

Rodes, R., Pham, T.-T., Jensen, J., Gibbon, T., and Monroy, I. (2010-B). Energy-efficient VCSEL-based multiGigabit IR-UWB over fiber with airlink transmission system.

2010 23rd Annual Meeting of the IEEE Photonics Society, 222-223. Denver, CO: IEEE. doi:10.1109/PHOTONICS.2010.5698839.

Rodes, R., Yu, X., Caballero, A., Jensen, J. B., Gibbon, T. B., Gonzalez, N. G., and Monroy, I. T. (2010-A). Range extension and channel capacity increase in impulse-radio ultra-wideband communications. Tsinghua Science and Technology, 169-173. doi:10.1016/S1007-0214(10)70046-8.

Roy, M., and Jamadagni, H. (2010). Comparative Study of Adaptive Frequency Hopping with Power Control to Avoid WLAN Interference in WPAN Systems like Bluetooth. Consumer Communications and Networking Conference (CCNC), 2010 7th IEEE, 1-5. Las Vegas, NV: IEEE. doi:10.1109/CCNC.2010.5421722.

Roy, S., Foerster, J., Somayazulu, V., and Leeper, D. (2004). Ultrawideband radio design: the promise of high-speed, short-range wireless connectivity. *Proceedings of the IEEE, 92*(2), 295-311. doi:10.1109/JPROC.2003.821910.

Sakib, M., Huang, T., Gross, W., and Liboiron-Ladouceur, O. (2011). Low-Density Parity-Check Coding in Ultra-Wideband-Over-Fiber Systems. IEEE Photonics Technology Letters, *23*(20), 1493-1495. doi:10.1109/LPT.2011.2162231.

Scholtz, R. (1993). Multiple access with time-hopping impulse modulation. Military Communications Conference, 1993. MILCOM '93. Conference record. Communications on the Move., 447-450. Boston, MA. doi:10.1109/MILCOM.1993.408628.

Senior, J. M. (2009). Optical Fiber Communications: Principles and Practice (3 ed.). Pearson Education Limited.

Sheng, H., Orlik, P., Haimovich, A., Cimini, L., and Jinyun Zhang. (2003). On the spectral and power requirements for ultra-wideband transmission. Communications, 2003. ICC '03. IEEE International Conference on. 738-742. doi:10.1109/ICC.2003.1204271.

Tan, C., Ong, L., Yee, M., Luo, B., and Tang, P. (2005). Direct transmission of ultra wide band signals using single mode radio-over-fiber system. Microwave Conference Proceedings, 2005. APMC 2005. Asia-Pacific Conference Proceedings. 2. doi:10.1109/APMC.2005.1606524.

Thotahewa, K., Redoute, J.-M., and Yuce, M. (2014). A Low-Power Wearable Dual-Band Wireless Body Area Network System: Development and Experimental Evaluation. IEEE Transactions on Microwave Theory and Techniques, *62*(11), 2802-2811. doi:10.1109/TMTT.2014.2360681.

Tong, Y., Chan, L., and Tsang, H. (1997). Fibre dispersion or pulse spectrum measurement using a sampling oscilloscope. Electronics Letters, *33*(11), 983-985. doi:10.1049/el:19970663.

Torres-Company, V., Leaird, D., and Weiner, A. (2011). Coherent frequency-to-time mapping revisited: Breaking the Fraunhofer limit to achieve ultrabroad radio-

frequency waveforms. Microwave Photonics, 2011 International Topical Meeting on and Microwave Photonics Conference, 2011 Asia-Pacific, MWP/APMP, 141-144. Singapore: IEEE. doi:10.1109/MWP.2011.6088689.

Trevor, J. H., Maldonado-Basilio, R., Abdul-Majid, S., Seregelyi, J., Li, R., Antolín-Pérez, I., and Liu, H. (2013). Radio-over-Fibre access for sustainable Digital Cities. annals of telecommunications - annales des télécommunications, *68*(1), 3-21. doi:10.1007/s12243-012-0346-3.

Valente, T., and Cartaxo, A. (2010). Distribution of IR-UWB Signals With PAM Modulation in Long-Reach FTTH Networks. IEEE/OSA Journal of Optical Communications and Networking, *2*(11), 892-900. doi:10.1364/JOCN.2.000892.

Verma, L., Fakharzadeh, M., & Choi, S. (2013). Wifi on steroids: 802.11AC and 802.11AD. IEEE Wireless Communications, *20*(6), 30-35. doi:10.1109/MWC.2013.6704471.

ViaLite. (2016). Mining & Public Safety. Reference obtained from: http://www.vialite.com/market-sectors/mining-and-public-safety/

Villarreal-Reyes, S. (2007). Convolutional coding schemes with convenient power spectral density characteristics. PhD thesis, Loughborough University.

Villarreal-Reyes, S., Edwards, R., Villasenor-Gonzalez, L., Conte-Galvan, R., and Aquino-Santos, R. (2011). Maximum Free Distance Rate 1/2 Spectral Line Free Convolutional Codes for BPSK/Q-BOPPM TH-IR UWB Systems. Microwave and Wireless Components Letters, *21*(3), 166-168. doi:10.1109/LMWC.2010.2103398.

VPIphotonics Design Automation. (2016-A) Publications. Reference obtained from: http://www.vpiphotonics.com/Services/Downloads/DownloadArea/Publications/

VPIphotonics Design Automation. (2016-B) Publications. Reference obtained from: http://www.vpiphotonics.com/Applications/TransmissionSystems/

Wake, D., Nkansah, A., and Gomes, N. (2010). Radio Over Fiber Link Design for Next Generation Wireless Systems. Journal of Lightwave Technology, *28*(16), 2456-2464. doi:10.1109/JLT.2010.2045103.

Wake, D., Webster, M., Wimpenny, G., Beacham, K., and Crawford, L. (2004). Radio over fiber for mobile communications. IEEE International Topical Meeting on Microwave Photonics, 2004. MWP'04. 2004, 157-160. doi:10.1109/MWP.2004.1396863.

Wang, C., Zeng, F., and Yao, J. (2007). All-Fiber Ultrawideband Pulse Generation Based on Spectral Shaping and Dispersion-Induced Frequency-to-Time Conversion. IEEE Photonics Technology Letters, *19*(3), 137-139. doi:10.1109/LPT.2006.888966.

Wang, J., Zhu, H., and Gomes, N. (2012). Distributed Antenna Systems for Mobile Communications in High Speed Trains. IEEE Journal on Selected Areas in Communications, *30*(4), 675-683. doi:10.1109/JSAC.2012.120502.

Wang, Q., and Yao, J. (2006). UWB doublet generation using nonlinearly-biased electro-optic intensity modulator. Electronics Letters, *42*(22), 1304-1305. doi:10.1049/el:20062134.

Wang, X., Fan, S., Tang, H., Lin, L., Liu, J., Fang, Q., and Zhao, B. (2011). A Whole-Chip ESD-Protected 0.14-pJ/p-mV 3.1–10.6-GHz Impulse-Radio UWB Transmitter in 0.18-umCMOS. IEEE Transactions on Microwave Theory and Techniques, *59*(4), 1109-1116. doi:10.1109/TMTT.2011.2114170.

Weiwei Zhang, Sun Junqiang, Jian Wang, Cheng Cheng, and Xinliang Zhang. (2009). Ultra-Wideband Pulse Train Generation Based on Turbo-Switch Structures. IEEE Photonics Technology Letters, *21*(5), 271-273. doi:10.1109/LPT.2008.2010628.

Win, M., and Scholtz, R. (1998). Impulse radio: how it works. Communications Letters, *2*(2), 36-38. doi:10.1109/4234.660796.

Win, M., and Scholtz, R. (2000). Ultra-wide bandwidth time-hopping spread-spectrum impulse radio for wireless multiple-access communications. IEEE Transactions on Communications, *48*(4), 679-689. doi:10.1109/26.843135.

Wong, S., and Lau, F. (2008). Impacts of UWB Interference on Selected Radio Systems used by the Government. Circuits andSystems for Communications, 2008. ICCSC 2008. 4th IEEE International Conference on, 525-529. Shanghai: IEEE. doi:10.1109/ICCSC.2008.117.

Wu, W.-D., Wang, C.-H., and Chao, C.-c. (2003). Effects of hopping codes in TH-SS UWB signals. Vehicular Technology Conference, 2003. VTC 2003-Fall. 2003 IEEE 58th. 2, 1308-1312. doi:10.1109/VETECF.2003.1285234.

Xianbin Yu, Gibbon, T., Pawlik, M., Blaaberg, S., and Tafur Monroy, I. (2009). A photonic ultra-wideband pulse generator based on relaxation oscillations of a semiconductor laser. *Optics Express, 17*, 9680-9687. doi:10.1364/OE.17.009680.

Xianbin Yu, Gibbon, T., Rodes, R., Tien-Thang Pham, and Monroy, I. (2013). System Wide Implementation of Photonically Generated Impulse Radio Ultra-Wideband for Gigabit Fiber-Wireless Access. Journal of Lightwave Technology, *31*(2), 264-275. doi:10.1109/JLT.2012.2228629.

Xu, K., LI, J.-q., Yin, J., Zhang, Y., Hao, H., and Jin-tong, L. (2009). Microwave photonic signal processing techniques and radio-over-fiber. The Journal of China Universities of Posts and Telecommunications, *16*, 6-9. doi:10.1016/S1005-8885(08)60367-2.

Xu, X., Zhou, E., Liang, Y., Yuk, T., Lui, K., and Wong, K. (2011). Power-efficient photonic BPSK coded ultrawideband signal generation. Optical Fiber Communication Conference and Exposition (OFC/NFOEC), 2011 and the National Fiber Optic Engineers Conference (pp. 1-3). Los Angeles, CA.

Yao, J. (2009). Photonics for ultrawideband communications. IEEE Microwave Magazine, *10*(4), 82-95. doi:10.1109/MMM.2009.932287.

Yao, J., Zeng, F., and Wang, Q. (2007). Photonic generation of ultra-wideband signals, J. Lightw. *Journal of Lightwave Technology, 25*, 3219-3235.

Yao, Q. W. (2007). Switchable optical UWB monocycle and doublet generation using a reconfigurable photonic microwave delay-line filter. Optics Express*, 15*, 14667-14672 . doi:10.1364/OE.15.014667.

Yick, J., Biswanath Mukherjee, and Dipak Ghosal. (2008). Wireless sensor network survey. Computer Networks, *52*(12), 2292-2330.

You Min Chang, Junsu Lee, and Ju Han Lee. (2010). Ultrawideband doublet pulse generation based on nonlinear polarization rotation of an elliptically polarized beam and its distribution over a fiber/wireless link. Optics Express, *18*, 20072-20085. doi:10.1364/OE.18.020072.

Yuan, T., and Wu, H. (2014). Analysis of Coverage Efficiency of Radio-over-Fiber Network for Railway LOCOTROL Wireless Communication System. Vehicular Technology Conference (VTC Fall), 2014 IEEE 80th (pp. 1-5). Vancouver: IEEE. doi:10.1109/VTCFall.2014.6965877.

Zeinalpour-Yazdi, Z., and Nasiri-Kenari, M. (2006). Performance analysis and comparisons of different ultra-wideband multiple access modulation schemes. IEE Proceedings - Communications, *153*(5), 705 – 718. doi:10.1049/ip-com:20050591.

Zeng, F., and Yao, J. (2004). All-optical bandpass microwave filter based on an electro-optic phase modulator. Optics Express, *12*, 3814-3819. doi:10.1364/OPEX.12.003814.

Zeng, F., and Yao, J. (2005). Frequency domain analysis of fiber bragg grating based phase modulation to intensity modulation conversion. Photonic Applications in Nonlinear Optics, Nanophotonics, and Microwave Photonics, 5971. Toronto, Canada. doi:10.1117/12.628628.

Zeng, F., and Yao, J. (2006-A). An approach to ultrawideband pulse generation and distribution over optical fiber. Photonics Technology Letters, *18*(7), 823-825. doi:10.1109/LPT.2006.871844.

Zeng, F., and Yao, J. (2006-B). Ultrawideband Impulse Radio Signal Generation Using a High-Speed Electrooptic Phase Modulator and a Fiber-Bragg-Grating-Based Frequency Discriminator. IEEE Photonics Technology Letters, *18*(19), 2062-2064. doi:10.1109/LPT.2006.883310.

Zeng, F., Wang, Q., and Yao, J. (2007). All-optical UWB impulse generation based on cross-phase modulation and frequency discrimination. Electronics Letters, *43*(2), 121-122. doi:10.1049/el:20073432.

Zhang, H., and Gulliver, T. (2005). Biorthogonal pulse position modulation for time-hopping multiple access UWB communications. IEEE Transactions on Wireless Communications, *4*(3), 1154-1162. doi:10.1109/TWC.2005.846969.

Zhang, J., Orlik, P., Sahinoglu, Z., Molisch, A., and Kinney, P. (2009-A). UWB Systems for Wireless Sensor Networks. Proceedings of the IEEE, 97(2), 313-331. doi:10.1109/JPROC.2008.2008786.

Zhang, M., Zheng, J., Wang, A., Wang, Y., Jiang, J., and Liu, T. (2013). Chaotic ultra-wideband over fiber link based on optical feedback laser diode. Microwave and Optical Technology Letters, *55*, 1504–1507. doi:10.1002/mop.27615.

Zhang, W., Sun, J., Wang, J., Cheng, C., and Zhang, X. (2009-B). Ultra-Wideband Pulse Train Generation Based on Turbo-Switch Structures. IEEE Photonics Technology Letters, *21*(5), 271-273. doi:10.1109/LPT.2008.2010628.

Zheng, J., Zhu, N., Wang, H., Du, Y., Wang, L., and Liu, J. (2013). Photonic-Assisted Ultrawideband Pulse Generator With Tunable Notch Filtering Based on Polarization-to-Intensity Conversion. IEEE Photonics Journal, *5*(3), 7900909-7900909.

Zhifeng Lin, Wei Lei, and Kaihang Li. (2010). Design of ADTR-DSSS-IR-UWB Transmitter for BPSK Modulation. Communications and Intelligence Information Security (ICCIIS), 2010 International Conference on, 236-239. Nanning: IEEE. doi:10.1109/ICCIIS.2010.22.

Zhiquan Bai, Wei Liu, Shaoyi Xu, Weihua Zhang, and Kyungsup Kwak. (2005). DS-BPAM UWB system-coded and uncoded scheme. Communications and Information Technology, 2005. ISCIT 2005. IEEE International Symposium on. 1, pp. 689-692. IEEE. doi:10.1109/ISCIT.2005.1566948.

Zhu, J., Waltho, A., Yang, X., and Guo, X. (2007). Multi-Radio Coexistence: Challenges and Opportunities. Proceedings of 16th International Conference on Computer Communications and Networks, 2007., 358-364. doi:10.1109/ICCCN.2007.4317845.

Zhu, M., Zhang, L., Wang, J., Cheng, L., Liu, C., & Chang, G.-K. (2013). Radio-Over-Fiber Access Architecture for Integrated Broadband Wireless Services. Journal of Lightwave Technology, *31*(23), 3614-3620. doi:10.1109/JLT.2013.2286564.